

Aus der Mannheimer Institut für Intelligente Systeme in der Medizin (MIISM)
der Medizinischen Fakultät Mannheim
(Direktor: Prof. Dr. med. Frank Anton Giordano)

The Radiochemical Basis of FLASH and Minibeam Radiotherapy:
Investigating H₂O₂ Production and Diffusion

Inauguraldissertation
zur Erlangung des Doctor scientiarum humanarum (Dr. sc. hum.)
der
Medizinischen Fakultät Mannheim
der Ruprecht-Karls-Universität
zu
Heidelberg

vorgelegt von
Tengda Zhang

aus
Liaoning, China
2025

Dekan: Prof. Dr. med. Sergij Goerd

Referent: Prof. Dr. rer. nat. Jürgen W. Hesser

TABLE OF CONTENTS

	Page
PREFACE	1
LIST OF ABBREVIATIONS	2
1 INTRODUCTION	4
1.1 FLASH radiotherapy: technical insights	4
1.1.1 Proton conformal FLASH-RT techniques	5
1.1.2 Treatment planning considerations	12
1.1.3 Advances in conformal FLASH-RT planning	13
1.1.4 Future perspectives	18
1.2 Current hypotheses behind FLASH effect	19
1.3 Radiochemistry in FLASH-RT	21
1.4 Radiochemical surrogate in Minibeam-RT	24
2 PUBLICATIONS	27
3. DISCUSSION	53
4. SUMMARY	55
5. ZUSAMMENFASSUNG	59
6. LITERATURE	63
7. APPENDIX	73

8. CURRICULUM VITAE.....74

9. ACKNOWLEDGMENT75

PREFACE

The doctoral committee has previously examined whether my publications are suitable for a cumulative dissertation, and this is a final overview of the publications contained in my cumulative thesis.

1. List of peer-reviewed publications included in the cumulative dissertation. For each publication, provide a complete list of authors, title, journal, journal impact factor, and whether the manuscript has been accepted for publication, is in revision after peer review, or has been submitted and is awaiting peer review. Shared first authorships should be clearly indicated. Please also indicate whether the publication is an original research report, a review, or another type of article.

Publication 1 **Tengda Zhang**, Daniel García-Calderón, Miguel Molina-Hernández, Joana Leitão, Jürgen Hesser, Joao Seco, *A theoretical study of H₂O₂ as the surrogate of dose in minibeam radiotherapy, with a diffusion model considering radical removal process*, **Medical Physics**, impact factor: 3.2, accepted for publication, doi: 10.1002/mp.16570. Original research report

Publication 2 **Tengda Zhang**, Christina Stengl, Larissa Derksen, Kristaps Palskis, Konstantinos Koritsidis, Klemens Zink, Sebastian Adeberg, Gerald Major, David Weishaar, Ulrike Theiß, Jing Jin, Maria Francesca Spadea, Elpida Theodoridou, Jürgen Hesser, Kilian-Simon Baumann, Joao Seco, *Analysis of Hydrogen Peroxide Production in Pure Water: Ultrahigh versus Conventional Dose-Rate Irradiation and Mechanistic Insights*, **Medical Physics**, impact factor: 3.2, accepted for publication, doi: 10.1002/mp.17335. Original research report

Publication 3 Yangguang Ma, **Tengda Zhang (co-first author)**, Balaji Selvaraj, Jiajian Shen, Shouyi Wei, Chingyun Cheng, Hao Gao, Per Rugaard Poulsen, Heng Li, Eric Diffenderfer, Jan Schuemann, Liyong Lin, Michael Folkerts, Zachary Morris, Benjamin Durkee, Jürgen Hesser, Haibo Lin, Charles B Simone, II, Minglei Kang, Hui Wu. *Advancing Proton Conformal FLASH Radiation Therapy: Innovations, Techniques, and Clinical Potentials*, **International Journal of Radiation Oncology, Biology, Physics**, impact factor: 6.4, awaiting peer review, Review paper.

2. Summary of the doctoral student's contribution to the work reported in each manuscript

Work steps	Publication 1	Publication 2	Publication 3
Conception (%)	100	100	50
Literature search (%)	100	100	50
Ethics proposal (%)	No need	No need	No need
Animal experimentation proposal (%)	No need	No need	No need
Data collection (%)	100	100	50
Data analysis (%)	100	100	50
Interpretation of results (%)	100	100	50
Manuscript writing (%)	100	100	80
Revision (%)	100	100	100
Indicate which figures and tables resulted from your dissertation work.	All figures and tables are included in my dissertation	All figures and tables are included in my dissertation	All figures and tables are included in my dissertation

I hereby certify that this is a true representation of the doctoral student's contribution to the publications listed.

LIST OF ABBREVIATIONS

RT – radiation therapy;

IMPT – intensity-modulated proton therapy;

OARs – organs at risk;

TB – transmission beam;

SEBP – single-energy Bragg peak;

SESOBP – single-energy spread-out Bragg peak;

MESOBP – multiple-energy spread-out Bragg peak;

PB – Bragg peak;

RC – range compensator;

RF – ridge filter;

URS – universal range shifters;

UHDR – ultra-high dose rates;

CONV – conventional dose-rate radiation;

DMF – dose modifying factor;

PBS – pencil beam scanning;

ROI – region of interest;

DADR – dose averaged dose rate;

DTDR – dose threshold dose rate;

PBSDR – pencil beam scanning dose rate;

LET – Linear Energy Transfer;

MLC – multileaf collimators;

SDDRO – simultaneous dose and dose rate optimization;

SDSMO – simultaneous dose and spot map optimization;

ALARA – as low as reasonably achievable principle;

MU – monitor unit;

FEM – FLASH effectiveness model;

ROS – reactive oxygen species;
RRR – radical-radical recombination;
SFRT – spatially fractionated radiation therapy;
BBRT – broad-beam radiotherapy;
PVDR – peak-valley dose ratio;
CTC – center-to-center distance;
MBRT – minibeam radiotherapy;
FDM – free diffusion model;
DMCR – diffusion model considering removal.

1 INTRODUCTION

Radiation, a ubiquitous phenomenon, is energy transmitted in the form of waves or particles. It originates from both natural sources, such as cosmic rays and radioactive decay, and artificial sources, including nuclear reactors and medical devices. Radiation is broadly classified into non-ionizing and ionizing types. Non-ionizing radiation, such as ultraviolet light and microwaves, lacks the energy to remove electrons from atoms but plays critical roles in applications like communication and heating. In contrast, ionizing radiation, including X-rays, gamma rays, electrons, and particle radiation (e.g., protons and carbon ions), possesses enough energy to ionize matter and is widely employed in medical applications. In medicine, ionizing radiation is indispensable for diagnostic imaging techniques like X-rays radiography and CT scans, which have revolutionized disease detection and monitoring. While ionizing radiation carries inherent risks, its therapeutic potential is harnessed in radiotherapy (RT). By carefully delivering controlled doses, radiotherapy transforms this otherwise harmful phenomenon into a powerful tool against cancer, offering precise and effective control over tumor growths while minimizing damage to healthy tissues.

1.1 FLASH radiotherapy: technical insights

This section is derived from my review paper, “*Advancing Proton Conformal FLASH Radiation Therapy: Innovations, Techniques, and Clinical Potentials*“, which is currently under peer review. This review provides a concise introduction to FLASH-RT and discusses various proton FLASH techniques that are currently applicable in clinical settings. It serves as a reference for future research and clinical implementation of related technologies. For complex and uncertain mechanisms, approaching FLASH-RT from a technical perspective facilitates a clearer understanding of its principles. Moreover, the clinical implementation of FLASH-RT is not necessarily hindered by an incomplete understanding of the underlying FLASH effect mechanisms. This is evidenced by the fact that proton FLASH-RT clinical trials are already underway^{1,2}.

FLASH-RT, delivered at ultra-high dose rates (UHDR), typically exceeding 40 Gy/s, has been demonstrated to spare organs at risk (OARs) while maintaining equivalent tumor control³⁻¹⁰. This protective effect from UHDR can be described by the dose modifying factor (DMF)⁴, which refers to the ratio of the doses delivered at FLASH and conventional dose rates that produce equivalent biological effects. To implement FLASH-RT, several critical and interconnected technical aspects must be considered, including total dose, dose rate, delivery mode, field size, dose conformity, and irradiation time structure. Proton therapy offers a superior dosimetric distribution compared to photons due to the Bragg peak¹¹. It is particularly suited for FLASH-RT due to the ability to treat deep-seated tumors with conformity compared to electron and photon RT^{12,13}. Current proton pencil beam scanning (PBS) treatment systems, which use multiple energy layers to cover the target, face significant challenges in delivering UHDR due to the energy layer switch time, typically greater than 200 ms for cyclotron and over 1000 ms for synchrotron. The resulting prolonged treatment duration reduces mean dose rates in OARs, which can make it more challenging to achieve the FLASH dose rate threshold¹²⁻¹⁷. To address these challenges, the use of single-energy proton beams for FLASH irradiation has proven effective^{12,18,19}.

Unlike electron and passive scattering proton therapy, which deliver a uniform dose to the entire field simultaneously, PBS necessitates the sequential delivery of

hundreds of pencil beam spots to cover the entire target volume, complicating the dose rate calculations¹³. Various approaches have been proposed to calculate the dose rate within specific regions of interest (ROIs), including dose averaged dose rate (DADR)¹⁷, dose threshold dose rate (DTDR)¹³, and pencil beam scanning dose rate (PBSDR)²⁰. DADR is calculated as the mean dose rate in a voxel, weighted by the dose contribution from each individual spot, without considering the delivery time or time intervals between spots. In contrast, PBSDR incorporates both delivery and scanning time, providing a more conservative dose rate estimate. DTDR applies a dose threshold to exclude the contribution from spots that deliver a dose below the predefined threshold. These different approaches can result in significant variations in dose rate calculations, further complicating the implementation of FLASH-RT.

Despite these challenges, a first proton FLASH clinical trial has been successfully completed using transmission beams and demonstrating the feasibility of FLASH treatment in humans². Following the insights gained from this trial, a second proton FLASH trial has been approved and is now enrolling patients to evaluate the treatment for thoracic bone metastases¹. This review aims to provide a comprehensive overview of the current research status of proton conformal FLASH technologies, offering insights for optimizing these techniques and guiding future preclinical and clinical applications.

1.1.1 Proton conformal FLASH-RT techniques

In conventional intensity-modulated proton therapy (IMPT), multiple energy layers are used to achieve conformity and uniformity in the target. Most research has proposed various single-energy proton FLASH delivery techniques in the very high end of the energy range to mitigate the impact of switch time on dose rate and to increase the beam transmission efficiency from the accelerator to the patient, providing higher dose rates. These techniques include transmission beams (TB), single-energy Bragg peak beams (SEBP), single-energy spread-out Bragg peak beams (SESOBP), and hybrid methods. These approaches sacrifice some of the dose conformity achievable with IMPT to maximize dose rates. Additionally, the concept of multiple-energy spread-out Bragg peak (MESOBP) FLASH on a superconducting gantry has also been proposed²¹. Furthermore, proton arc FLASH therapy has been introduced as a potential approach, though its clinical implementation requires biological evidence confirming the existence of the FLASH effect^{22,23}.

1.2.1.A Transmission beam (TB) FLASH-RT

The TB FLASH^{2,12,24-27}, also known as the shoot-through FLASH technique^{17,28,29}, utilizes the plateau region of protons to irradiate the tumor, thereby eliminating the need for multiple energy layers required in conventional IMPT. This approach offers the advantages of achieving higher dose rates more easily and maintaining uniform dose distribution in the target. However, it also has notable drawbacks: the technique positions the Bragg peak (BP) outside the patient's body, which does not fully take advantage of the superior physical properties of protons. This inevitably results in a higher exit dose beyond the target. By superimposing multiple fields from various angles, this technique achieves a high-dose and high-dose-rate region with conformity to the target area. This technique is pioneering for achieving FLASH dose rates with proton beams²⁸. The pertinent studies on this technique³⁰ have demonstrated its effectiveness in mitigating uncertainties related to dose-averaged Linear Energy Transfer (LET) distributions and proton range while ensuring adequate

target coverage. Multiple research teams compared TB with IMPT^{13,17,20,24,26,31} and found that by increasing beam intensities, reducing the number of scanning spots, and employing hypofractionation¹⁷, TB can achieve FLASH dose rates (>40 Gy/s) while producing plans comparable in quality to IMPT.

1.2.1.B Single-energy Bragg peak (SEBP) FLASH-RT

SEBP was first introduced by researchers to leverage the Bragg peaks to eliminate the exit doses in TB FLASH technique³². This technique utilizes multiple-field optimization (MFO) and beam-specific range pull-back devices³³ to achieve IMPT-equivalent dosimetric distribution. The highest single-energy setting of the cyclotron machine is used to achieve a sufficient beam current for FLASH-RT. Using an inverse algorithm, this method optimizes multiple fields by ensuring that each spot within the field is delivered within only one energy layer. Through MFO, this approach ultimately creates a clinically acceptable treatment plan. A ray-tracing algorithm³⁴ is then employed to calculate the range pull-back for each spot and to generate range compensators (RC) and universal range shifters (URS) for each field. The combination of single-energy beams with range compensation from URS and RC enables precise adaptation of the proton range to the target's distal edge. To further improve the dose rate, a relatively sparse spot map is achieved by multiple iterations of merging low-weighted spots into nearby ones while considering the dose constraints for the target and OARs. Consequently, the number of spots is reduced while the new sparse spot map can achieve a dose distribution that is comparable to the original one. Compared to the TB method, SEBP eliminates exit dose to OARs beyond the tumor while still preserving FLASH dose rate delivery.

1.2.1.C Single-energy spread-out Bragg peak beams (SESOBP) FLASH-RT

The SESOBP mainly employs patient-specific ridge filters (RFs) generated through inverse optimization to achieve proton SOBPs. The RFs broaden the BP for a given energy of protons, potentially with only a single field to achieve the target dose coverage with a FLASH dose rate.

1) 3D static ridge filter

The primary objective of an RF is to convert an initially monoenergetic proton beam, characterized by a sharp Bragg peak, into a beam with uniform depth doses over a designated range^{35,36}. RFs enable conformal coverage of the target area by an SOBPs while reducing the number of energy layers required for proton irradiation, thereby decreasing the overall irradiation time³⁷⁻³⁹. So far, this method has been widely used in preclinical studies⁴⁰⁻⁴³. However, the utilization of range modulation devices (e.g., URS, RCs, RFs) introduces additional neutron doses. Study suggests using low-Z materials can help minimize neutron contamination, emphasizing the importance of material selection for patient safety⁴⁴. Besides, accurate positioning of the static RFs is crucial for effective proton FLASH delivery due to the pyramid or pin-shaped ridges' submillimeter size.

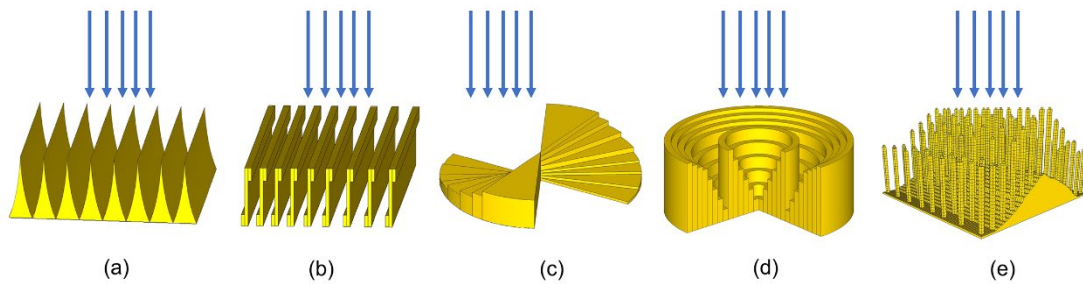


Figure 1. Several 2D (a-d) and 3D (e) designs of ridge filters (RFs): grating-type RFs (a, b), propeller wheel modulators (c), spiral RFs (d), and 3D pyramid-type RFs.

Early 2D RFs had a variety of shapes (Figure 1(a)-(d))⁴⁵⁻⁵⁰. The recent 3D RF design (Figure 1(e)) features a cylindrical pyramid structure with multiple layers tailored to achieve the desired width of the SOBP at each spot. The pyramid's height corresponds to the SOBP width, whereas each layer's width represents beam intensity. By carefully positioning pyramid structures within the RFs, a 3D RF is created (named pin-shaped RFs, 3D range-modulators, non-uniform SOBP modulators, mini-RFs, and others^{18,51-54}). As shown in Figure 2, when used alone or combined with range shifters or patient-specific compensators, this method allows three-dimensional conformal SOBP within the target area using single-energy, single-field irradiation. It is currently the primary approach for utilizing RFs in proton conformal FLASH-RT^{18,51-61}. The challenges mainly involve generating and optimizing the pyramid structure and its distribution while maintaining high precision.

The evolved form of this technique is similar to the SEBP solution, where the ridges are modulated to deliver non-uniform doses from individual beams. By combining multiple fields, a conformal dose distribution is achieved. Liu et al.⁵¹ introduced a sparse RF, which differs from regular RFs by selectively removing pins at specific locations. This selective pin removal ensures a higher dose rate while preserving adequate SOBP dose coverage. Multiple beams are needed to generate a uniform dose distribution in the whole target volume. User-defined pin removal thresholds result in different filter designs. For larger targets, a 50% pin removal threshold is suggested, whereas a 30% threshold is recommended for smaller targets.

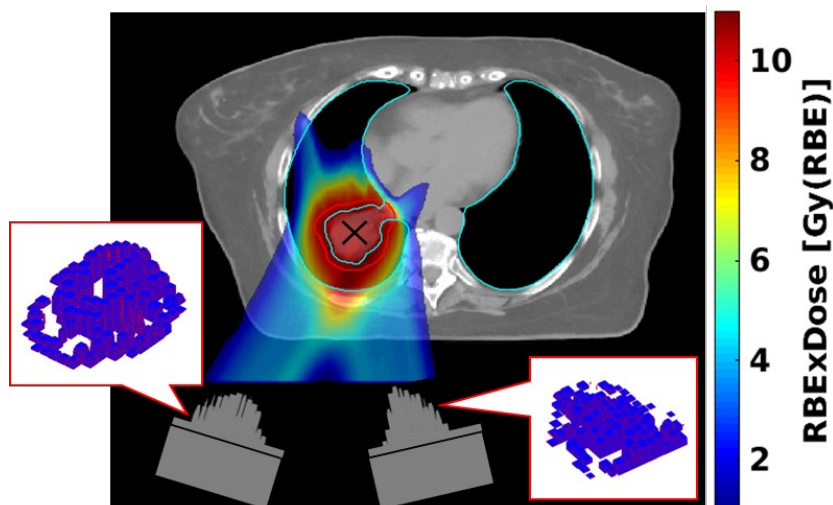


Figure 2. 3D pyramid-shaped RFs used with a URS to enable uniform target dose coverage in a lung cancer case.

2) Dynamic RFs

The RFs discussed above, known as static RFs, are customized for each patient and field, and adjustments between treatment fractions necessitate new RFs, leading to poor reusability and high costs. To address these limitations, dynamic RF designs have been proposed. However, the stringent motion speed and precision requirements restrict its application in FLASH-RT, and it remains conceptual for now. Nevertheless, advancements in industrial technology may pave the way for future implementation. In light of this, two intriguing dynamic RF designs were introduced.

One idea involves moving the universal RFs during irradiation to broaden the Bragg peak^{47,56}. Maradia et al.⁵⁶ proposed to position two identical universal RFs back-to-back and move them simultaneously to adjust the thickness differences of the degrader material (as shown in Figure 3a). This technique allowed for varying degrees of Bragg peak broadening, significantly reducing the number of energy layers required to achieve the desired SOBP and thus shortening the treatment time. However, the proposed design can only achieve a narrow SOBPs of around 3 cm, which limits its usage clinically.

Zhang et al. [52] proposed a more flexible design that is a bit similar to the dynamic three-dimensional beam modification technique proposed by Varian Medical Systems, Inc (Palo Alto, CA)⁶². This dynamic RF resembles multileaf collimators (MLCs), consisting of two opposing rows (Figure 3b). However, unlike traditional MLCs, where the thickness (or height) and width of the leaves are fixed, this RF allows the height of each pin to vary. Additionally, the combination of layers with a different cross-sectional area in each pin can be dynamically adjusted during treatment as well. This variability is driven by multiple motors on both sides, which move simultaneously with the proton scanning process. The dynamic RF must be adjusted quickly enough to match the speed of PBS while maintaining accuracy to achieve the FLASH dose rate. Currently, this level of performance is not feasible, making it a conceptual solution that has yet to be implemented.

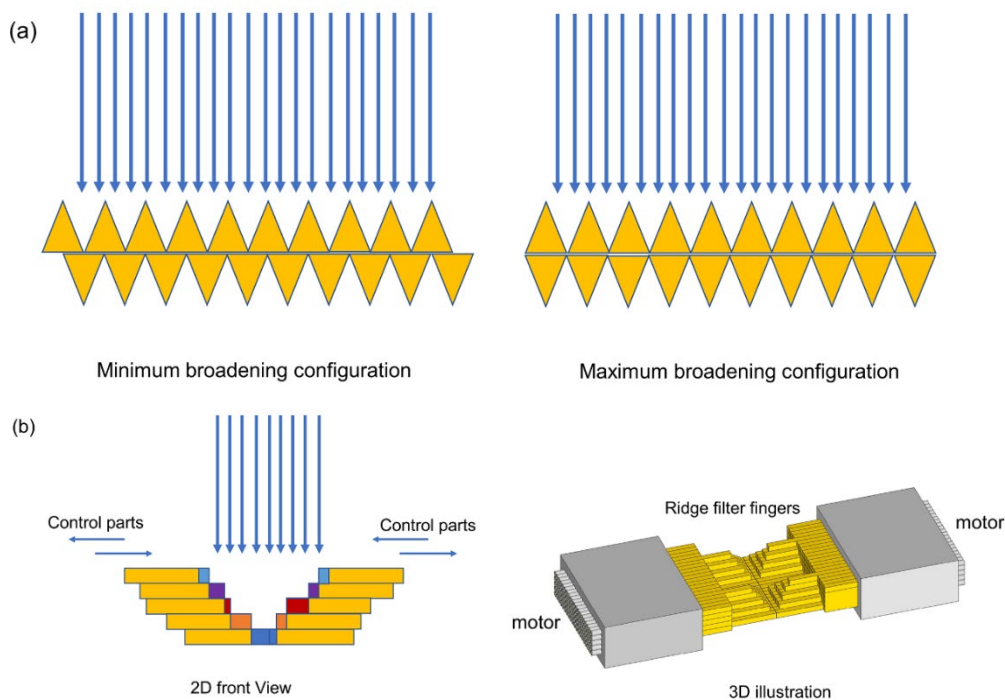


Figure 3. Two designs of dynamic RFs were proposed for SESOBP. (a) two identical back-to-back universal RFs; (b) multilayer dynamic RFs similar to MLC.

Examples of the dose and dose rate distribution of these monoenergetic FLASH techniques are shown in Figure 4, compared with IMPT.

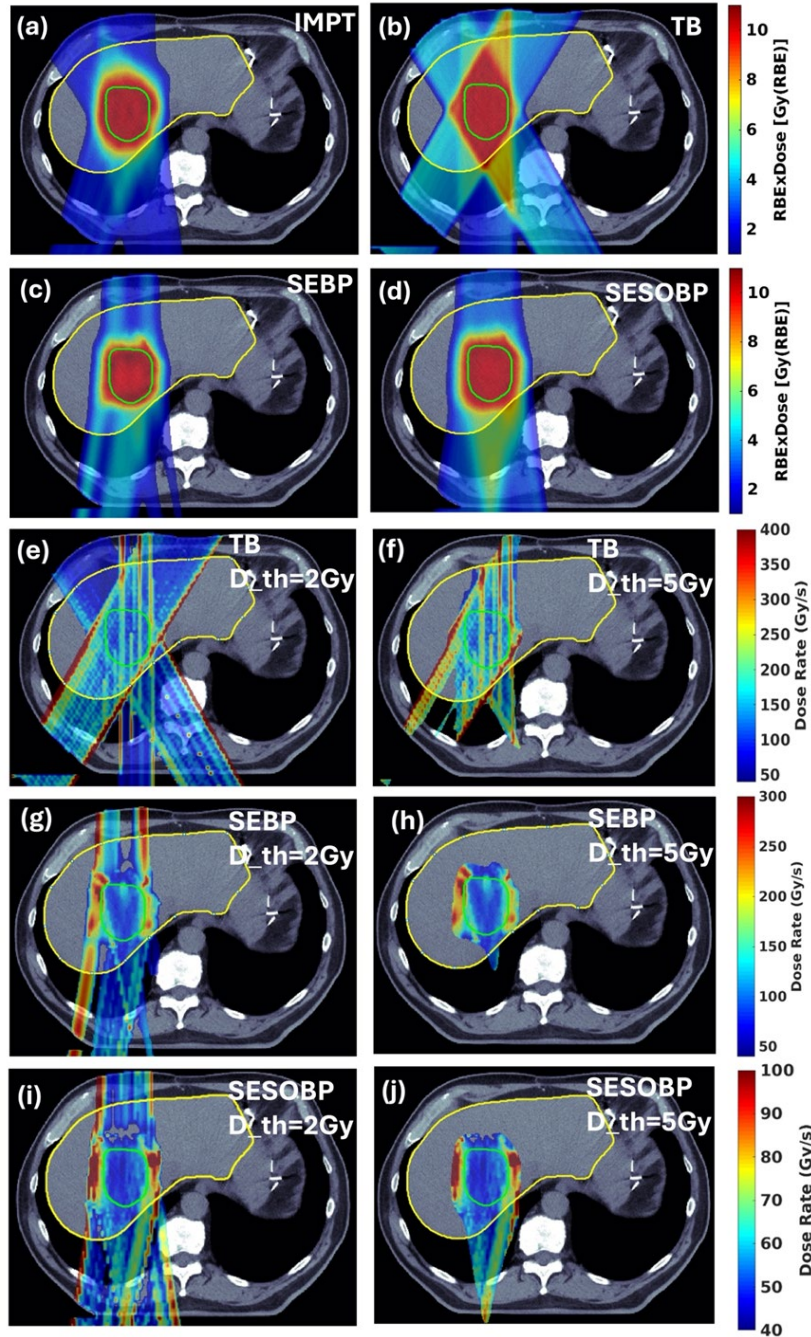


Figure 4. A schematic comparison of monoenergetic proton FLASH irradiation techniques, including Transmission Beam (TB), Single-Energy Bragg Peak (SEBP), and Single-Energy Spread-Out Bragg Peak (SESOBP), for a liver case ($10 \text{ GyRBE} \times 5 \text{ fraction}$, 3 fields for each technique) shown in panels (b)-(d). The conventional Pencil Beam Scanning (PBS) treatment depicted in panel (a) serves as a reference. Panels (e)-(j) illustrate the 2D dose rate distribution, calculated for each beam individually using the pencil beam scanning dose rate (PBSDR) method, with dose thresholds of 2 GyRBE and 5 GyRBE for FLASH-sparing effect.

1.2.1.D Hybrid FLASH-RT

Although all three of the aforementioned techniques can achieve FLASH dose rates in treatment planning, each has its advantages and disadvantages. Therefore, researchers have proposed combining two of these techniques to further improve treatment plans.

Lin et al.⁶³ proposed a method that combines TB with IMPT, referred to as TB-BP. Unlike conventional optimizers that focus solely on dose distribution, this method employs simultaneous dose and dose rate optimization (SDDRO)²⁹ and automatically selects the optimal combination of BP and TB with optimized spot selection and weighting. Since the FLASH effect primarily serves to protect OARs as opposed to the tumor itself, the TB technique is used to irradiate the tumor boundary adjacent to normal tissues, while the BPs target the tumor core. Additionally, including BPs reduces the exit dose and improves target conformity. Compared to the TB-only approach, this hybrid optimization method maintained the same FLASH dose rate coverage on OARs while significantly reducing the dose to the surrounding normal tissue. Moreover, its conformal index was even slightly better than that of IMPT (0.92 vs. 0.90). The authors suggested that this might be attributed to the increased optimization degrees of freedom offered by the TB-BP approach. Unlike traditional IMPT, which can only use BPs to deliver dose at the tumor boundary, this hybrid method allows TB to be used for uniform dose delivery within the target area.

Furthermore, Ma et al.⁶⁴ investigated the combination of TB with SESOBP to achieve FLASH (TB-SESOBP). Although SESOBP alone can achieve conformal FLASH-RT, the presence of RFs as scatterers increases the spot size and thereby reduces the spot dose rate, which may hinder the optimal realization of the FLASH effect. The addition of TB can help mitigate this limitation to some extent. The authors developed a hybrid inverse optimization method that generates SESOBP using pre-designed general bar RFs and places SESOBP within the target while using TB to cover the target boundaries and maintain FLASH dose rate coverage for surrounding normal tissues. Compared to the customized RFs, these pre-designed general RFs can only form a uniform dose distribution in a cuboid region to facilitate adaptive proton radiotherapy used in previously mentioned SESOBP approaches. Thereby, the conformity was improved by the use of multiple beams and TB. The hybrid TB-SESOBP demonstrated the same FLASH dose rate coverage as the TB-only while significantly reducing the dose to the OARs. The researchers also compared TB-SESOBP with TB-BP in lung cancer cases, which is discussed later.

1.2.1.E Multiple-energy spread-out Bragg peak (MESOBP) FLASH-RT

Energy layer switching is a major obstacle in achieving BP FLASH, which is a leading reason why most researchers use single-energy beams. However, Zeng et al.²¹ proposed a MESOBP FLASH approach using a superconducting gantry. In conventional systems, bending magnetic fields must be adjusted to accommodate the proton energy changes for accurate beam positioning. Due to the larger momentum acceptance of superconducting magnets, the magnetic field strength of the bending magnets does not need to change for protons within a specific energy range, enabling ultra-fast energy switching. The authors divided the energy range of 70-218 MeV into three bands, with an energy switching time of only 16 ms within each band. They selected the highest energy band (150-218 MeV) and combined it

with URS of varying thicknesses³², as discussed in section 1.1.1.B about SEBP, the proton beam should be pulled back with a depth range of 0-30 cm.

Although superconducting magnets enable extremely fast energy switching, treatment time for PBS increases with the addition of energy layers. To address this, the authors developed a simultaneous dose and spot map optimization (SDSMO) algorithm. SDSMO reduces the total number of spots by merging low-weighted spots into adjacent ones, and it also merges low-weighted energy layers into other layers to decrease the number of layers, thereby increasing the dose rate. Compared to TB plans, the MESOBP approach can achieve equivalent FLASH dose rate coverage, better target conformity, and significantly reduced doses to normal tissues.

As we discussed above, the advantages and disadvantages of all proton conformal techniques mentioned are summarized in Table 1.

Table 1. The pros and cons of various proton conformal FLASH techniques.

Technique	Pros	Cons	Additional accessories
TB	<ol style="list-style-type: none"> 1. The highest dose rate among all techniques 2. Improved robustness against proton range uncertainties 3. The only clinically tested proton FLASH technology 4. Enables proton portal imaging beyond the patient 5. Capable of delivering FLASH-RT using a single beam 	<ol style="list-style-type: none"> 1. Unavoidable exit dose on normal tissue 2. Inefficient use of protons' high LET 3. Maximum beam path through patient ~30cm 4. Conformal dose requires multiple beams 	
SEBP	<ol style="list-style-type: none"> 1. Comparable plan quality to IMPT 2. Eliminates exit dose beyond the target 3. Better conformity than TB 4. Higher dose rate and a more robust setup than SESOBP 	<ol style="list-style-type: none"> 1. Requires beam-specific RCs for each patient 2. Multiple beams may minimize the FLASH-sparing effect 3. URS and RCs produce extra neutrons and increase the spot sizes 	URS, beam-specific RCs
SESOBP	<ol style="list-style-type: none"> 1. Comparable plan quality to IMPT 2. Eliminates exit dose beyond the target 3. Better conformity than TB 4. Capable of delivering FLASH-RT using a single beam 	<ol style="list-style-type: none"> 1. Requires beam-specific RCs for each patient 2. Involves a complex RF design and optimization process 3. Requires accurate positioning of the RFs 4. URS and RFs produce extra neutrons and increase the spot sizes 5. SOBP decreases dose rate 	URS, beam-specific RFs
TB-BP	<ol style="list-style-type: none"> 1. Less exit dose and better conformity than TB 2. Higher dose rate on OARs than SEBP and SESOBP 	<ol style="list-style-type: none"> 1. Multiple beams may minimize the FLASH-sparing effect 2. Still delivers exit dose on normal tissue 3. Reduced robustness compared to TB 	
TB-SESOBP	<ol style="list-style-type: none"> 1. Less exit dose and better conformity than TB 2. Higher dose rate on OARs than SEBP and SESOBP 3. Enables adaptive FLASH-RT by utilizing general bar RFs, compared to SEBP and SESOBP 	<ol style="list-style-type: none"> 1. Multiple beams may minimize the FLASH-sparing effect 2. Still delivers exit dose on normal tissue 3. Reduced robustness compared to TB 4. URS and RFs might produce extra neutrons and increase the spot sizes 	General bar RFs, URS
MESOBP	<ol style="list-style-type: none"> 1. Comparable plan quality to IMPT 2. Ultra-fast energy switching 	<ol style="list-style-type: none"> 1. Reduced dose rate due to energy switching 	

3. Eliminates exit dose beyond the target
4. Better conformity than TB
5. Capable of delivering FLASH-RT using a single beam

2. Limited accessibility of superconducting gantry

1.1.2 Treatment planning considerations

Technical advancements have made conformal FLASH-RT using proton beams clinically feasible; however, significant challenges must be considered. Current biological evidence indicates that there is likely a dose threshold besides a dose rate threshold for the FLASH effect. If the delivered dose to an ROI does not meet the necessary thresholds, the FLASH protective effect is not expected to be achieved⁶⁵⁻⁶⁷. Consequently, when planning FLASH-RT, dose and dose rate constraints for OARs must be incorporated. However, the complexity of dose delivery patterns in PBS introduces various factors to consider, such as individual spot dose rate, field dose rate, dwelling time, switch time, dose threshold, and spot dose weights, making dose rate definition more intricate. Sørensen et al.⁶⁷ have shown that although the field dose rate is the same, repainting in proton therapy can compromise the sparing effect. DADR¹⁷, PBSDR²⁰, and DTDR¹³ have been used to assess the FLASH protective effect for critical OARs. Most studies on FLASH have utilized a threshold of 40 Gy/s¹⁰. Nevertheless, researchers have observed different dose rate thresholds to achieve protective effects on different biological models⁶⁷⁻⁶⁹. In a murine model, researchers found that animals could progressively benefit from increasing the mean dose rate from 0.7 Gy/s to 2 Gy/s to 5.5 Gy/s to 20 Gy/s to 40 Gy/s⁶⁷. FLASH sparing was not triggered abruptly at a specific dose rate but started gradually at relatively low dose rates. Treatment plan optimization should probably not only focus on increasing the dose rate to above 40 Gy/s but also on increasing lower dose rates to medium dose rates. However, further investigation is necessary to fully comprehend the dose rate requirement for different OARs.

Minimum dose thresholds were also proposed during treatment planning^{28,31,60}. However, due to the incomplete understanding of the FLASH mechanism, the correlation of dose with the FLASH-sparing effect remains unclear. While some studies suggested 10 Gy as the dose threshold, other research has also shown different thresholds, such as 4 Gy⁷⁰ in the humanized mouse model. However, the exact selection of the dose thresholds remains undetermined, posing challenges to developing clinical protocols. Despite the potential of achieving additional FLASH-sparing effects, treatment planning practices still need to adhere to the current guidance to follow as low as reasonably achievable (ALARA) principles.

Besides the phenomenological models, the feasibility of integrating FLASH mechanistic models into treatment planning was demonstrated⁶⁰, in which the FLASH DMF was modeled via the radiolytic oxygen depletion⁷¹ and the treatment planning was optimized directly in terms of FLASH effective dose as a product of DMF and physical dose. While the exact understanding of the FLASH mechanism is unclear, the proposed general framework and optimization method for integrating FLASH phenomenological or mechanistic models into treatment planning⁶⁰ can be used to address the tradeoff between the physical dose coverage and the biological FLASH coverage by modeling and optimizing both effects as one quantity, i.e., FLASH effective dose, to quantify the net improvement of FLASH.

Another important consideration is how multiple beams affect the FLASH-sparing effect. Currently, most proton conformal FLASH-RT techniques rely on multiple beams, except for SESOBP, which allows single-beam irradiation. MacKay et al. discussed potential treatment options for future FLASH therapy delivery using multiple beams⁶⁵, and they found that single-field plans exhibited a greater plan-specific FLASH effect compared to multifield plans (14.7% vs. 3.7%). Recent studies investigated the impact of multiple beams on the FLASH effect in mice, revealing that interruptions in delivery time can compromise the FLASH-sparing effect in areas of beam overlap^{67,72}. The time gap between overlapping beams and the spatial arrangement of the delivered beams are critical parameters for FLASH studies. The studies suggest that the impact of multiple beams requires further research on different types of OARs⁷².

Notably, the choice of fractionation scheme in radiotherapy significantly affects the sparing effect of FLASH radiotherapy on certain OARs⁷³. MacKay et al. revealed that the threshold dose and the dose per fraction strongly impacted the FLASH effect, and smaller fractionated doses pose challenges in optimizing plan quality and achieving adequate FLASH coverage of OARs⁶⁵. Similarly, Kang et al. compared 34 Gy in a single fraction and 45 Gy in 3 fractions for lung cancer and observed significant variations in FLASH dose rate distribution using the same planning parameters. Their findings revealed that the treatment plans with a lower fraction dose (15 Gy per fraction) require a smaller minimum monitor unit (MU) per spot to achieve a more uniform dose distribution. However, the reduced minimum MU per spot diminished the FLASH coverage for critical OARs because of current machine limitations of the minimal spot duration¹³. Many biological studies have focused on delivering a single high dose^{3,6,10,68,74-76}, which is not directly applicable to treating many human tumors that could benefit from normal tissue sparing. For clinical use, a hypofractionation approach often would be more suitable to reduce the potential long-term toxicities observed in animal studies^{77,78}. Sørensen et al.⁶⁷ explored that splitting the total dose into 2, 3, 4 or 6 identical deliveries with 2-minute pauses still preserves the FLASH-sparing effect but with a largely reduced protective benefit compared to delivery in a single delivery. As research progresses, clinical scenarios involving dose interruptions are expected to become more common, highlighting the need for further investigation.

1.1.3 Advances in conformal FLASH-RT planning

The development of techniques such as TB, SEBP, SESOBP, hybrid, and MESOBP proton conformal FLASH methods has shown promising dosimetric results in various anatomical regions. Here, we summarize the utilization of these techniques in the head and neck, lung, breast, and abdomen cases in Table 2.

Table 2. The utilization of proton conformal FLASH techniques across various anatomical regions.

Treatment sites	FLASH Technique	Number of fields	Fraction dose (Gy)	Dose-rate calculation methods (Gy)	Dose threshold (Gy)	DMF
Head and neck	van de Water et al. ¹⁷	117	2/6	DADR		
	van Marlen et al. ²⁴	10	1.55/2	DADR (0.005-0.04)*		
	Verhaegen et al. ²⁶	4	1.8	DADR		2
	Kneepkens ³⁰	≤5	1.8			1.5
	Gao et al. ³¹	3/4	15/16	DADR	8	1.43
	Pennock et al. ⁷⁹	SEBP	3/4	6/10	DADR	
Thorax	Kang et al. ¹³	5	15/34	DADR/PBSDR (0.1)		

				/DTDR (0.1)		
	Wei et al. ²⁷	3/5	34	PBSDR		
	van Marlen et al. ²⁸	10	18	DADR (0.01)		
	Gao et al. ³¹	3	12	DADR	8	1.43
	Kang et al. ³²	5	34	DADR		
	Wei et al. ⁸⁰	SEBP	2-4	34	PBSDR (0.1)	0.1/1/5
	Liu et al. ⁵¹	3	10	DADR	4	
	Ma et al. ⁵⁷	3	34	FEM**	5	1.49
	Ma et al. ⁶⁴	TB- SESOBP	3+3***	34	DADR/PBSDR (0.1)	
	Lin et al. ⁶³	TB-BP	3+3	6	DADR	
	Zeng et al. ²¹	MESOBP	1/5	9	DADR	4
Breast	van Marlen et al. ⁸¹	TB	1	5.7/9.74/14.32	DADR (0.01)	4
	Lattery et al. ⁸²	SEBP	3	8	PBSDR (0.1)	0.1/1/5
Abdomen	Wei et al. ¹²	TB	2/5	4.5	PBSDR	
	Gao et al. ³¹		2	12	DADR	8
	Wei et al. ¹⁹				DADR/PBSDR (0.1)	5
		SEBP	3	10	/DTDR (0.1)	
		Kaulfers et al. ⁸³	4	8	PBSDR	0.1/1/5
	Zeng et al. ²¹	MESOBP	1/5	9	DADR	4

* The dose threshold in dose-rate calculations;

** FLASH effectiveness model⁸⁴;

*** Hybrid FLASH technique: 3 TB +3SESOBP

1.2.3.A Head and neck cancers

Research on proton conformal FLASH-RT for head and neck tumors has predominantly focused on the use of TB^{17,24,26,30,31}, with only a few studies exploring the techniques of BP FLASH⁷⁹.

1) Transmission FLASH-RT

van de Water et al.¹⁷ conducted a study using four head-and-neck cancer cases. They employed 117 TBs to simulate proton arc therapy and compared the dosimetric outcomes with clinical treatment plans. The study found that TB proton arc therapy reduced the Dmax of the brainstem from 64% of the prescription dose to 47%, and the Dmean of the lacrimal gland decreased from 58% to 44.5%. Additionally, improvements were observed in the Dmax for both eyes (from 92.5% to 86.5%) and for the lenses (from 80.5% to 46%). However, the reduction in OAR doses is likely attributable to the arc therapy composed of 117 fields rather than directly related to TB FLASH. Nonetheless, their study demonstrated that, combined with hypofractionation, this TB proton arc therapy technique could achieve a DADR of 73.2 Gy/s. It is important to note that the radiobiological and clinical significance of DADR, a dose rate concept frequently used in FLASH treatment planning studies, remains unclear. The higher skin toxicity seen in mice with PBS repainting than without repainting despite the dose and DADR being the same⁶⁷ directly demonstrates that DADR is a too simple dose rate concept to represent the full biological effect. Similarly, van Marlen et al.²⁴ randomly selected 10 head and neck cancer cases to compare IMPT plans with 10-field TB plans. They found that, while achieving comparable PTV coverage, the TB plans generally performed worse than the IMPT plans when the FLASH effect was not considered. For instance, the Dmax for the spinal cord and brainstem increased from 36 Gy and 23.8 Gy in the IMPT plans to 40.6 Gy and 35.3 Gy in the TB plans, respectively. Additionally, the Dmean for the oral cavity increased from 25.2 Gy to 29.3 Gy. These results are not surprising given TB's unavoidable exit doses and poor dose modulation capacity.

When the FLASH effect is taken into account, the comparison results could be entirely different. Verhaegen et al.²⁶ compared 4-field IMPT and TB plans in a neurological cancer case. Although specific dose values were not provided, the DVH analysis showed that, without considering the FLASH effect, OARs like the chiasm, hippocampi, and brainstem received higher doses in the TB plan than in the IMPT plan. However, when applying the DMF in dose calculation, the brainstem dose in the TB plan was lower than in the IMPT plan. It's important to note that the study used a very bold DMF of 2, which would require further justification and validation. Regular TB planning only focus on dose distribution without considering dose rate in the optimization. Gao et al.³¹ introduced the SDDRO method for TB, which can significantly improve FLASH coverage. In this study, the Dmean for the esophagus, larynx, and ROI (a ring of normal tissue surrounding the target) in the IMPT plan were 31.6, 38.6, and 38.4 Gy, respectively. In contrast, these values were higher in the TB plan without considering DMF, at 36.8, 40.4, and 44.8 Gy, respectively. However, when a DMF of 1.43 was incorporated into the dose calculation, the Dmean for these OARs dropped to 28.0, 31.8, and 30.8 Gy, respectively, lower than in the IMPT plan.

The examples above illustrate that the protection of OARs by TB is highly dependent on the presence and magnitude of the FLASH effect. If the FLASH effect is absent or if the DMF is not sufficiently high, IMPT would be superior to the TB technique in dose distribution. It is worth noting that TB, compared to IMPT, results in a lower dose-averaged LET (LET_D) in OARs³⁰, although research has suggested that SOBP is similar to entrance plateau regarding to the FLASH sparing effect⁴³.

2) SEBP FLASH-RT

In addition to the TB technique mentioned above, Pennock et al. investigated the use of BP FLASH techniques⁷⁹, and compared IMPT, TB, and SEBP plans in eight cases of recurrent head and neck cancer at 6 and 10 Gy per fraction. Given that hypofractionation favors FLASH coverage, they showed the comparison of OAR doses at 10 Gy per fraction, which is similar to 6 Gy/fraction. As expected, without considering any DMF, TB provided less favorable dosimetric distribution to OARs compared to IMPT: in the IMPT plans, the Dmax of the mandible and spinal cord were 81.2% and 34.6% of the prescription dose, respectively, while the Dmean of the left and right parotid glands were 6.3% and 9.3%; In contrast, in the TB plans, the Dmax of the mandible and spinal cord increased to 104.6% and 65.8%, with the Dmean of the left and right parotid glands rising to 18.6% and 14.8%, respectively. Treatment plans using SEBP technology showed no statistically significant differences in OAR dose metrics compared to IMPT plans. Although direct evidence of the FLASH effect in these OARs is still lacking, the fact that SEBP achieves similar results to IMPT even without considering the DMF highlights the superiority of this technique, making it a clinically feasible option with potential for clinical FLASH trials with uncompromised dose conformation.

1.2.3.B Thoracic cancers

Numerous studies have explored proton conformal FLASH-RT for thoracic cancer cases, utilizing various techniques, including TB^{13,27-29,31}, SEBP^{32,80}, SESOBP^{51,57,58}, hybrid methods^{63,64}, and MESOBP²¹. When treating thoracic malignancies with radiotherapy, several critical OARs are at risk, such as the lungs, proximal bronchial

tree, heart, great vessels, spinal cord, brachial plexus, and esophagus. However, lung doses are the only metrics consistently reported in each study. Therefore, we will primarily focus on comparing lung dose metrics in this section.

1) Transmission FLASH-RT

Similar to head and neck cases, TB FLASH-RT offers less lung protection than IMPT when DMF is not considered^{27,29,31}, mainly due to the unavoidable exit dose. A study²⁸ comparing TB with VMAT showed similar dose metrics for the ipsilateral lung: Dmean (5.7 vs. 5.6 Gy), V5Gy (29% vs. 33.1%), V10Gy (17.9% vs. 18.2%), and V20Gy (7.9% vs. 7%). However, 10 non-coplanar fields in TB plans provide a greater degree of freedom in optimization. Therefore, further comparison between non-coplanar VMAT and TB is still required. TB may not be the optimal solution regarding dose distribution, but it offers better robustness in thoracic radiotherapy, given the impact of respiratory motion²⁷.

2) SEBP FLASH-RT

Kang et al.³² reported that SEBP (using a higher MMU constraint) provided comparable FLASH dose rate coverage (V40Gy/s) to TB, while significantly reducing lung dose metrics like V7Gy (492.6 ± 325.2 vs. 724.9 ± 416.3 cc) and V7.4Gy (468.7 ± 310.7 vs. 672.8 ± 398.6 cc) according to RTOG0915 constraints. SEBP not only outperformed TB in lung protection, but Wei et al.⁸⁰ also demonstrated that SEBP achieved plan quality comparable to IMPT, with no significant differences in lung dose metrics.

3) SESOBP FLASH-RT

The SESOBP FLASH technique requires beam-specific RFs for individual patients. Researchers^{51,57,58} have explored different approaches to RF design, with a common strategy of sparse RFs to increase the dose rate. However, overly sparse RFs may compromise the plan quality. Although these studies did not provide specific dose metrics for OARs, the DVH analysis and the authors' discussions suggest that SESOBP is able to achieve comparable target coverage and OAR protection to IMPT, even without considering DMF. This outcome is understandable, given SESOBP's characteristics.

4) Hybrid FLASH technology

Hybrid FLASH techniques leverage the strengths of multiple approaches for lung cancer treatment. Specifically, two strategies, TB-BP⁶³ and TB-SESOBP⁶⁴, were proposed and compared in recent studies. TB inevitably irradiated more healthy lungs, but the hybrid techniques reduced the proportion of TB by incorporating BP and SESOBP, thereby offering better protection for OARs. The DVH clearly showed that, compared to TB-only, these hybrid techniques significantly reduced lung dose. Ma et al.⁶⁴ reported specific lung dose metrics for TB-only, TB-BP, and TB-SESOBP plans: V7Gy(cc) were 360.8 ± 177.9 , 313.1 ± 170.2 , and 300.8 ± 156.9 , respectively; V7.4Gy(cc) were 349.4 ± 172.6 , 305.3 ± 165.6 , and 292.1 ± 150.2 , respectively. While no statistically significant difference was found between TB-BP and TB-SESOBP, both were superior to TB-only. Additionally, no difference in FLASH dose rate coverage was observed between the two hybrid techniques. However, TB-SESOBP outperformed TB-BP in OAR sparing for larger PTV, particularly for the

lungs. The researchers attributed this to the higher weighting of the TB component in the TB-BP plans than the TB-SESOBP for larger targets, which led to less favorable dose distribution. This finding suggests that applying minimal weighting constraints on the BP component in the TB-BP optimizer may be necessary to achieve optimal results.

5) MESOBP FLASH-RT

Zeng et al.²¹ compared MESOBP with TB in both single and multiple field plans across 10 lung cancer cases. Just like other BP FLASH techniques, MESOBP demonstrated superior lung protection. Specifically, for single field plans, MESOBP achieved a lower Dmean (3.5 ± 1.8 Gy vs. 6.2 ± 3.1 Gy) and V12.8Gy ($9.1 \pm 4.7\%$ vs. $16.6 \pm 9.0\%$) compared to TB. Similarly, in multiple field plans, MESOBP continued to outperform TB, with a lower Dmean (2.8 ± 1.5 Gy vs. 3.4 ± 1.9 Gy) and V12.8Gy ($8.1 \pm 4.6\%$ vs. $10.3 \pm 5.9\%$) in lungs. Although MESOBP and TB showed no difference in FLASH dose rate coverage above 40 Gy/s, TB delivered dose rates exceeding 1000 Gy/s to over 90% of the lungs, while MESOBP maintained this high dose rate in only a small portion of the lung.

1.2.3.C Breast cancer

We identified only two studies on FLASH-RT for breast cancer. One used a single tangential TB⁸¹, and the other employed a multiple-field SEBP method⁸². For whole breast irradiation, the dose distribution is typically tangential to both sides of the target, suggesting that TB could be a promising technique for this application. However, the authors did not report any OAR dose metrics; instead, they focused on achieving TB FLASH and analyzing the impact of various machine parameters on the target dose. Future research on TB FLASH treatment plans for breast cancer should explore the differences in dose distribution between TB and IMPT. Regarding SEBP, it achieved the FLASH dose rate and is consistent with results in other anatomical sites, showing no statistically significant differences in OAR dose metrics compared to IMPT.

1.2.3.D Abdominal cancer

In the abdomen, researchers have investigated the use of TB^{12,31}, SEBP^{19,83}, and MESOBP²¹ techniques in treating liver cancers. SEBP has consistently achieved comparable dose distributions to IMPT, similar to results observed in other anatomical sites^{19,83}. Study on TB¹² in liver cancer, the effects of varying the number of fields (2 and 5) and minimum spot times (0.5 and 2 ms) on treatment plan quality were examined. Although these combinations produced different OAR dose metrics and FLASH dose rate coverage, none provided the same level of OAR protection as IMPT. For instance, in the best scenario of TB, the kidney's V18Gy was 15.8%, compared to just 5.6% in the IMPT plan.

1.2.3.E Pelvic cancer

There are limited proton FLASH treatment planning studies for pelvic cancers. In one prostate cancer study^{19,83}, patients were treated with proton SBRT using PBS (40 Gy in five fractions). SEBP FLASH plans with a four-beam setup produced dose distributions similar to conventional opposing beams. Dose comparisons for rectum, bladder, femoral heads, large bowel, and penile bulb showed no significant

differences between clinical and SEBP plans, except for a higher maximum dose (Dmax) in the FLASH plans (116.9% vs. 103.3%). The rectum V40Gy/s reached 94%, and the FLASH ratio neared 100% with a 5 GyRBE threshold.

1.1.4 Future perspectives

Based on different dose rate definitions, all the aforementioned techniques can achieve "FLASH dose rate" while complying with clinical dose constraints. However, numerous challenges still hinder their clinical translation.

A major limitation is the beam current insufficiency in commercially available cyclotron or synchrotron systems in reaching an averaged field dose rate above 40Gy/s for large-volume targets. Ongoing research aims to enhance machine capabilities to meet the demands of large-volume treatments. Additionally, further radiobiological studies are urgently needed to determine which dose rate definition, whether the instantaneous dose rate per pulse or the average dose rates such as DADR, DTDA, and PBSDR, is most relevant to the FLASH-sparing effect¹³. If the former, the current machines may already suffice; if the latter, optimization methods for the spot delivery sequences will be essential^{85,86}.

Many current treatment planning studies use the open-source toolkit matRad⁸⁷. So far, TB FLASH treatment planning is available in Eclipse (Varian Medical Systems) and SESOBP FLASH treatment planning is available in RayStation (RaySearch Laboratories, Stockholm, Sweden), while treatment planning modules for SEBP FLASH-RT are still under development⁸⁸. The availability of a universal treatment planning system will facilitate research for both preclinical and clinical applications. The current treatment planning studies on different anatomical sites may not be sufficient to draw definitive conclusions due to the limited data. However, once TPS tools are developed in commercial versions, more extensive studies are expected to provide robust evidence for designing future clinical trials. This advancement will significantly enhance the reliability and applicability of FLASH-RT in clinical settings.

In the end, further investigation into the mechanisms underlying the FLASH effect is essential. Understanding which OARs can achieve the FLASH-sparing effect under specific conditions and determining the magnitude of DMF, will be pivotal in guiding treatment planning strategies⁶⁰, potentially leading to the exclusion of certain techniques. FLASH technique researchers must consider not only the physical aspects but also the radiobiological mechanisms, as overlooking the latter could render proposed concepts and techniques clinically irrelevant.

1.2 Current hypotheses behind FLASH effect

Preclinical studies first observed this FLASH effect, with mice subjected to UHDR irradiation exhibiting reduced normal tissue toxicity compared to conventional dose rates¹⁰. Specifically, studies documented diminished fibrosis, inflammation, and other radiation-induced side effects, while tumor suppression remained uncompromised. These findings have positioned FLASH as a promising innovation in clinical radiotherapy. Extensive preclinical research has explored the mechanisms behind the FLASH sparing effects. Animal models, including those involving mice, cats, and pigs, have consistently shown significant protection of normal tissue. These studies revealed that normal tissues exposed to FLASH radiation maintained structural integrity and function far better than those exposed to conventional rates while maintaining tumor control. This dual advantage has captured widespread interest as a potential paradigm shift in radiotherapy, but the underlying mechanisms remain incompletely understood. One of the earliest and most consistent findings related to the FLASH effect is the critical involvement of oxygen. Both an absence of oxygen (anoxia) and an excess of oxygen (normoxia) appear to negate the FLASH sparing effect, implying that oxygen availability within the irradiated medium must be finely tuned^{74,89-91}. Historically, the significance of oxygen in radiobiology has been explained by the oxygen fixation hypothesis (OFH). According to OFH, the presence of oxygen during radiation exposure “fixes” otherwise transient, potentially repairable DNA radical damage into permanent, non-reversible lesions⁹²⁻⁹⁴. In conventional radiation (CONV), OFH and associated oxygen-dependent mechanisms explain why well-oxygenated tissues and tumors are generally more radiosensitive than hypoxic regions.

Building on the OFH, many researchers hypothesized that the FLASH effect arises from rapid oxygen depletion. Under UHDR conditions, the intense burst of initial free radicals supposedly consumes local oxygen so quickly that normal tissues become transiently hypoxic, preventing the fixation of damage. This oxygen depletion theory gained traction because it aligns with familiar principles: high instantaneous radical production would outpace oxygen diffusion and replenishment, leaving insufficient oxygen to lock in the damage. Such a model seemed plausible for low linear energy transfer (LET) radiation, such as electrons, X-rays, or protons, where a substantial fraction of DNA damage is indirect—mediated by reactive oxygen species (ROS) formed when radiation interacts with water. However, this explanation conflicts with several recent findings: 1) High-LET radiation, such as carbon ions can cause densely clustered, complex, and non-repairable DNA damage without requiring oxygen’s presence. As a result, the Oxygen Enhancement Ratio (OER) for carbon ions is close to 1, indicating that oxygen plays a negligible role in modulating their cytotoxicity⁹⁵⁻⁹⁷. Thus, under traditional assumptions, if the FLASH effect were fundamentally rooted in OFH and oxygen depletion, then it should not manifest when using carbon ions, since the damage they inflict does not rely on the presence or absence of oxygen. However, recent *in vitro* and *in vivo* studies conducted in Heidelberg and GSI have shown a clear FLASH effect when carbon and helium ions under UHDR, even within the Bragg Peak region^{90,98,99}. This finding directly contradicts the idea that OFH-driven oxygen depletion is a prerequisite for the FLASH effect. Furthermore, direct *in vivo* and *in vitro* oxygen partial pressure measurements have demonstrated that FLASH irradiation consumes less oxygen per unit dose compared to CONV irradiation with various radiation modalities (X-ray, electron, proton, carbon, and oxygen ions), contrary to what one might expect if oxygen depletion were the central

mechanism, and this reduction is insufficient to induce hypoxic conditions in the irradiated tissue¹⁰⁰⁻¹⁰².

The radical-radical recombination (RRR) hypothesis is another proposed mechanism to explain the FLASH effect¹⁰³. The RRR hypothesis in FLASH radiotherapy arises from the idea that, at UHDR, a dense population of free radicals is generated within an extremely short time frame, leading many of them to recombine before they can inflict significant biological damage on healthy tissues. In conventional radiotherapy, free radicals, primarily hydroxyl radicals ($\bullet\text{OH}$) produced through the radiolysis of water, diffuse through cells and interact with critical biomolecules such as DNA, proteins, and lipids, thereby contributing to cell damage and death. With FLASH, however, the argument is that because so many free radicals are formed almost simultaneously, they recombine with each other to form more neutral or less reactive species, such as hydrogen peroxide (H_2O_2), the product of $\bullet\text{OH}$ recombination, thus reducing the overall burden of damage in normal tissues. In principle, this rapid radical quenching could account for a protective effect, leaving healthy tissue relatively unscathed by the radiation. Some early computational models of radiolysis and chemical reactions in radiotherapy^{71,104-109}, have shed light on how radicals might interact in dense clusters under different dose rates, providing a theoretical framework to explore whether radical-radical interactions might be dose-rate dependent.

Despite the initial appeal of this RRR mechanism, scientific investigations have revealed complexities that challenge its plausibility as the primary explanation for the FLASH effect. For instance, one key finding in FLASH radiotherapy research is that the protective effect is strongly dependent on proper oxygen concentration in the environment, as we discussed previously. Oxygen is well-known to enhance radiation-induced damage by stabilizing radical-induced DNA lesions, forming peroxy radicals that are harder to repair. If radical-radical recombination alone were responsible for the FLASH effect, it should, in theory, manifest similarly in both oxygenated and hypoxic conditions. Additionally, due to the rapid recombination of $\bullet\text{OH}$ presented in RRR, the H_2O_2 production should be increased compared to CONV. Although there is no consensus about dose rate dependency of H_2O_2 production, but recent experiments have all shown a decreased H_2O_2 production under UHDR^{74,110-112}. Meanwhile, investigators at the University of Oxford have proposed that the potential outcome of RRR is the formation of crosslinks¹¹³. By positing that the high concentration of reactive species could drive radical-radical couplings that bridge biomolecules, they hypothesized that RRR might generate harmful crosslinks instead of simply neutral byproducts. Their studies, however, did not detect any notable crosslink formation difference between FLASH and CONV. The absence of such evidence led these researchers to conclude that RRR alone is unlikely to explain the sparing of normal tissue observed in FLASH. Instead, the research community is increasingly looking into other hypotheses, ranging from lipid peroxidation, to transient immune or vascular effects, to modifications of cell signaling pathways triggered by extremely rapid irradiation^{3,114}. Although RRR remains an interesting component of the broader discussion on free radical chemistry in radiobiology, the collective evidence thus far suggests it is not the principal driver behind the FLASH effect and its well-documented dependence on oxygen. Nevertheless, radiochemistry under UHDR still warrants further study.

1.3 Radiochemistry in FLASH-RT

Ionizing radiation induces DNA damage via two main pathways: direct and indirect damage. Direct damage occurs when radiation deposits energy directly into the DNA molecule, breaking chemical bonds. Indirect damage, on the other hand, is mediated by ROS generated primarily from water radiolysis. For low LET radiation, the indirect damage pathway accounts for up to 70% of total DNA damage¹¹⁵. This makes ROS generation critically important for understanding radiation effects. Radiation-induced indirect damage proceeds through three major stages—physical, chemical, and biological—that together underlie much of the harm ionizing radiation can inflict on living systems^{116,117}. In the physical stage, which occurs within femtoseconds to picoseconds after radiation exposure, the incoming photons or charged particles deposit their energy in tissue, resulting in ionization and excitation of atoms and molecules. This phase is characterized by extremely rapid physical interactions: electrons are stripped from molecules (ionization), leaving behind charged species or excited states. Because biological matter is predominantly water, a large proportion of these initial events happen in water molecules. Consequently, the physical stage sets the groundwork for subsequent chemical reactions by creating reactive species, sometimes termed “primary species,” such as free electrons, ionized water (H_2O^+), and excited water (H_2O^*). Following the physical stage, the chemical stage spans from picoseconds to seconds. During this interval, the primary species generated by the initial ionization begin to undergo secondary reactions, most notably the formation of ROS such as the hydroxyl radical. These highly reactive ROS readily interact with surrounding substances, and since much of human tissue is aqueous, water radiolysis is the dominant process. These ROS can diffuse short distances and initiate chain reactions that ultimately alter nearby biological macromolecules. Free radicals can oxidize lipids in cell membranes, break chemical bonds in proteins, and even damage DNA. A key aspect of indirect damage is that the radiation itself does not always directly strike critical targets—like DNA—yet the reactive species formed can still cause severe biological effects. Consequently, this chemical phase serves as a bridge between the initial physical energy deposit and the eventual damage observed at the cellular and systemic levels. Lastly, the biological stage unfolds over minutes to years, encompassing a wide array of processes that begin once the reactive chemical species interact with vital cellular components. During this stage, damaged DNA or other macromolecules trigger responses such as cell cycle arrest, DNA repair mechanisms, or apoptosis. If the damage is not adequately repaired, mutations can accumulate, leading to genomic instability and potentially carcinogenesis. At the tissue or organism level, various signaling pathways may be activated to orchestrate immune responses, inflammation, or tissue remodeling. Additionally, non-targeted effects—such as bystander effects, where non-irradiated cells respond to signals from irradiated neighbors—can amplify the overall impact of radiation damage.

Radiation does not only produce oxidizing species (e.g., hydroxyl radicals); it also generates reducing species, such as solvated electrons (e_{aq}^-). These solvated electrons are just as significant as their oxidizing counterparts, as they influence redox balance within the irradiated system. The subtle interplay between oxidizing and reducing species, and their subsequent reactions with biomacromolecules, sets the stage for intricate redox cycling within cells. When reducing species (like solvated electrons) react with biomolecules, the resulting products often remain reducing in character, ready to scavenge or react with oxidizing molecules. Conversely, when oxidizing species react with biomolecules, the products remain oxidizing,

perpetuating oxidative stress. This delicate balance of redox cycling has profound implications for the overall burden of cellular damage.

If FLASH-RT reduces ROS production, it could indeed play a role in the lower radiation toxicity observed with UHDR. However, since most ROS have extremely short half-lives and are difficult to measure, research has primarily focused on H₂O₂, a relatively stable ROS and an end product of water radiolysis^{104,106,109,118}. This makes H₂O₂ a crucial marker in studies investigating the FLASH effect. H₂O₂ is considered a relatively weak ROS, which enables it to function effectively as a signaling molecule. Its moderate reactivity allows it to diffuse across cell membranes and modulate various physiological processes. For instance, in DNA damage repair processes, where key signaling proteins such as ATM and ATR can be activated by H₂O₂, even in the absence of DNA double-strand breaks to initiate downstream DNA damage response pathways¹¹⁹⁻¹²¹. Additionally, the interaction of H₂O₂ with DNA poses a significant threat. Due to the presence of phosphate groups, DNA molecules carry a negative charge and can form coordination bonds with free iron ions in the cell, resulting in metal–DNA complexes. When H₂O₂ diffuses near DNA, it undergoes decomposition via the Fenton reaction, producing highly reactive •OH that can cause severe DNA damage¹²²⁻¹²⁴. Therefore, it is critical to understand the impact of dose rates on H₂O₂ production.

Previous studies have reported contradictory findings regarding the dose-rate dependence of H₂O₂ production in pure water^{74,110-112,125-130}. While several recent experiments have indicated that UHDR results in a lower G-value (molecules/100 eV) for H₂O₂ (G(H₂O₂)) without an explanation, most of Monte Carlo simulation studies have suggested the opposite. Consequently, there is no consensus on whether UHDR increases or decreases H₂O₂ yield compared with conventional irradiation. In addition, in previous research on H₂O₂ production, the hypoxic water samples did not contain carbon dioxide (CO₂) dissolved in the water. In contrast, there was 5% CO₂ in cell experiments to equilibrate the pH value of the medium. In addition to the dose-rate dependency, the influence of CO₂ on the H₂O₂ yield also warrants investigation. Therefore, in our publication titled “*Analysis of Hydrogen Peroxide Production in Pure Water: Ultrahigh versus Conventional Dose-Rate Irradiation and Mechanistic Insights*”, we aim to resolve this long-standing debate by determining whether UHDR produces more or less H₂O₂, and elucidating the underlying mechanisms

As we mentioned earlier, radiation not only generates oxidizing species but also produces reducing species, such as e_{aq}⁻ and hydrogen radicals (H•). Between these two, the yield of e_{aq}⁻ is by several-fold higher than H•, making e_{aq}⁻ the primary reducing species¹³¹. e_{aq}⁻ is trapped in the surrounding network of hydrogen-bonded water molecules, and it remains inherently unstable and exhibits exceptionally strong reducing properties¹³²⁻¹³⁴. We hypothesize that FLASH alters the radiochemical kinetics, making the reducing e_{aq}⁻ play a more important role in radiochemical kinetics, leading to a lower H₂O₂ yield. The two main reasons why e_{aq}⁻ results in reduced H₂O₂ production under UHDR are:

1. **Enhanced Scavenging of •OH:** The e_{aq}⁻ reacts with •OH at a high rate, effectively reducing the availability of •OH, which is a precursor to H₂O₂. Under UHDR, this scavenging effect is further amplified due to the increased instantaneous radical concentration, leading to a shift in the competition between reactions that consume •OH.

-
2. **Diffusion-Limited Effects:** , the diffusion coefficients¹⁰⁹ of e_{aq^-} , OH^- and $\bullet OH$ are 4.9, 5.3, and 2.2×10^{-9} m²/s, which means that e_{aq^-} will benefit more from inter-tract effect of UHDR¹³⁵ due to the lower diffusion rate.

A more detailed explanation, along with a diagram illustrating these mechanisms, is provided in my published article and will not be repeated here. To test this hypothesis, I conducted experiments using e_{aq^-} scavengers, specifically N_2O and $NaNO_3$ ¹³⁶. The former is a gas that dissolves in water, with a saturation solubility of approximately 25 mM at 25°C and 1 atm, while the latter is a salt. Both compounds are commonly used as e_{aq^-} scavengers in radiation chemistry experiments, and they do not react with other ROS, such as the $\bullet OH$, precursor of H_2O_2 . If our hypothesis is correct, that UHDR produces less H_2O_2 due to the influence of e_{aq^-} , then the addition of these scavengers should eliminate the differences in the G-value of H_2O_2 between UHDR and CONV dose rates. This is precisely what we observed in our experiments, further supporting our proposed mechanism.

Many Monte Carlo simulation studies^{125-127,129,130} have predicted a trend opposite to our experimental findings and those of other studies^{74,110-112}, suggesting that UHDR results in a higher H_2O_2 yield than CONV. To explain this discrepancy, these studies propose that certain relatively long-lived radicals, such as $O_2^{\bullet-}$ and HO_2^{\bullet} , gradually accumulate in solution under the lower dose rate conditions of CONV, ultimately influencing H_2O_2 production. To test this hypothesis, we designed an experiment to verify its validity. We compared 3-spilled UHDR irradiation with 1-spilled UHDR irradiation, where each spill was separated by a 5-second interval. During 3-spilled UHDR irradiation, long-lived radicals in the water progressively accumulated with each spill, potentially affecting the $G(H_2O_2)$ of the third spill. If the Monte Carlo prediction were correct, we would expect $G(H_2O_2)$ in 3-spilled UHDR to be lower than that in 1-spilled UHDR, as the multi-spill irradiation more closely resembles the conditions of CONV. However, our experimental results did not fully support this hypothesis.

This experimental study primarily aimed to determine the dose-rate dependency of H_2O_2 production, which is crucial for a deeper understanding of radiochemical kinetics in FLASH. As discussed earlier, radiochemistry plays a significant role in radiation damage, and our research extends beyond this experimental work. Through theoretical simulations, we further explored the potential role of H_2O_2 in minibeam-RT, which has a similar effect to the FLASH-RT, providing additional insights into the radiochemical effects in these novel treatment modalities.

1.4 Radiochemical surrogate in Minibeam-RT

Recently, radiation oncologists have increasingly explored optimizing the spatial distribution of radiation doses to enhance treatment efficacy while minimizing toxicity. Preclinical and clinical studies have demonstrated improved local control rates using these methods, known as spatially fractionated radiotherapy (SFRT). Unlike conventional external radiation therapy, SFRT alternates high-dose regions and low-dose regions within the target area.

The origins of this approach trace back to 1909 in the era of two-dimensional radiotherapy when German radiobiologist Alban Köhler¹³⁷ first reported the use of GRID therapy to treat malignant tumors, effectively reducing skin toxicity. In certain palliative cases, this method also alleviated symptoms, improved response rates, and reduced side effects¹³⁸⁻¹⁴⁰. More recently, advancements in radiation physics and the development of synchrotron technology have paved the way for microbeam radiotherapy (MRT), a novel SFRT approach with beam widths typically in the range of tens of micrometer. Studies indicate that while normal tissues generally exhibit lower toxicity and better repair capacity after MRT, and poorly differentiated and immature tumors are unable to repair the damage as effectively^{141,142}. However, due to MRT's extremely narrow beam widths and high doses, implementing it with standard clinical radiotherapy equipment is highly challenging. To make this approach more feasible for clinical use, researchers have broadened the beam width, giving rise to the concept of minibeam radiotherapy (MBRT). MBRT represents a novel SFRT technique, characterized by beam widths in the millimeter or sub-millimeter range, as shown in Figure 5. Moreover, unlike Grid and Lattice radiotherapy, which are primarily used for palliative care, MBRT has shown curative potential in animal studies¹⁴³. In glioma-bearing rats, even a superior survival rate to standard radiotherapy has also been observed¹⁴⁴⁻¹⁴⁶.

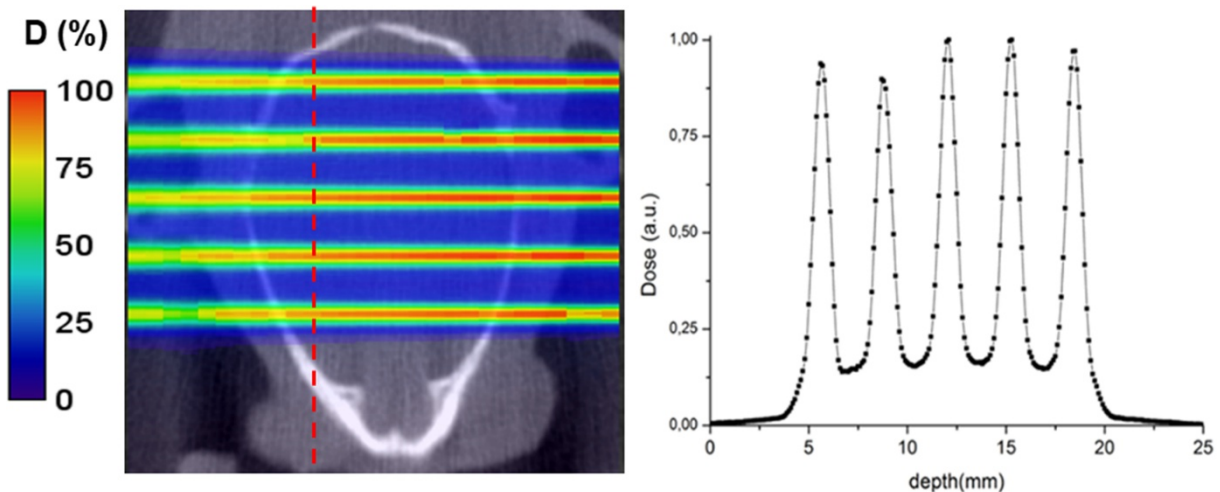


Figure 5. MBRT dose distribution. Left: 2D dose map in the rat head (coronal view). The red line marks the approximate position of the center of the tumor. Right: Corresponding lateral dose profile at the tumor position¹⁴⁶.

In general, similar to the FLASH effect, the minibeam effects also encompass two key aspects: (1) sparing normal tissue and (2) maintaining tumor control. Therefore, the appropriate application of MBRT can also widen the therapeutic window. Although the minibeam effect shares similarities with the FLASH effect and may even exhibit synergistic interactions, the two techniques should not be conflated.

Moreover, experimental findings suggest that MBRT is not a particularly robust approach. In certain scenarios, it can achieve tumor control comparable to BBRT at the same volumetric-averaged dose¹⁴⁷, while some studies have even reported inferior outcomes with MBRT¹⁴⁸. Because of the presence of low-dose regions, it is not hard to understand why MBRT can reduce the lesion of normal tissue. Animal experiments have found that even when there is an inter-fraction shift of beamlets, MBRT can still provide more protection to normal tissue than broad-beam radiotherapy (BBRT)^{149,150}. However, the underlying reason why MBRT can achieve tumor control despite the presence of underdosed valley regions within tumors remains unclear. According to conventional radiotherapy theories, these low-dose valleys should compromise local tumor control. Yet, experimental results contradict this expectation, indicating that current theoretical models do not fully explain MBRT's biological mechanisms. Moreover, unlike conventional radiotherapy, where treatment can typically be defined by a single parameter, such as the prescribed dose, MBRT involves multiple parameters to characterize the treatment: peak dose, valley dose, mean dose, peak width, and valley width. Additionally, several derived parameters are commonly used: 1) the peak-valley dose ratio (PVDR), the ratio of peak dose to valley dose; 2) the center-to-center distance (CTC), the sum of peak width and valley width. Each of these parameters only partially describes the minibeam dose distribution. Even if two treatments have the same CTC, their spatial dose distributions may differ significantly due to variations in peak and valley widths. So far, no single variable comprehensively captures all aspects of MBRT, making it challenging to perform direct comparisons across different MBRT studies. This complexity highlights the need for a standardized approach to characterizing MBRT dose distributions to better understand its unique radiobiological effects.

As we discussed before, ionizing radiation can cause DNA damage directly or cause water radiolysis first and then damage the DNA by consequent reactive oxygen species. The human body is roughly 60 % water by weight, so the indirect damage plays a vital role. Because dose is a physical parameter and it is hard to describe MBRT with simple dosimetric quantity, we propose to select a product from the chemical stage as the surrogate of dose.

A previous study¹⁵¹ has discussed the standard of a potential surrogate in the chemical stage: 1) it should be relatively stable to allow diffusion to reach the low-dose valley region; 2) its production and removal in the radiolysis process should reach a steady state; 3) it should have oxidizing capacity to trigger downstream biological effects. Therefore, as we mentioned before, hydrogen peroxide (H_2O_2) is a perfect candidate as a potential surrogate of dose. The previous study¹⁵¹ introduced a H_2O_2 diffusion model based on the convolution method. In this approach, a Gaussian function representing the diffusion of H_2O_2 over time was derived from Monte Carlo simulations and data fitting. This function was then used as a convolution kernel with the dose distribution, allowing the model to estimate the irradiation time required to achieve a certain uniformity of H_2O_2 distribution in pure water under different MBRT conditions. However, this model presents several limitations:

1. Accuracy of the Gaussian Function Parameters – The parameters of the Gaussian function, obtained through Monte Carlo simulations and data fitting, may not be the most accurate representation of the actual diffusion process. Since Monte Carlo codes for water radiolysis rely on an underlying diffusion

equation, it would be more rigorous to solve the diffusion problem analytically rather than relying on numerical fitting.

2. Mismatch Between H_2O_2 Uniformity and Physical Dose – The model primarily calculates the time required to achieve a certain uniformity in the H_2O_2 distribution. However, if H_2O_2 or another radiolysis product is to be used as a chemical indicator for MBRT, the concentration distribution, rather than uniformity, should be the chemical counterpart of the physical dose.
3. Oversimplification of Diffusion in Biological Tissues – The model assumes free diffusion of radicals in pure water, which does not accurately represent conditions in biological tissues. Unlike pure water, tissues consist of cells that actively metabolize and eliminate ROS. Therefore, a free diffusion model is insufficient for simulating the behavior of H_2O_2 in MBRT under physiological conditions.
4. Unrealistic Assumption of Instantaneous H_2O_2 Generation – The model assumes that all radiation instantaneously produces H_2O_2 throughout the entire tissue at the same time, with diffusion beginning from a uniform starting point. In reality, H_2O_2 is generated continuously during irradiation rather than appearing simultaneously. This oversimplification neglects the spatial and temporal dynamics of radiolysis product formation, making the model inconsistent with actual H_2O_2 production in MBRT.

These limitations highlight the need for a more sophisticated modeling approach that incorporates realistic tissue environments, cellular metabolism of ROS, and a more precise analytical framework for H_2O_2 diffusion dynamics in MBRT. To address these issues, we developed a new diffusion model that accounts for H_2O_2 removal. We propose that H_2O_2 can serve as a surrogate for dose, and by modeling its diffusion and elimination dynamics with the MBRT parameters used in previous animal studies and comparing the treatment outcome with our simulated H_2O_2 concentration in the valley region, we can gain insights into MBRT's ability to maintain tumor control despite a non-uniform dose distribution. This part of work is published in Medical Physics titled "*A theoretical study of H_2O_2 as the surrogate of dose in minibeam radiotherapy, with a diffusion model considering radical removal process*".

Overall, ROS play a crucial role in radiation-induced damage and radiotherapy, serving as key mediators of cellular responses to ionizing radiation. These ROS can cause oxidative stress, leading to DNA damage, lipid peroxidation, and protein oxidation, ultimately affecting cell survival and therapeutic outcomes. Our research focuses on radiochemistry, specifically the production of ROS in two emerging non-conventional dose delivery techniques: FLASH radiotherapy and MBRT. Among various ROS, we primarily investigate H_2O_2 , a relatively stable and long-lived species that is the end product of water radiolysis. Given its persistence and ability to diffuse across cellular compartments, H_2O_2 plays a significant role in modulating radiation-induced biological effects. By understanding its production and dynamics under FLASH and MBRT conditions, we aim to elucidate how these advanced irradiation modalities influence oxidative stress, DNA repair mechanisms, and normal tissue responses, ultimately contributing to the optimization of radiotherapy strategies.

2 PUBLICATIONS

Analysis of hydrogen peroxide production in pure water: Ultrahigh versus conventional dose-rate irradiation and mechanistic insights

Tengda Zhang^{1,2} | Christina Stengl^{3,4} | Larissa Derksen⁵ | Kristaps Palskis^{6,7} |
Konstantinos Koritsidis^{1,8} | Klemens Zink^{5,9,10} | Sebastian Adeberg^{9,10,11} |
Gerald Major^{12,13,14} | David Weishaar⁵ | Ulrike Theiß^{10,15} | Jing Jin^{16,17} |
Maria Francesca Spadea¹⁸ | Elpida Theodoridou^{1,8} | Jürgen Hesser^{2,19} |
Kilian-Simon Baumann^{5,9,10} | Joao Seco^{1,20}

¹Division of Biomedical Physics in Radiation Oncology, German Cancer Research Center, Heidelberg, Germany

²MIISM, Medical Faculty Mannheim, Heidelberg University, Mannheim, Germany

³Division of Medical Physics in Radiation Oncology, German Cancer Research Center, Heidelberg, Germany

⁴Medical Faculty Heidelberg, Heidelberg University, Heidelberg, Germany

⁵University of Applied Sciences, Institute of Medical Physics and Radiation Protection, Giessen, Germany

⁶CERN, Geneva, Switzerland

⁷Riga Technical University, Riga, Latvia

⁸Faculty of Physics, The Aristotle University of Thessaloniki, Thessaloniki, Greece

⁹Department of Radiotherapy and Radiation Oncology, Marburg University Hospital, Marburg, Germany

¹⁰Marburg Ion-Beam Therapy Center (MIT), Marburg, Germany

¹¹Universitäres Centrum für Tumorerkrankungen (UCT) Frankfurt - Marburg, Marburg, Germany

¹²Department of Radiation Oncology, Heidelberg University Hospital, Heidelberg, Germany

¹³Heidelberg Institute of Radiation Oncology (HIRO), Heidelberg, Germany

¹⁴National Center for Tumor Diseases (NCT), Heidelberg, Germany

¹⁵Department of Radiotherapy and Radiation Oncology, Philipps-University, Marburg, Germany

¹⁶State Key Laboratory of Molecular Oncology and Department of Radiation Oncology, National Cancer Center/National Clinical Research Center for Cancer/Cancer Hospital, Chinese Academy of Medical Sciences (CAMS) and Peking Union Medical College (PUMC), Beijing, China

¹⁷Department of Radiation Oncology, National Cancer Center/National Clinical Research Center for Cancer/Cancer Hospital & Shenzhen Hospital, CAMS and PUMC, Shenzhen, China

¹⁸Institute of Biomedical Engineering, Karlsruhe Institute of Technology (KIT), Karlsruhe, Germany

¹⁹Interdisciplinary Center for Scientific Computing (IWR), Central Institute for Computer Engineering (ZITI), CZS Heidelberg Center for Model-Based AI, Heidelberg University, Heidelberg, Germany

²⁰Department of Physics and Astronomy, Heidelberg University, Heidelberg, Germany

Correspondence

Kilian-Simon Baumann, University of Applied Sciences, Institute of Medical Physics and Radiation Protection, Giessen, Germany.
Email:
kilian-simon.baumann@staff.uni-marburg.de

Abstract

Background: Ultrahigh dose-rate radiation (UHDR) produces less hydrogen peroxide (H_2O_2) in pure water, as suggested by some experimental studies, and is used as an argument for the validity of the theory that FLASH spares the

This is an open access article under the terms of the [Creative Commons Attribution-NonCommercial-NoDerivs](https://creativecommons.org/licenses/by-nc-nd/4.0/) License, which permits use and distribution in any medium, provided the original work is properly cited, the use is non-commercial and no modifications or adaptations are made.

© 2024 The Author(s). *Medical Physics* published by Wiley Periodicals LLC on behalf of American Association of Physicists in Medicine.

Joao Seco, Division of Biomedical Physics in Radiation Oncology, German Cancer Research Center, Heidelberg, Germany. Email: j.seco@dkfz-heidelberg.de

Tengda Zhang, Christina Stengl, and Larissa Derksen are Co-shared first authors. Killian-Siman Baumann and Joao Seco are Co-shared senior authors.

Funding information

Federal Ministry of Education and Research, Grant/Award Number: 02NUK076A; Hessen State Ministry of Higher Education, Research, and the Arts (HMWK), Grant/Award Numbers: LOEWE/2/16/519/03/09.001(0001)/101, 13FH726IX6; Deutsche Krebshilfe (DKH), Grant/Award Numbers: 70115332, 70115445

normal tissue due to less reactive oxygen species (ROS) production. In contrast, most Monte Carlo simulation studies suggest the opposite.

Purpose: We aim to unveil the effect of UHDR on H_2O_2 production in pure water and its underlying mechanism, to serve as a benchmark for Monte Carlo simulation. We hypothesized that the reaction of solvated electrons (e_{aq}^-) removing hydroxyl radicals ($\cdot\text{OH}$), the precursor of H_2O_2 , is the reason why UHDR leads to a lower G-value (molecules/100 eV) for H_2O_2 ($G[\text{H}_2\text{O}_2]$), because: 1, the third-order reaction between e_{aq}^- and $\cdot\text{OH}$ is more sensitive to increased instantaneous ROS concentration by UHDR than a two-order reaction of $\cdot\text{OH}$ self-reaction producing H_2O_2 ; 2, e_{aq}^- has two times higher diffusion coefficient and higher reaction rate constant than that of $\cdot\text{OH}$, which means e_{aq}^- would dominate the competition for $\cdot\text{OH}$ and benefit more from the inter-track effect of UHDR. Meanwhile, we also experimentally verify the theory of long-lived radicals causing lower $G(\text{H}_2\text{O}_2)$ in conventional irradiation, which is mentioned in some simulation studies.

Methods and materials: H_2O_2 was measured by Amplex UltraRed assay. 430.1 MeV/u carbon ions (50 and 0.1 Gy/s), 9 MeV electrons (600 and 0.62 Gy/s), and 200 kV x-ray tube (10 and 0.1 Gy/s) were employed. For three kinds of water (real hypoxic: 1% O_2 ; hypoxic: 1% O_2 and 5% CO_2 ; and normoxic: 21% O_2), unbubbled and bubbled samples with N_2O , the scavenger of e_{aq}^- , were irradiated by carbon ions and electrons with conventional and UHDR at different absolute dose levels. Normoxic water dissolved with sodium nitrate (NaNO_3), another scavenger of e_{aq}^- , and bubbled with N_2O was irradiated by x-ray to verify the results of low-LET electron beam.

Results: UHDR leads to a lower $G(\text{H}_2\text{O}_2)$ than conventional irradiation. O_2 and CO_2 can both increase $G(\text{H}_2\text{O}_2)$. N_2O increases $G(\text{H}_2\text{O}_2)$ of both UHDR and conventional irradiation and eliminates the difference between them for carbon ions. However, N_2O decreases $G(\text{H}_2\text{O}_2)$ in electron conventional irradiation but increases $G(\text{H}_2\text{O}_2)$ in the case of UHDR, ending up with no dose-rate dependency of $G(\text{H}_2\text{O}_2)$. Three-spilled carbon UHDR does not have a lower $G(\text{H}_2\text{O}_2)$ than one-spilled UHDR. However, the electron beam shows a lower $G(\text{H}_2\text{O}_2)$ for three-spilled UHDR than for one-spilled UHDR. Normoxic water with N_2O or NaNO_3 can both eliminate the dose rate dependency of H_2O_2 production for x-ray.

Conclusions: UHDR has a lower $G(\text{H}_2\text{O}_2)$ than the conventional irradiation for both high LET carbon and low LET electron and x-ray beams. Both scavengers for e_{aq}^- , N_2O and NaNO_3 , eliminate the dose-rate dependency of $G(\text{H}_2\text{O}_2)$, which suggests e_{aq}^- is the reason for decreased $G(\text{H}_2\text{O}_2)$ for UHDR. Three-spilled UHDR versus one-spilled UHDR indicates that the assumption of residual radicals reducing $G(\text{H}_2\text{O}_2)$ of conventional irradiation may only be valid for low LET electron beam.

KEYWORDS

hydrogen peroxide, solvated electron, ultrahigh dose rate, water radiolysis

1 | INTRODUCTION

Ultra-high dose rate (UHDR) irradiation used in FLASH radiotherapy, is a novel technique that delivers a high dose of radiation in a very short time to achieve a dose rate higher than 40 Gy/s. Several preclinical studies^{1–3} have shown that FLASH radiotherapy can reduce normal tissue toxicity while maintaining tumor control, compared to conventional radiotherapy. This phenomenon, known as the FLASH effect, suggests

that FLASH radiotherapy can widen the therapeutic window and has the potential to further increase the prescription dose against tumors that are radioresistant to conventional radiotherapy.

However, the radiobiological mechanisms underlying the FLASH effect are not yet fully understood. Ionizing radiation can cause direct deoxyribonucleic acid (DNA) damage but also ionize or excite water molecules in the human body, which is a physical process that generates various reactive oxygen species (ROS). These

TABLE 1 Reactions in water radiolysis and their reaction rate constants.^{23,24,27}

Reaction no.	Reaction	Rate constant ($10^{10} \text{ M}^{-1} \text{ s}^{-1}$)	Reaction no.	Reaction	Rate constant ($10^{10} \text{ M}^{-1} \text{ s}^{-1}$)
1	$\cdot\text{OH} + \text{H}_2 \rightarrow \text{H}\cdot + \text{H}_2\text{O}$	0.0036	23	$\text{H}^+ + \text{HO}_2^- \rightarrow \text{H}_2\text{O}_2$	2
2	$\cdot\text{OH} + \text{H}_2\text{O}_2 \rightarrow \text{HO}_2\cdot + \text{H}_2\text{O}$	0.0033	24	$\text{H}_2\text{O}_2 \rightarrow \text{H}^+ + \text{HO}_2^-$	3.56×10^{-12}
3	$\cdot\text{OH} + \text{O}_2\cdot^- \rightarrow \text{O}_2 + \text{OH}^-$	0.9	25	$\text{HO}_2\cdot + \text{H}^+ \rightarrow \text{O}_2\cdot^-$	8×10^{-5}
4	$\text{H}\cdot + \text{O}_2 \rightarrow \text{HO}_2\cdot$	1.8	26	$\text{H}^+ + \text{OH}^- \rightarrow \text{H}_2\text{O}$	14.3
5	$\text{H}\cdot + \text{O}_2\cdot^- \rightarrow \text{HO}_2^-$	2	27	$\text{H}_2\text{O} \rightarrow \text{H}^+ + \text{OH}^-$	2.6×10^{-15}
6	$e_{\text{aq}}^- + \text{O}_2 \rightarrow \text{O}_2\cdot^-$	1.9	28	$\text{H}\cdot + \cdot\text{OH} \rightarrow \text{H}_2\text{O}$	2
7	$e_{\text{aq}}^- + \text{H}_2\text{O}_2 \rightarrow \cdot\text{OH} + \text{OH}^-$	1.2	29	$\text{H}\cdot + \text{H}\cdot \rightarrow \text{H}_2$	1
8	$e_{\text{aq}}^- + \text{O}_2\cdot^- \rightarrow \text{HO}_2^- + \text{OH}^-$	1.3	30	$\cdot\text{OH} + \text{OH}^- \rightarrow \text{O}\cdot^- + \text{H}_2\text{O}$	1.2
9	$e_{\text{aq}}^- + \text{H}^+ \rightarrow \text{H}\cdot$	2.2	31	$\text{O}\cdot^- + \text{H}_2\text{O} \rightarrow \cdot\text{OH} + \text{OH}^-$	0.00017
10	$e_{\text{aq}}^- + \text{H}_2\text{O} \rightarrow \text{H}\cdot + \text{OH}^-$	2×10^{-9}	32	$\cdot\text{OH} + \text{O}\cdot^- \rightarrow \text{HO}_2^-$	0.1
11	$e_{\text{aq}}^- + \text{HO}_2^- \rightarrow \text{O}\cdot^- + \text{OH}^-$	0.35	33	$\cdot\text{OH} + \text{O}_3\cdot^- \rightarrow \text{O}_2\cdot^- + \text{HO}_2\cdot$	0.85
12	$e_{\text{aq}}^- + \text{H}\cdot \rightarrow \text{H}_2 + \text{OH}^-$	2.5	34	$\text{O}\cdot^- + \text{O}_2 \rightarrow \text{O}_3\cdot^-$	0.3
13	$e_{\text{aq}}^- + e_{\text{aq}}^- \rightarrow \text{H}_2 + 2\text{OH}^-$	0.5	35	$\text{O}\cdot^- + \text{H}_2 \rightarrow \text{H}\cdot + \text{OH}^-$	0.008
14	$e_{\text{aq}}^- + \cdot\text{OH} \rightarrow \text{OH}^-$	3	36	$\text{O}\cdot^- + \text{H}_2\text{O}_2 \rightarrow \text{H}_2\text{O} + \text{O}_2\cdot^-$	0.02
15	$\cdot\text{OH} + \cdot\text{OH} \rightarrow \text{H}_2\text{O}_2$	0.55	37	$\cdot\text{OH} + \text{HO}_2^- \rightarrow \text{HO}_2\cdot + \text{OH}^-$	0.5
16	$\cdot\text{OH} + \text{HO}_2\cdot \rightarrow \text{H}_2\text{O} + \text{O}_2$	1.2	38	$\text{HO}_2^- + \text{O}\cdot^- \rightarrow \text{OH}^- + \text{O}_2\cdot^-$	0.08
17	$\text{H}\cdot + \text{HO}_2\cdot \rightarrow \text{H}_2\text{O}_2$	2	39	$\text{O}_3\cdot^- + \text{H}_2\text{O}_2 \rightarrow \text{O}_2\cdot^- + \text{O}_2 + \text{H}_2\text{O}$	0.00016
18	$\text{H}\cdot + \text{H}_2\text{O}_2 \rightarrow \text{H}_2\text{O} + \cdot\text{OH}$	0.009	40	$\text{O}_3\cdot^- + \text{HO}_2^- \rightarrow \text{O}_2\cdot^- + \text{O}_2 + \text{OH}^-$	8.9×10^{-5}
19	$\text{H}\cdot + \text{OH}^- \rightarrow e_{\text{aq}}^- + \text{H}_2\text{O}$	0.0021	41	$\text{O}_3\cdot^- \rightarrow \text{O}_2 + \text{O}\cdot^-$	3×10^{-8}
20	$\text{HO}_2\cdot + \text{O}_2\cdot^- \rightarrow \text{O}_2 + \text{HO}_2^-$	0.0089	42	$\text{O}_3\cdot^- + \text{H}_2 \rightarrow \text{O}_2 + \text{H}\cdot + \text{OH}^-$	2.5×10^{-5}
21	$\text{HO}_2\cdot + \text{HO}_2\cdot \rightarrow \text{H}_2\text{O}_2 + \text{O}_2$	0.0002	43	$\text{O}_2\cdot^- + \text{H}_2\text{O}_2 \rightarrow \cdot\text{OH} + \text{O}_2 + \text{OH}^-$	1.3×10^{-11}
22	$\text{OH}^- + \text{H}_2\text{O}_2 \rightarrow \text{HO}_2^- + \text{H}_2\text{O}$	0.0471	44	$\text{HO}_2\cdot + \text{H}_2\text{O}_2 \rightarrow \cdot\text{OH} + \text{O}_2$	5×10^{-11}

ROS react with each other because of free radical chain reactions, and they undergo diffuse transport simultaneously (shown in Table 1). This process, which lasts for about one microsecond, is called the inhomogeneous chemical reaction stage.⁴ After that, the ROS distribution becomes relatively homogeneous, and the chemical reactions continue. This period of time is called the homogeneous chemical stage. ROS damages various molecules in the cell, including DNA, and triggers the subsequent biological response process. Since 60% of the human body is composed of water,⁴ and since this radio-protective effect of UHDR has been observed in bacteria^{5,6} as well, radiochemistry may play a significant role in the FLASH mechanism. Hydrogen peroxide (H_2O_2) is an important end product in the water radiolysis process and is also a major source of cellular oxidative stress and DNA damage due to the Fenton reaction.^{7–10}

Previous studies have shown contradictory results regarding the dose-rate dependency of H_2O_2 production in pure water,^{11–20} and most of Monte Carlo simulation studies have shown the opposite to recent experimental measurements. So far, there is no consensus on whether UHDR increases or decreases H_2O_2 yield compared with conventional irradiation. In addition, in previous research on H_2O_2 production, the

hypoxic water samples did not contain carbon dioxide (CO_2) dissolved in the water. In contrast, there was 5% CO_2 in cell experiments to equilibrate the pH value of the medium. In addition to the dose-rate dependency, we also studied the role of CO_2 in the H_2O_2 yield.

Recent experimental^{11,13,14,16} results suggest that UHDR has a lower G-value (molecules/100 eV) for H_2O_2 ($G[\text{H}_2\text{O}_2]$) without an explanation. We hypothesize that the mechanism behind this is that solvated electrons (e_{aq}^-) eliminate hydroxyl radicals ($\cdot\text{OH}$), the precursor to H_2O_2 , reducing $G(\text{H}_2\text{O}_2)$. In the case of UHDR, this scavenging of $\cdot\text{OH}$ becomes more effective since (Figure 1):

I. The reaction between the e_{aq}^- and $\cdot\text{OH}$ (reaction [14] shown in Table 1) has the highest reaction rate constant in the water radiolysis process except for the background reaction (26).



The product of reaction (14) can also serve as the scavenger of $\cdot\text{OH}$.



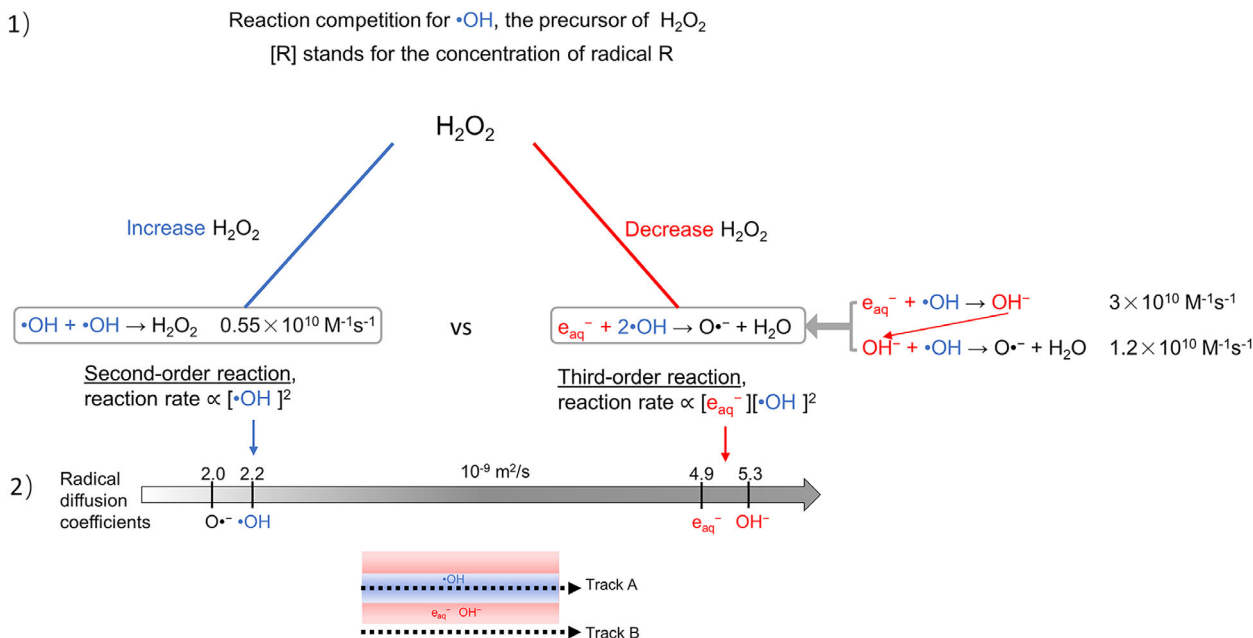
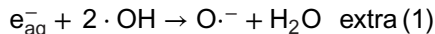
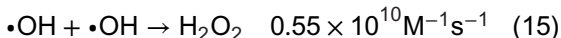


FIGURE 1 Two reasons why e_{aq}^- cause less H_2O_2 production in UHDR. (1), Third-order reaction is more sensitive to radical concentration change than second-order reaction, so the competition balance in conventional irradiation will shift toward the right side with UHDR increasing instantaneous radical concentration; (2), e_{aq}^- and OH^- have higher diffusion coefficients and higher reaction rate constants than $\cdot\text{OH}$, which means they would benefit more from the intertrack effect of UHDR, and remove $\cdot\text{OH}$. H_2O_2 , hydrogen peroxide; OH , hydroxyl radicals; UHDR, ultrahigh dose-rate radiation.

Therefore, we can combine reactions (14) and (30) into one reaction shown as the following:



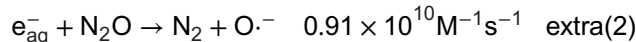
The main source of H_2O_2 is the recombination of $\cdot\text{OH}$ ^{12,21} which is the precursor to H_2O_2 , as shown in the reaction (15).



Evidently, there is a competition for $\cdot\text{OH}$ between reactions extra (1) and (15). Note that reaction (15) is a second-order reaction, while extra (1) is a third-order reaction. In conventional irradiation, these two reactions reach a competitive equilibrium. However, UHDR can increase the instantaneous radical concentration by several orders of magnitude in the same period of time, resulting in different enhancement of reaction rate because reaction extra (1), a third-order reaction, will benefit more from this concentration increase in the competition than reaction (15), a second-order reaction. The reaction rate for reaction extra (1) is $k_{\text{extra}(1)}[e_{\text{aq}}^-][\cdot\text{OH}]^2$ while the rate for reaction (15) is $k_{15}[\cdot\text{OH}]^2$, where $k_{\text{extra}(1)}$ and k_{15} stand for the reaction rate constant of each reaction and [radical] stands for the radical concentration. So, reaction extra (1) is more sensitive to concentration change than reaction (15). Hence, UHDR can shift the competition for $\cdot\text{OH}$ in conventional irradiation towards the reaction removing $\cdot\text{OH}$, and lead to less H_2O_2 production.

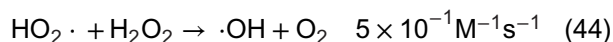
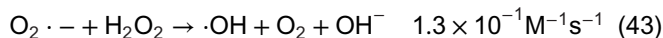
II. Since both reactions (14) and (30) have higher reaction rate constants than $\cdot\text{OH}$ self-reaction and the primary yield^{22,23} of e_{aq}^- is higher than the rest of radicals and molecules except for $\cdot\text{OH}$ and H^+ , e_{aq}^- will dominate the competition for $\cdot\text{OH}$. Also, the diffusion coefficients²⁴ of e_{aq}^- , OH^- and $\cdot\text{OH}$ are 4.9, 5.3, and $2.2 \times 10^{-9} \text{ m}^2/\text{s}$, which means that e_{aq}^- will benefit more from inter-track effect of UHDR²⁵ due to the higher diffusion rate.

To test the above hypothesis about e_{aq}^- , nitrous oxide (N_2O) gas, a solvate electron scavenger,²⁶ was used in our experiments. We expect to see that when e_{aq}^- is removed by N_2O , the H_2O_2 production has no difference in UHDR and conventional irradiation.



Most of the Monte Carlo simulations and analytical analysis^{12,15,17,19,20} have shown that $G(\text{H}_2\text{O}_2)$ increases with increasing dose rate, which is the opposite of recent experimental results.^{11,13,14,16} A model using molecular dynamics combined with Monte Carlo simulation suggests that UHDR produces less ROS, including H_2O_2 , although it does not specifically show a decrease in only H_2O_2 .¹⁸ One assumption of higher $G(\text{H}_2\text{O}_2)$ by UHDR is that higher instantaneous $\cdot\text{OH}$ concentration increases the possibility of $\cdot\text{OH}$ recombination (reaction [15] in Table 1).¹⁷ However, this assumption ignores that UHDR also increases the instantaneous concentration of e_{aq}^- , the scavenger of $\cdot\text{OH}$, which has a higher reaction rate constant and

higher diffusion coefficient than $\cdot\text{OH}$. Another explanation is that in conventional irradiation, the accumulation of relatively long-lived radicals in homogenous chemical stage, such as $\text{O}_2\cdot^-$ and $\text{HO}_2\cdot$, will affect the competition kinetics for the chemical species generated by the following pulses and remove H_2O_2 molecules,^{12,15,19} as shown in reactions (43) and (44) in Table 1.



To test this theory, we compared the H_2O_2 production of one-spilled UHDR and three-spilled UHDR. In three-spilled UHDR, each spill delivered the same dose as one-spilled UHDR, and there was at least a 5 s interval between each spill. In this way, the first UHDR spill would generate long-lifetime radicals that create the chemical environment described above to influence the chemical reactions of the radicals generated by the subsequent UHDR spills. So, we should observe that the $G(\text{H}_2\text{O}_2)$ of three-spilled UHDR is lower than that of one-spilled UHDR.

Previous studies^{11,13,14,16} have used electron or proton UHDR to study H_2O_2 production. In our experiment, in addition to an electron beam, we used a carbon ion beam for the first time to study H_2O_2 production. Carbon ions and electron beams can deliver the same volume-averaged dose, but their microscopic dose distributions are entirely different because of the relatively high linear energy transfer (LET) of the carbon beam compared with the electron beam, which also results in different spatial distributions of ROS. This difference could have an impact on the chemical kinetics.

In conclusion, four main topics will be discussed in the following:

1. To test the theory of solvated electrons leading to low H_2O_2 production in UHDR with scavengers.
2. To define the impact of CO_2 on H_2O_2 production.
3. To test the long-lived radical theory by one-spilled UHDR versus three-spilled UHDR.
4. To determine the difference between high-LET carbon ions and low-linear energy transfer (low-LET) sources.

2 | MATERIALS AND METHODS

2.1 | Sample preparation

Water samples were prepared with varying oxygen concentrations by keeping Milli-Q water in a hypoxic chamber for at least 24 h:

1. hypoxic water with 1% O_2 and 5% CO_2 ,

2. real hypoxic water with 1% O_2 and 0.1% CO_2 (0% CO_2 is not allowed due to the hypoxic chamber setting limits),
3. and normoxic water with 21% O_2 .

Therefore, three different water samples were used in the experiments. Different water samples were filled into 200 μL Eppendorf polymerase chain reaction (PCR) tubes, which are free of metal components (metal atoms would decompose H_2O_2 molecules), ensuring that there were no bubbles in the tubes. Pure N_2O gas (Gutttroff, Germany) was used to bubble water at room temperature for 40 min in a gas-washing bottle to prepare the samples with N_2O . Sodium Nitrate (NaNO_3), another e_{aq}^- scavenger, was dissolved in normoxic water with the final concentrations of 25 and 250 μM and used in x-ray experiments. The pH values of water samples before and after dissolving N_2O and NaNO_3 were recorded using the Mettler Toledo pH Probe (Germany).

2.2 | Experimental setup and irradiation

2.2.1 | Carbon ion beam

A carbon ion beam was produced by synchrotron in the Marburg Ion-Beam Therapy Center. In our experiment, carbon ions were accelerated to 430.1 MeV/u, with a frequency of 6.74 MHz. 7.0×10^8 particles were injected into the synchrotron, which is the maximum number of particles that can be injected in one spill. The extraction time was 150 ms because after that, the extraction efficiency of the carbon ions decreased sharply (Figure 2a). Therefore, to achieve 40 Gy/s, at least 6 Gy was required within 150 ms. Even though the dose distribution in the sample is inhomogeneous, we expect the dose rate of each irradiated part of the sample to be higher than 40 Gy/s, so we do not need to worry about the ROS diffusion between the UHDR region and the non-UHDR region leading to any problem. The inner diameter of the 200 μL tube is approximately 5.5 mm. As shown in the dose profile in Figure 2b, the diameter of the region with a dose higher than 6 Gy is approximately 6 mm. Therefore, the samples were placed parallel to the beam direction with a 3D-printed sample holder (see Figure 2c) to ensure that the UHDR region covered the entire sample. An EBT-3 film was placed in front of each sample to record the received dose. One-spilled UHDR irradiation can deliver a volume-averaged dose of approximately 7 Gy, with a volume-averaged dose rate of approximately 50 Gy/s. Based on the dose measured from the one-spilled UHDR, conventional dose-rate irradiation (0.1 Gy/s) was adjusted to deliver a comparable dose. Three kinds of water samples with and without N_2O were irradiated under UHDR and conventional dose-rate conditions.

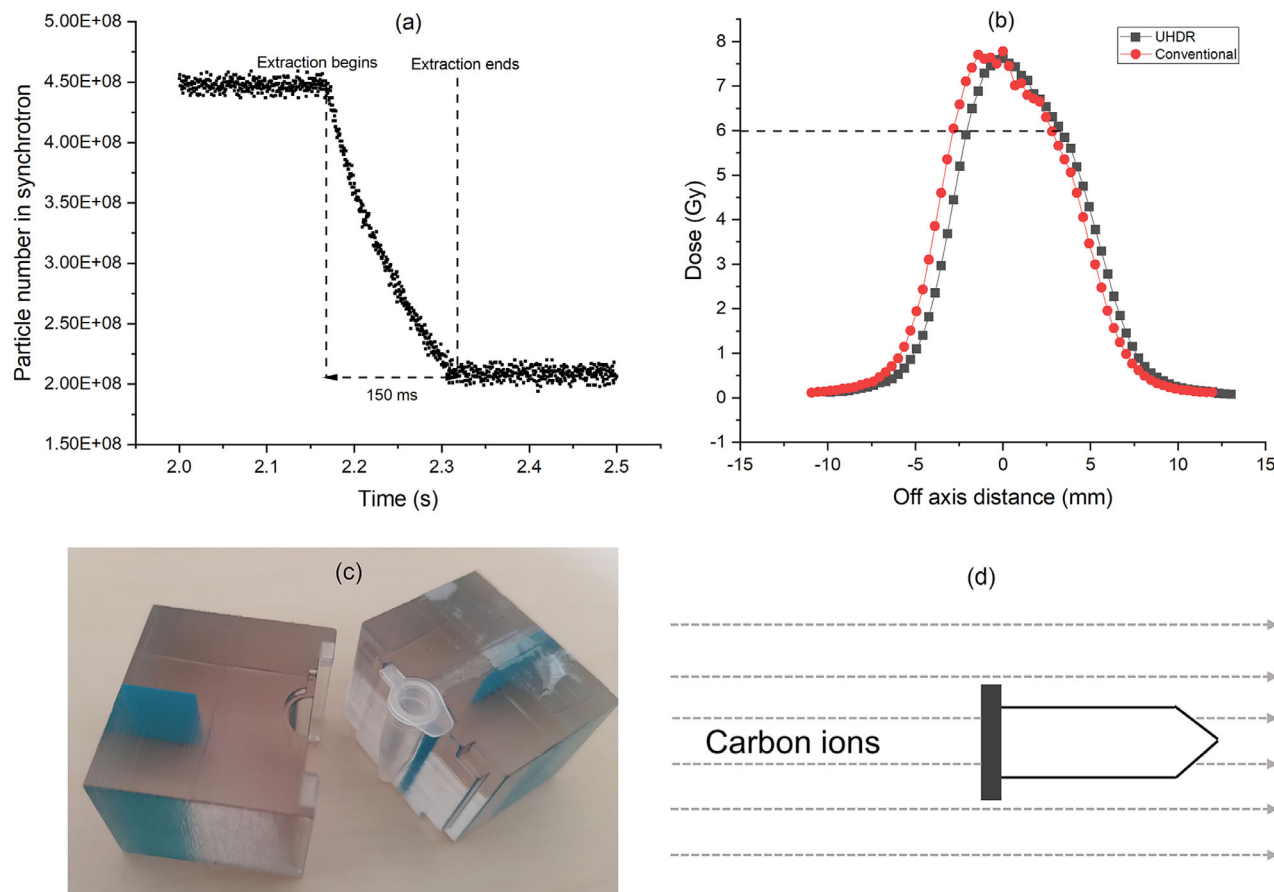


FIGURE 2 The irradiation setup used in carbon ion experiments. (a) The carbon ions extraction for UHDR lasting for 150 ms. (b) Exemplary dose profiles using carbon ions with UHDR and conventional dose rates. (c) The 3D-printed sample holder used to provide enough lateral scattering dose. (d) Sample tubes were placed horizontally. UHDR, ultrahigh dose-rate radiation.

For the comparison of the $G(\text{H}_2\text{O}_2)$ for one-spilled UHDR and three-spilled UHDR, the synchrotron requires at least 5 s of particle refilling time between two spills. We can assume that the first spill UHDR generates long-lifetime radicals that can affect the following chemical kinetics. In this experiment, only samples without N_2O were used.

2.2.2 | Electron beam

A 9 MeV electron source generated by a Mobetron unit (IntraOp Medical, Sunnyvale, CA, USA) with a field size of 6 cm was used in the experiment. The dose rate achieved for UHDR was 600 and 0.62 Gy/s for conventional irradiation. Dosimetry was performed using a FlashDiamond Detector T60025 (PTW, Freiburg, Germany). Mobetron can deliver a pulsed beam up to 3.6 μs pulse width with a pulse repetition frequency up to 120 Hz. Four-pulsed irradiation can achieve approximately 20 Gy within around 33.2 ms. To be consistent with the terminology of the carbon ion experiment, one-spilled UHDR consists of four pulses. The sample holder and experimental setup are shown in Figure 3. The irra-

diation schedule for the electron beam was the same as that for the carbon ions.

2.2.3 | x-Ray irradiation

As shown in Figure 4, MultiRad 225 (Precision, USA) irradiator was used to produce x-ray with dose rates of 0.1 and 10 Gy/s in the experiments, which is below the commonly recognized dose-rate threshold of 40 Gy/s for FLASH. The filter was removed to increase the dose rate. To further increase the dose rate, samples were placed close to the source by an elevatable rack. The voltage of the x-ray tube was set at 200 kV, and the current intensity was 17.8 mA. The irradiation dose for each sample is around 30 Gy.

2.3 | H_2O_2 measurement and statistics

CO_2 dissolves in water and forms carbonic acid, which lowers the pH of water. When the samples were saturated in a hypoxic chamber containing 5% CO_2 , the pH decreased to around 6.4. Therefore, in the pH range of 6

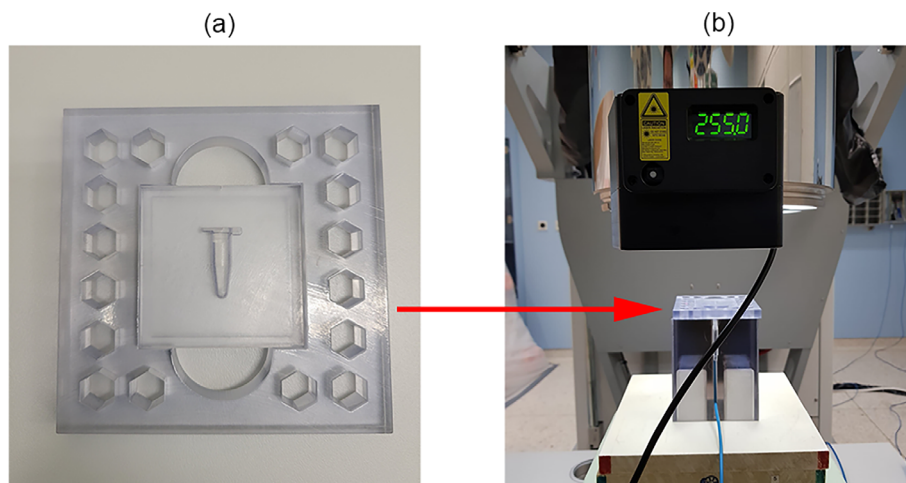


FIGURE 3 The experimental setup used in the 9 MeV electron irradiation. (a) The 3D-printed sample hold used in the experiments. (b) The electron facility, Mobetron, provides UHDR and conventional irradiation. UHDR, ultrahigh dose-rate radiation.

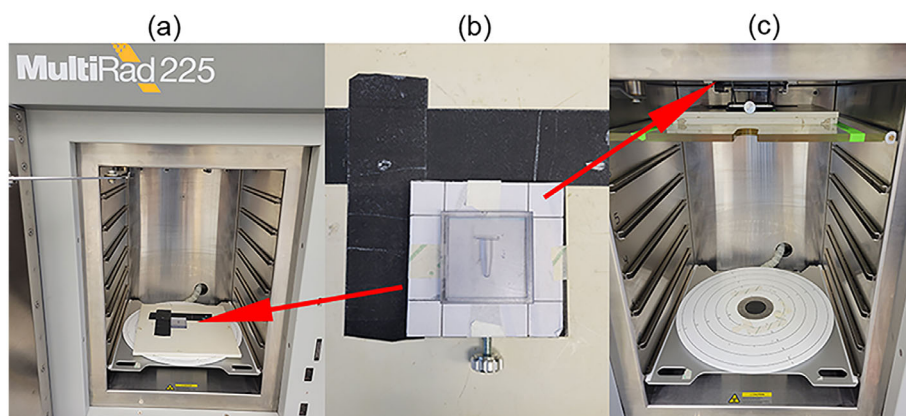


FIGURE 4 The experimental setup used in x-ray irradiation. (a) 0.1 Gy/s was achieved by positioning the samples on the lowest shelf. (b) The sample holder used in the experiment. (c) The samples were positioned on an elevatable rack to achieve around 10 Gy/s.

to 8, a pH-independent Amplex UltraRed assay (Thermo Fisher Scientific Inc, America), instead of the Amplex Red assay, was used to determine the concentration of H_2O_2 generated by irradiation. 50 μL of each irradiated sample was pipetted up and mixed with 50 μL of 100 μM Amplex UltraRed solution in a 96-well plate. The plate was covered with aluminum foil and incubated at room temperature for 40 min. Then, a plate reader was used to measure fluorescence intensity (excitation: 530 nm, emission: 590 nm). The system was fully calibrated by a series of fixed concentration of H_2O_2 solution. There were three samples for each oxygen condition, and the measurements of each sample were performed in triplicate. The Independent Samples *t*-test was used to assess the significance between the two groups. $P < 0.05$ was considered statistically significant.

3 | RESULTS

At extremely low pH values, the $G(\text{H}_2\text{O}_2)$ can dramatically increase. Therefore, the pH values of different

water samples were monitored. Pure water has a pH of around 7. N_2O gas does not change the pH value. However, water samples dissolved 250 μM NaNO_3 and equilibrated at 5% CO_2 , respectively, have pH values of 6.7 and 6.4.

3.1 | $G(\text{H}_2\text{O}_2)$ of the different kinds of water samples irradiated by carbon ions

As shown in Figure 5a, although hypoxic sample contains only 1% oxygen, similar to real hypoxic sample, it has the highest $G(\text{H}_2\text{O}_2)$ among three kinds of water because of the presence of 5% CO_2 . Normoxic samples have a lower $G(\text{H}_2\text{O}_2)$ than hypoxic samples but higher than real hypoxic samples. It can be concluded that oxygen can increase the H_2O_2 production (real hypoxic vs. normoxic sample), and CO_2 can also markedly boost the H_2O_2 production (real hypoxic vs. hypoxic sample). Because the solubility of CO_2 is approximately 30 times higher than that of oxygen, hypoxic water equilibrated with 5% CO_2 has a higher H_2O_2 yield even than

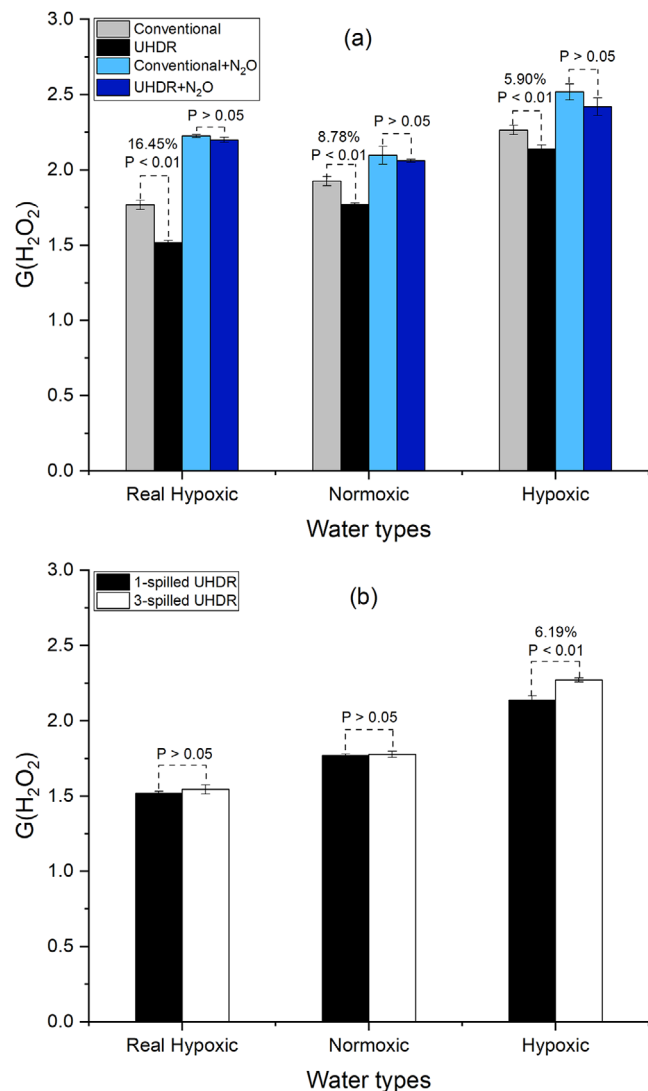


FIGURE 5 Radiolytic H_2O_2 yields of water samples with various O_2 and CO_2 concentrations irradiated by 430.1 MeV/u carbon ions. (a) The comparison of UHDR with conventional dose-rate irradiation for samples with and without N_2O . (b) $G(\text{H}_2\text{O}_2)$ of one-spilled UHDR and three-spilled UHDR. CO_2 , carbon dioxide; H_2O_2 , hydrogen peroxide; N_2O , nitrous oxide; OH, hydroxyl radicals; UHDR, ultrahigh dose-rate radiation.

normoxic water samples with 21% oxygen (hypoxic vs. normoxic sample).

Furthermore, as we can see in Figure 5a, UHDR always produces less H_2O_2 than conventional irradiation for any type of sample without N_2O , which is similar to recent experimental results mentioned before. However, the difference between UHDR and conventional irradiation became statistically insignificant ($P > 0.05$) for all three kinds of samples with N_2O . Note that N_2O increases both $G(\text{H}_2\text{O}_2)$ of UHDR and conventional irradiation, while this effect is more pronounced for UHDR, resulting in eliminating the dose-rate dependency of H_2O_2 production.

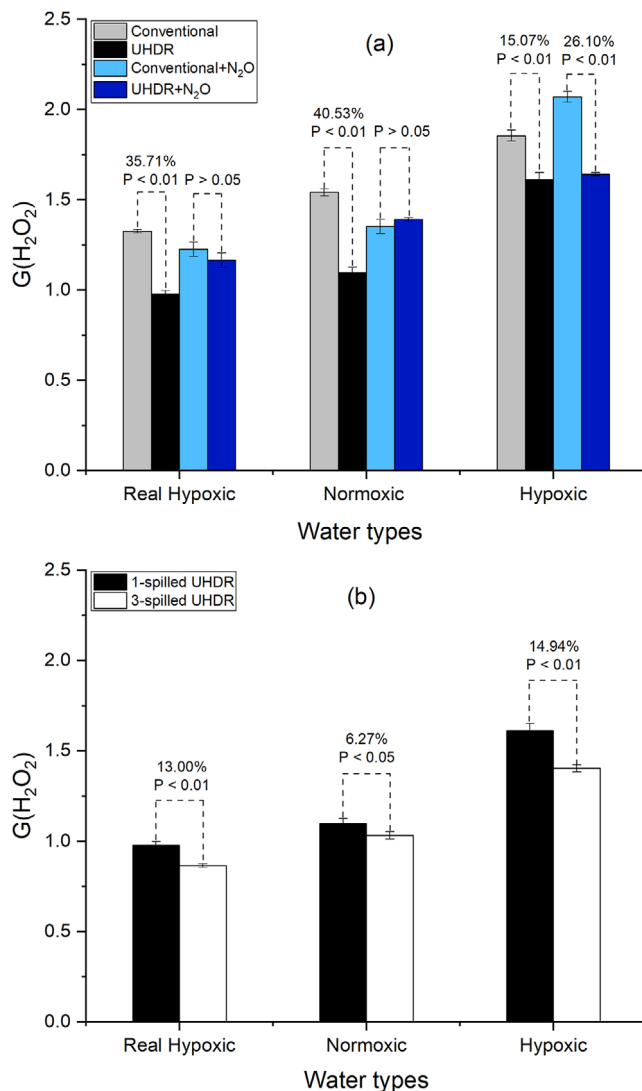


FIGURE 6 Radiolytic H_2O_2 yields of water samples with various O_2 and CO_2 concentrations irradiated by 9 MeV electron beam. (a) The comparison of UHDR with conventional dose-rate irradiation for samples with and without N_2O . (b) $G(\text{H}_2\text{O}_2)$ of one-spilled UHDR and three-spilled UHDR. CO_2 , carbon dioxide; H_2O_2 , hydrogen peroxide; N_2O , nitrous oxide; OH, hydroxyl radicals; UHDR, ultrahigh dose-rate radiation.

In the end, as shown in Figure 5b, there is no significant difference in $G(\text{H}_2\text{O}_2)$ between one-spilled UHDR and one-spilled UHDR for both real hypoxic and normoxic water conditions, despite one-spilled UHDR appearing to produce slightly more H_2O_2 . However, for hypoxic water with CO_2 , one-spilled UHDR has a higher $G(\text{H}_2\text{O}_2)$ than one-spilled UHDR does.

3.2 | $G(\text{H}_2\text{O}_2)$ of various kinds of water samples irradiated by electron source

As shown in Figure 6a, like carbon ions, electron UHDR also has a lower $G(\text{H}_2\text{O}_2)$ than conventional irradiation,

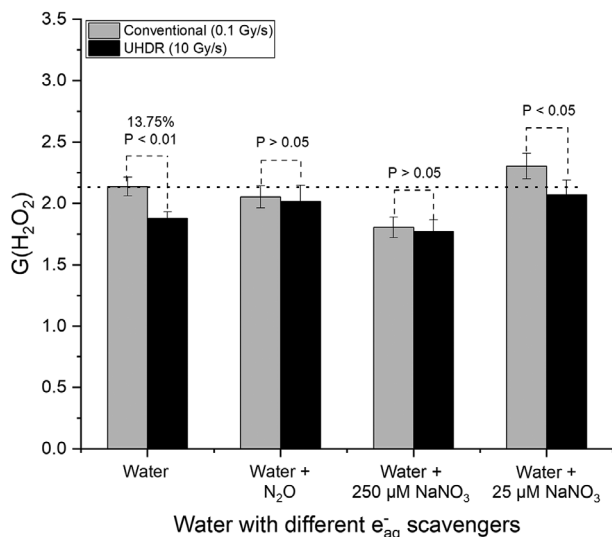


FIGURE 7 Radiolytic H₂O₂ yields of normoxic water samples with different e_{aq}⁻ scavengers, irradiated by 200 kV x-ray. $P < 0.05$ means statistically significant. H₂O₂, hydrogen peroxide.

but the difference between UHDR and conventional is even more significant. For real hypoxic water, the difference in $G(\text{H}_2\text{O}_2)$ can be up to around 35%, and for normoxic water, it can reach around 40%. For the three different water samples, we can still observe that $G(\text{H}_2\text{O}_2)_{\text{hypoxic}} > G(\text{H}_2\text{O}_2)_{\text{normoxic}} > G(\text{H}_2\text{O}_2)_{\text{real hypoxic}}$, which is consistent with the $G(\text{H}_2\text{O}_2)$ of carbon ions. For carbon ions, N₂O increases both UHDR and conventional $G(\text{H}_2\text{O}_2)$ while eliminating the discrepancy between them. However, we can see that N₂O has a different impact on H₂O₂ production with electron beams than with carbon ions. (1), for real hypoxic and normoxic samples, N₂O can also eliminate the difference in H₂O₂ yield between electron UHDR and electron conventional irradiation by decreasing the $G(\text{H}_2\text{O}_2)$ of conventional irradiation, which is opposite to carbon ions but increasing the $G(\text{H}_2\text{O}_2)$ of UHDR, resulting in the previous 35.71% and 40.53% difference between UHDR and conventional becoming statistically insignificant. (2), for hypoxic water with CO₂, on the contrary, N₂O increases the $G(\text{H}_2\text{O}_2)$ of conventional irradiation but does not have the same effect on the UHDR. The results of the comparison of $G(\text{H}_2\text{O}_2)$ between one-spilled UHDR and three-spilled UHDR are shown in Figure 6b. Unlike carbon ion, the $G(\text{H}_2\text{O}_2)$ of three-spilled electron UHDR is always lower than that of one-spilled UHDR, and this effect is the same on three kinds of water samples.

3.3 | G(H₂O₂) of water with different scavengers irradiated by kV x-ray

There is around 13.75% difference in $G(\text{H}_2\text{O}_2)$ of pure water between x-ray conventional and UHDR, as shown in Figure 7. N₂O can also eliminate the dose-rate depen-

dency of $G(\text{H}_2\text{O}_2)$ in x-ray experiments, just like in carbon ion and electron beam experiments. However, compared to carbon ions, x-ray is also a low LET source, just like the electron beam, and its $G(\text{H}_2\text{O}_2)$ is similarly modified by N₂O as the previous electron beam, that is, N₂O only increases the $G(\text{H}_2\text{O}_2)$ of UHDR. Another e_{aq}⁻ scavenger, NaNO₃, can also eliminate or narrow the difference in H₂O₂ production between conventional and UHDR, resulting in no statistical significance ($P > 0.05$). Note that 250 μM NaNO₃ decreases $G(\text{H}_2\text{O}_2)$ of the conventional dose rate irradiation, but 25 μM NaNO₃ increases the G-value.

4 | DISCUSSION

About 60 years ago,^{28–30} when researchers discovered that ultra-high dose rate mode could improve the survival fraction of cells after irradiation, radical-radical recombination was a popular hypothesis proposed in the early days.³¹ Due to the higher instantaneous radical concentration produced by ultra-high dose rate irradiation, the probability of radical recombination increases, resulting in less ROS production, thereby improving the survival fraction of cells after irradiation. H₂O₂, as a relatively stable ROS, is an important end product of water radiolysis. Recent studies^{11,13,14,16} have shown that compared with conventional irradiation, UHDR generates less H₂O₂ without providing an explanation. However, except for one study,¹⁸ most Monte Carlo simulations and analytical analyses have shown the opposite.^{12,15,17,19,20} Therefore, even with regard to the question of H₂O₂ production in UHDR, there is no consensus in the academic community. An assumption from studies claiming UHDR increases $G(\text{H}_2\text{O}_2)$ is that higher instantaneous •OH concentration favors •OH recombination (reaction [15] in Table 1), resulting in more H₂O₂.¹⁷ Another assumption claiming UHDR produces more H₂O₂ attributes this to some long-lived radicals, such as O₂•⁻ and HO₂•, accumulating in conventional irradiation and affecting the subsequent chemical reaction kinetics, resulting in conventional irradiation producing less H₂O₂ than UHDR.^{12,15,19}

From our results, we can see that for the three water samples with different O₂ and CO₂ concentrations, whether using an electron beam with a uniform microscopic dose distribution or a carbon ion beam with a very heterogeneous microscopic dose distribution, UHDR always decreases $G(\text{H}_2\text{O}_2)$ compared to conventional irradiation. •OH is the precursor of H₂O₂, and previous studies^{12,21} have indicated that reaction (15) in Table 1 is the primary source of H₂O₂ produced by water radiolysis. As we described before, e_{aq}⁻ is the main scavenger of •OH because of its high rate constant and primary yield, and we showed the effects of e_{aq}⁻ on removing •OH is the reason behind less H₂O₂ production of UHDR.

4.1 | Solvated electron scavengers removing the dose-rate dependency of H_2O_2 production

4.1.1 | Carbon ion source

To verify our theory about e_{aq}^- mentioned before, we introduced N_2O in the experiment. N_2O can react with e_{aq}^- and generate chemically stable N_2 and oxygen atomic anion ($\text{O}\cdot^-$). $\text{O}\cdot^-$ can react with many kinds of radicals, including $\cdot\text{OH}$, but the reaction rate constant is only $0.1 \times 10^{10} \text{ M}^{-1}\text{s}^{-1}$, as shown in reaction (32) in Table 1, which is lower than that of the reaction between e_{aq}^- and $\cdot\text{OH}$ ($3 \times 10^{10} \text{ M}^{-1}\text{s}^{-1}$), and even lower than that of the self-reaction of $\cdot\text{OH}$ producing H_2O_2 ($0.55 \times 10^{10} \text{ M}^{-1}\text{s}^{-1}$). In the experiment with carbon ion beam, eliminating e_{aq}^- by N_2O reduces the scavenging capacity for $\cdot\text{OH}$, so we can see that the $G(\text{H}_2\text{O}_2)$ increase under both UHDR and conventional irradiation. Meanwhile, N_2O eliminates the third-order reaction extra (1), so the competition balance in conventional will not shift toward removing $\cdot\text{OH}$ when UHDR increases the instantaneous radical concentration; thus, there is no dose-rate dependency of $G(\text{H}_2\text{O}_2)$ for carbon-ion irradiation as shown in Figure 5a. Another experiment³² conducted in 1968 also supports our e_{aq}^- theory. In that experiment, researchers found out dose-rate independence of $G(\text{H}_2\text{O}_2)$ when they irradiated HClO_4 water solution with a $\text{pH} = 0.46$. In an extreme acid environment, all e_{aq}^- can be eliminated by H^+ (reaction [9] in Table 1) with an even higher rate constant than N_2O .

4.1.2 | Electron source

For real hypoxic and normoxic water with the electron beam, although N_2O still eliminates the difference in H_2O_2 production between UHDR and conventional irradiation, similar to its effect in the carbon ion experiment, it decreases the $G(\text{H}_2\text{O}_2)$ of conventional irradiation (Figure 6a). We can see this phenomenon because of the relatively high concentration of N_2O compared to ROS concentration.²¹ N_2O , as a scavenger of e_{aq}^- , can also react with e_{pre}^- (the precursor of e_{aq}^-) and molecular cation of water (H_2O^+) if the relative concentration is high enough. The dissociative recombination reaction of e_{pre}^- with H_2O^+ is one of two sources of $\cdot\text{OH}$. Therefore, a relatively high concentration of N_2O leads to lower $\cdot\text{OH}$ production. That study has shown that with increasing concentration of scavenger of e_{aq}^- , $G(\text{H}_2\text{O}_2)$ increases at the beginning and then decreases at high scavenger concentration (Figure 7 in that paper).²¹ In our experiment, we dissolved N_2O in water by bubbling the gas. It was hard to control the accurate scavenger concentration, so we chose to saturate N_2O to maintain the same experiment conditions each time. The reason why we see that N_2O still increases the $G(\text{H}_2\text{O}_2)$

of conventional irradiation of carbon ion beam is that the relatively high LET of carbon ions leads to the microscopic dose distribution being very heterogeneous. Although the volume-averaged dose is only a few Gy, the microscopic dose near the carbon ion tracks can exceed 1000 Gy,^{33,34} so the local dose rate is significantly higher than 50 Gy/s used in carbon ion UHDR. Most of the ROS produced by carbon ions are distributed in the vicinity of carbon ion tracks, so the local ROS concentration is very high even under conventional irradiation, unlike the ROS produced by electron beam, which are uniformly distributed. This highly concentrated local ROS distribution makes N_2O concentration relatively low, resulting in the increased $G(\text{H}_2\text{O}_2)$ under conventional irradiation of carbon ion beam.

However, N_2O does not eliminate the dose-rate dependency of H_2O_2 production for hypoxic samples (1% O_2 , 5% CO_2) with the electron source, as shown in Figure 6a. Apparently, this is because of the extra 5% CO_2 . As for why we cannot see similar results using a carbon ion source, we believe it also relates to the relative concentration of CO_2 and N_2O compared to local ROS concentration. High local ROS concentration produced by high LET carbon ions minimizes the influence of CO_2 and N_2O . We will discuss the role of CO_2 in the following section.

In addition to e_{aq}^- , $\text{H}\cdot$ also serves as the scavenger for $\cdot\text{OH}$ with a relatively high reaction rate constant ($2.5 \times 10^{10} \text{ M}^{-1}\text{s}^{-1}$). The reason why we mainly focus on e_{aq}^- is that the primary yield of $\text{H}\cdot$ is only one-fifth of e_{aq}^- .²³ The “scavenging capacity” mentioned before is equal to the reaction rate constant \times concentration,¹⁵ so the concentration of the reactant is as important as the reaction rate constant in determining the scavenging capacity. Therefore, $\text{H}\cdot$ is not as important as e_{aq}^- , but we admit that $\text{H}\cdot$ also has an impact on H_2O_2 production.

4.1.3 | x-Ray source

As discussed above, the $G(\text{H}_2\text{O}_2)$ of the water sample with e_{aq}^- scavenger depends on the relative scavenger concentration. With x-Ray source, we could also see the similar results shown in Figure 7. x-Ray, like the electron beam, is classified as low-LET radiation, characterized by a uniform spatial dose distribution, resulting in low local ROS concentrations. In contrast, the relative concentration of N_2O is higher, so even though it scavenges e_{aq}^- , it does not increase $G(\text{H}_2\text{O}_2)$. However, due to the removal of e_{aq}^- by N_2O , the dose rate dependency of $G(\text{H}_2\text{O}_2)$ is also eliminated. In our x-ray experiments, we used another scavenger of e_{aq}^- , NaNO_3 , which can also eliminate the dose rate dependency of $G(\text{H}_2\text{O}_2)$. We observed that 250 μM NaNO_3 not only eliminated the difference in H_2O_2 production between UHDR and conventional irradiation but also reduced the $G(\text{H}_2\text{O}_2)$ at conventional irradiation. Conversely, 25 μM NaNO_3

increased both UHDR and conventional $G(\text{H}_2\text{O}_2)$. However, because the concentration is not high enough, and its reaction rate constant with solvated electron is $0.97 \times 10^{10} \text{ M}^{-1}\text{s}^{-1}$, its scavenging capacity is not high enough to eliminate the dose rate dependency.

The previous study,²¹ along with our results in Figure 7 regarding different NaNO_3 concentrations, clearly demonstrate that the effect of the scavenger on $G(\text{H}_2\text{O}_2)$ depends on the relative concentration to ROS, which determines whether $G(\text{H}_2\text{O}_2)$ increases or decreases. Notably, NaNO_3 has a reaction rate constant with the precursor of e_{aq}^- that is at least an order of magnitude higher than that of N_2O ,²¹ but similar rate constant with e_{aq}^- , which means NaNO_3 tends to remove the precursor, compared to N_2O , easily leading to a lower $G(\text{H}_2\text{O}_2)$. Both compounds, serving as e_{aq}^- scavengers, eliminate the dose rate dependency of H_2O_2 production, strongly supporting our hypothesis.

4.2 | One-spilled UHDR versus three-spilled UHDR

Previous studies,^{12,17,20} especially Monte Carlo simulations, suggested that UHDR should increase the $G(\text{H}_2\text{O}_2)$, and explained that some radicals, such as $\text{O}_2^{\bullet-}$ and HO_2^{\bullet} , would persist for a much longer time in conventional irradiation than other radicals and affect the chemical reaction kinetics of the free radicals produced by subsequent irradiation, thereby reducing the production of H_2O_2 . This effect is insignificant for UHDR irradiation because UHDR delivers all dose in a very short time, so the $G(\text{H}_2\text{O}_2)$ of UHDR is higher than that of conventional irradiation. This theory seems reasonable to some extent, but it ignores the fact that the concentration of those residual long-lived radicals in the homogeneous chemical stage is very low, as shown in their own Monte Carlo studies. To verify this hypothesis, we designed an experiment of one-spilled UHDR versus three-spilled UHDR. In three-spilled UHDR irradiation, there is at least a 5 s interval between each spill, and the first spill produces many long-lived radicals that affect the chemical kinetics of the following two spills, just like conventional irradiation. If the hypothesis is true, we should see that the $G(\text{H}_2\text{O}_2)$ of three-spilled UHDR is lower than that of one-spilled UHDR. However, as shown in Figures 5b and 6b, the $G(\text{H}_2\text{O}_2)$ of three-spilled UHDR is lower than that of one-spilled UHDR in the experiment using electron beam, but we do not see the same situation with the carbon ions. One possible reason is the different spatial distribution of radicals produced by carbon ions and electrons. Although those long-lived radicals have been found to survive for hours after irradiation, their concentration becomes very low after 1 microsec of irradiation,^{12,35} which is the start of the homogeneous chemical stage. The radicals produced by carbon ion beams are highly

concentrated in the vicinity of the carbon ion tracks. The local concentration of the newly produced free radicals is several orders of magnitude higher than that of the previous residual free radicals, so the concentration of residual radicals is not high enough to affect the chemical kinetics of the radicals produced by subsequent carbon ion beams. The radical spatial distribution produced by the electron beam is homogeneous, and the local radical concentration is low. Therefore, residual radicals affecting subsequent chemical reactions only occur in low-LET beams like electron beams.

Another reason is that a high LET carbon ion beam can produce O_2 in tracks because of multiple ionization,^{7,8} and another study also suggested that carbon ions can generate highly oxygenated conditions in the tumor environment.³⁶ O_2 can increase H_2O_2 production so that it can counteract those long-lived radicals.

As for the reason why three-spilled carbon ion UHDR has a higher $G(\text{H}_2\text{O}_2)$ than one-spilled carbon ion UHDR for hypoxic water (1% O_2 and 5% CO_2), we will discuss the effect of CO_2 in the next section.

4.3 | The role of CO_2 in water radiolysis

Our experiment has shown that O_2 can increase H_2O_2 production. Studies on ROS production and radiosensitivity often only consider the role of O_2 and ignore CO_2 . Because the role of CO_2 in the cell culture environment is often only assumed to maintain physiological pH levels. According to Henry's law constants,³⁷ the solubility of CO_2 is around 26 times that of O_2 under the same conditions, and metabolically active tissues consume more O_2 and produce more CO_2 . If we want to study the role of ROS production in UHDR, CO_2 should not be ignored. Our experiments have shown that the hypoxic sample containing CO_2 has the highest $G(\text{H}_2\text{O}_2)$ among the three kinds of water samples, no matter for carbon ions or electron beam. As mentioned before, the pH value of water equilibrated with 5% CO_2 drops to around 6.4, and the acid chemical environment favors H^{\bullet} , which is the scavenger for $\bullet\text{OH}$. Although previous experimental results indicated that lower pH increased $G(\text{H}_2\text{O}_2)$,³² $G(\text{H}_2\text{O}_2)$ is stable in pH from 8 to 5. CO_2 radiolysis produces CO and O_2 , and both of them can serve as a scavenger for e_{aq}^- . Previous study³⁸ has shown that the G-value of O_2 produced by CO_2 radiolysis is 2.24 for 1.5 MeV protons at 27°C and 0.4 atm pressure. Therefore, increased $G(\text{H}_2\text{O}_2)$ of water containing CO_2 might originate from O_2 production. In addition, CO_2 can directly react with e_{aq}^- (rate constant = $0.77 \times 10^{10} \text{ M}^{-1}\text{s}^{-1}$),³⁹ and the reaction product, CO_2^- , can interact with various radicals and molecules, such as $\bullet\text{OH}$ and N_2O .⁴⁰ The detailed reason needs further investigation, and it would benefit

Monte Carlo radiochemical studies since CO_2 has been ignored in Monte Carlo codes.

We have discussed why, for real hypoxic water and normoxic water, the $G(\text{H}_2\text{O}_2)$ of three-spilled carbon ion UHDR is the same as that of three-spilled UHDR, unlike the experimental results with the electron beam. However, for hypoxic water, the $G(\text{H}_2\text{O}_2)$ of three-spilled carbon ion UHDR is higher than that of one-spilled UHDR. The only difference between hypoxic water and real hypoxic water is 5% CO_2 , so this phenomenon is caused by CO_2 . The possible reason is similar to CO_2 increasing the $G(\text{H}_2\text{O}_2)$: the first spill of carbon ion FLASH beam causes the CO_2 radiolysis to produce more O_2 in the environment, thereby increasing the $G(\text{H}_2\text{O}_2)$ of the subsequent spills, or the product of the reaction of CO_2 with e_{aq}^- , CO_2^- , participates in the subsequent reactions.

5 | LIMITATIONS

In our experiments, we bubbled water with pure N_2O gas for at least 40 min at room temperature. The main problem is we do not know the accurate N_2O concentration in each sample. First, we have to assume that N_2O molecules diffuse homogeneously in the bottle of water after 40 min of bubbling. Second, for real hypoxic water after bubbling N_2O , we brought the bottle of water back into the hypoxic chamber to fill water samples in 200 μL Eppendorf tubes. Therefore, the temperature change from room temperature to 37°C in the hypoxic chamber may have an impact on the N_2O concentration in the water. Besides, bubbling N_2O gas might influence the concentrations of other gases in the water. However, the conclusion is not affected since the comparison between UHDR, and conventional irradiation was done by the samples with the same solute gases. In future research, it would be beneficial to accurately measure the N_2O concentration in each sample and to test a range of different N_2O concentrations in the experiment. When considering these results in relation to the FLASH effect, one must be aware that these investigations were carried out in pure water, not in a biological system. Due to the existence of various antioxidant enzymes in living cells, radiochemistry might not be the same. What we found in water radiolysis needs to be investigated further with biologically relevant samples, such as an in-vitro study, to determine its significance in FLASH radiotherapy.

6 | CONCLUSION

For water samples with different O_2 and CO_2 concentrations (real hypoxic, normoxic, and hypoxic water), compared with conventional irradiation, UHDR always reduces the H_2O_2 production, regardless of whether

high-LET or low-LET beams are used. O_2 and CO_2 can both increase H_2O_2 production, and CO_2 has a much higher solubility than O_2 , which should not be ignored. The scavengers of e_{aq}^- , such as N_2O and NaNO_3 , can narrow the difference in H_2O_2 production between UHDR and conventional irradiation, making it statistically insignificant, which suggests that UHDR produces less H_2O_2 because e_{aq}^- scavenging $\cdot\text{OH}$, the precursor of H_2O_2 , benefits more from the instantaneous radical concentration increase than the $\cdot\text{OH}$ self-reaction. The long-lived radical theory from previous Monte Carlo simulation studies that suggested that UHDR should produce more H_2O_2 cannot explain the results of the carbon ion UHDR experiment, indicating that this hypothesis cannot be the reason for the difference in H_2O_2 production between UHDR and conventional irradiation.

AUTHOR CONTRIBUTIONS

Conceptualization: Tengda Zhang. *Experimental methodology:* Tengda Zhang, Joao Seco and Kilian-Simon Baumann. *Investigation and methodology:* Tengda Zhang, Christina Stengl, Larissa Derksen, Kilian-Simon Baumann, Gerald Major, Kristaps Palskis, David Weishaar, Ulrike Theiß and Konstantinos Koritsidis. *Software:* Tengda Zhang, Christina Stengl, Larissa Derksen, Kilian-Simon Baumann, Kristaps Palskis and Konstantinos Koritsidis. *Formal analysis:* Tengda Zhang, Larissa Derksen, Kristaps Palskis and Konstantinos Koritsidis. *Data curation:* Tengda Zhang, Christina Stengl, Larissa Derksen, Kilian-Simon Baumann, Gerald Major, Ulrike Theiß, Kristaps Palskis and Konstantinos Koritsidis. *Visualization:* Tengda Zhang and Larissa Derksen. *Consultation:* Joao Seco, Kilian-Simon Baumann, Jürgen Hesser, Klemens Zink, Sebastian Adeberg, Jing Jin and Ulrike Theiß. *Supervision:* Joao Seco, Kilian-Simon Baumann, Jürgen Hesser, Klemens Zink, Sebastian Adeberg and Jing Jin. *Writing—original draft preparation:* Tengda Zhang. *Writing—review and editing:* Tengda Zhang, Christina Stengl, Larissa Derksen, Klemens Zink, Sebastian Adeberg, Gerald Major, Maria Francesca Spadea, Jing Jin, Jürgen Hesser, Kilian-Simon Baumann and Joao Seco. *Funding acquisition:* Joao Seco, Kilian-Simon Baumann, Klemens Zink and Sebastian Adeberg. All authors have read and agreed to the published version of the manuscript.

ACKNOWLEDGMENTS

The authors thank the MIT accelerator team for the beam settings, and the Preclinical Trial Unit at the DKFZ for their assistance with the x-ray irradiation. The project was partially supported by the Federal Ministry of Education and Research within the scope of the grant 'Biological and physical optimization of particle beams: radiation protection for the patient' (PARTITUR, grant number 02NUK076A). This study was partially funded by the

Hessen State Ministry of Higher Education, Research, and the Arts (HMWK) via the LOEWE Research Cluster “ADMIT”, grant LOEWE/2/16/519/03/09.001(0001)/101. The experiments at MIT were supported by the Hessian state government. Larissa Derksen was supported by the Federal Ministry of Education and Research within the scope of the grant ‘Physikalische Modellierung für die individualisierte Partikel-Strahlentherapie und Magnetresonanztomographie’ (MiPS, Grant Number 13FH726IX6). Deutsche Krebshilfe (DKH) Grant with fördernummern 70115332, 70115445, and entitled “Dosisleistungsabhängige Ande-rung des Sauerstoffpartialdrucks während FLASH-Bestrahlung und deren Einfluss auf die strahlenbi-ologische Wirkung in Zebrafisch Embryonen”.

Open access funding enabled and organized by Projekt DEAL.

CONFLICT OF INTEREST STATEMENT

The authors declare no conflicts of interest.

REFERENCES

- Favaudon V, Caplier L, Monceau V, et al. Ultrahigh dose-rate FLASH irradiation increases the differential response between normal and tumor tissue in mice. *Sci Transl Med*. 2014;6(245):245ra93-245ra93.
- Rohrer Bley C, Wolf F, Goncalves Jorge P, et al. Dose- and volume-limiting late toxicity of FLASH radiotherapy in cats with squamous cell carcinoma of the nasal planum and in mini pigs. *Clin Cancer Res*. 2022;28(17):3814-3823.
- Vozenin MC, De Fornel P, Petersson K, et al. The advantage of FLASH radiotherapy confirmed in mini-pig and cat-cancer patients. *Clin Cancer Res*. 2019;25(1):35-42.
- Le Caër S. Water radiolysis: influence of oxide surfaces on H₂ production under ionizing radiation. *Water*. 2011;3(1):235-253.
- Weiss H. An equation for predicting the surviving fraction of cells irradiated with single pulses delivered at ultra-high dose rates. *Radiat Res*. 1972;50(2):441-452.
- Weiss H, Epp E, Heslin J, Ling C, Santomaso A. Oxygen depletion in cells irradiated at ultra-high dose-rates and at conventional dose-rates. *Int J Radiat Biol Relat Stud Phys Chem Med*. 1974;26(1):17-29.
- Dahm-Daphi J, Sass C, Alberti W. Comparison of biological effects of DNA damage induced by ionizing radiation and hydrogen peroxide in CHO cells. *Int J Radiat Biol*. 2000;76(1):67-75.
- Gülden M, Jess A, Kammann J, Maser E, Seibert H. Cytotoxic potency of H₂O₂ in cell cultures: impact of cell concentration and exposure time. *Free Radic Biol Med*. 2010;49(8):1298-1305.
- Park WH. Hydrogen peroxide inhibits the growth of lung cancer cells via the induction of cell death and G₁-phase arrest. *Oncol Rep*. 2018;40(3):1787-1794.
- Ogawa Y. Paradigm shift in radiation biology/radiation oncology—exploitation of the “H₂O₂ effect” for radiotherapy using low-LET (linear energy transfer) radiation such as x-rays and high-energy electrons. *Cancers*. 2016;8(3):28.
- Montay-Gruel P, Acharya MM, Petersson K, et al. Long-term neurocognitive benefits of FLASH radiotherapy driven by reduced reactive oxygen species. *Proc Natl Acad Sci*. 2019;116(22):10943-10951.
- D-Kondo JN, Garcia-Garcia OR, LaVerne JA, et al. An integrated Monte Carlo track-structure simulation framework for modeling inter and intra-track effects on homogenous chemistry. *Phys Med Biol*. 2023;68(12):125008.
- Kacem H, Psoroulas S, Boivin G, et al. Comparing radiolytic production of H₂O₂ and development of zebrafish embryos after ultra high dose rate exposure with electron and transmission proton beams. *Radiother Oncol*. 2022;175:197-202.
- Thomas W, Sunnerberg J, Reed M, et al. Proton and electron ultrahigh-dose-rate isodose irradiations produce differences in reactive oxygen species yields. *Int J Radiat Oncol Biol Phys*. 2024;118(1):262-267.
- Wardman P. Radiotherapy using high-intensity pulsed radiation beams (FLASH): a radiation-chemical perspective. *Radiat Res*. 2020;194(6):607-617.
- Sunnerberg JP, Zhang R, Gladstone DJ, Swartz HM, Gui J, Pogue BW. Mean dose rate in ultra-high dose rate electron irradiation is a significant predictor for O₂ consumption and H₂O₂ yield. *Phys Med Biol*. 2023;68(16):165014.
- Derksen L, Flatten V, Engenhardt-Cabillic R, Zink K, Baumann K-S. A method to implement inter-track interactions in Monte Carlo simulations with TOPAS-nBio and their influence on simulated radical yields following water radiolysis. *Phys Med Biol*. 2023;68:135017.
- Abolfath R, Grosshans D, Mohan R. Oxygen depletion in FLASH ultra-high-dose-rate radiotherapy: a molecular dynamics simulation. *Med Phys*. 2020;47(12):6551-6561.
- Wardman P. Mechanisms of the ‘FLASH’ effect: radiation chemistry should not be ignored in developing models. *Radiother Oncol*. 2023;184:109673.
- Lai Y, Jia X, Chi Y. Modeling the effect of oxygen on the chemical stage of water radiolysis using GPU-based microscopic Monte Carlo simulations, with an application in FLASH radiotherapy. *Phys Med Biol*. 2021;66(2):025004.
- Hiroki A, Pimblott SM, LaVerne JA. Hydrogen peroxide production in the radiolysis of water with high radical scavenger concentrations. *J Phys Chem A*. 2002;106(40):9352-9358.
- Boscolo D, Kramer M, Durante M, Fuss MC, Scifoni E. TRAX-CHEM: a pre-chemical and chemical stage extension of the particle track structure code TRAX in water targets. *Chem Phys Lett*. 2018;698:11-18.
- Boyd A, Carver M, Dixon R. Computed and experimental product concentrations in the radiolysis of water. *Radiat Phys Chem*. 1980;15(2-3):177-185.
- Plante I. A review of simulation codes and approaches for radiation chemistry. *Phys Med Biol*. 2021;66(3):03TR02.
- Baikalov A, Abolfath R, Schüler E, Mohan R, Wilkens JJ, Bartzsch S. Intertrack interaction at ultra-high dose rates and its role in the FLASH effect. *Front Phys*. 2023;11:1215422.
- Renault JP, Pommeret S. Seeing the solvated electron in action: first-principles molecular dynamics of NO₃⁻ and N₂O reduction. *Radiat Phys Chem*. 2022;190:109810.
- Frongillo Y, Goulet T, Fraser MJ, Cobut V, Patau JP, Jay-Gerin J-P. Monte Carlo simulation of fast electron and proton tracks in liquid water—II. nonhomogeneous chemistry. *Radiat Phys Chem*. 1998;51(3):245-254.
- Town CD. Radiobiology. Effect of high dose rates on survival of mammalian cells. *Nature*. 1967;215(5103):847-848.
- Epp ER, Weiss H, Santomaso A. The oxygen effect in bacterial cells irradiated with high-intensity pulsed electrons. *Radiat Res*. 1968;34(2):320-325.
- Berry RJ, Hall EJ, Forster DW, Storr TH, Goodman MJ. Survival of mammalian cells exposed to x rays at ultra-high dose-rates. *Brit J Radiol*. 1969;42(494):102-107.
- Limoli CL, Vozenin M-C. Reinventing radiobiology in the light of FLASH radiotherapy. *Annu Rev Cancer Biol*. 2023;7:1-21.
- Sehested K, Rasmussen OL, Fricke H. Rate constants of OH with HO₂, O₂⁻, and H₂O₂⁺ from hydrogen peroxide formation in pulse-irradiated oxygenated water. *J Phys Chem*. 1968;72(2):626-631.

33. Wang H, Vassiliev ON. Radial dose distributions from carbon ions of therapeutic energies calculated with Geant4-DNA. *Phys Med Biol*. 2017;62(10):N219-N227.
34. Tian Z, Jiang SB, Jia X. Accelerated Monte Carlo simulation on the chemical stage in water radiolysis using GPU. *Phys Med Biol*. 2017;62(8):3081-3096.
35. Pastina B, LaVerne JA. Effect of molecular hydrogen on hydrogen peroxide in water radiolysis. *J Phys Chem A*. 2001;105(40):9316-9322.
36. Zakaria AM, Colangelo NW, Meesungnoen J, Azzam EI, Plourde M-É, Jay-Gerin J-P. Ultra-high dose-rate, pulsed (FLASH) radiotherapy with carbon ions: generation of early, transient, highly oxygenated conditions in the tumor environment. *Radiat Res*. 2020;194(6):587-593.
37. Burkholder J, Sander S, Abbatt J, et al. Chemical kinetics and photochemical data for use in atmospheric studies; evaluation number 19. 2020. <https://jpldataeval.jpl.nasa.gov>
38. Kummeler R, Leffert C, Im K, Piccirelli R, Kevan L, Willis C. A numerical model of carbon dioxide radiolysis. *J Phys Chem*. 1977;81(25):2451-2463.
39. Buxton GV, Greenstock CL, Helman WP, Ross AB. Critical review of rate constants for reactions of hydrated electrons, hydrogen atoms and hydroxyl radicals ($\cdot\text{OH}/\cdot\text{O}^-$) in aqueous solution. *J Phys Chem Ref Data*. 1988;17(2):513-886.
40. Neta P, Huie RE, Ross AB. Rate constants for reactions of inorganic radicals in aqueous solution. *J Phys Chem Ref Data*. 1988;17(3):1027-1284.

How to cite this article: Zhang T, Stengl C, Derksen L, et al. Analysis of hydrogen peroxide production in pure water: Ultrahigh versus conventional dose-rate irradiation and mechanistic insights. *Med Phys*. 2024;51:7439–7452.
<https://doi.org/10.1002/mp.17335>

A theoretical study of H_2O_2 as the surrogate of dose in minibeam radiotherapy, with a diffusion model considering radical removal process

Tengda Zhang^{1,2} | Daniel García-Calderón^{1,3} | Miguel Molina-Hernández^{1,4,5} |
Joana Leitão^{1,4,5} | Jürgen Hesser² | Joao Seco^{1,3}

¹Division of Biomedical Physics in Radiation Oncology, German Cancer Research Center, Heidelberg, Germany

²Medical Faculty Mannheim, Heidelberg University, Mannheim, Germany

³Department of Physics and Astronomy, Heidelberg University, Heidelberg, Germany

⁴Laboratory of Instrumentation and Experimental Particle Physics (LIP), Lisbon, Portugal

⁵Instituto Superior Técnico, Universidade de Lisboa, Lisbon, Portugal

Correspondence

Joao Seco, Division of Biomedical Physics in Radiation Oncology, German Cancer Research Center, Heidelberg D-69120, Germany.
Email: j.seco@dkfz-heidelberg.de

Funding information

Deutscher Akademischer Austauschdienst (DAAD), Grant/Award Number: 57450037

Abstract

Background: Minibeam radiation therapy (MBRT) is an innovative dose delivery method with the potential to spare normal tissue while achieving similar tumor control as conventional radiotherapy. However, it is difficult to use a single dose parameter, such as mean dose, to compare different patterns of MBRT due to the spatially fractionated radiation. Also, the mechanism leading to the biological effects is still unknown.

Purpose: This study aims to demonstrate that the hydrogen peroxide (H_2O_2) distribution could serve as a surrogate of dose distribution when comparing different patterns of MBRT.

Methods: A free diffusion model (FDM) for H_2O_2 developed with Fick's second law was compared with a previously published model based on Monte Carlo & convolution method. Since cells form separate compartments that can eliminate H_2O_2 radicals diffusing inside the cell, a term describing the elimination was introduced into the equation. The FDM and the diffusion model considering removal (DMCR) were compared by simulating various dose rate irradiation schemes and uniform irradiation. Finally, the DMCR was compared with previous microbeam and minibeam animal experiments.

Results: Compared with a previous Monte Carlo & Convolution method, this analytical method provides more accurate results. Furthermore, the new model shows H_2O_2 concentration distribution instead of the time to achieve a certain H_2O_2 uniformity. The comparison between FDM and DMCR showed that H_2O_2 distribution from FDM varied with dose rate irradiation, while DMCR had consistent results. For uniform irradiation, FDM resulted in a Gaussian distribution, while the H_2O_2 distribution from DMCR was close to the dose distribution. The animal studies' evaluation showed a correlation between the H_2O_2 concentration in the valley region and treatment outcomes.

Conclusion: DMCR is a more realistic model for H_2O_2 simulation than the FDM. In addition, the H_2O_2 distribution can be a good surrogate of dose distribution when the minibeam effect could be observed.

KEYWORDS

diffusion model, hydrogen peroxide, minibeam radiation therapy, spatial fractionation

This is an open access article under the terms of the [Creative Commons Attribution](https://creativecommons.org/licenses/by/4.0/) License, which permits use, distribution and reproduction in any medium, provided the original work is properly cited.

© 2023 The Authors. *Medical Physics* published by Wiley Periodicals LLC on behalf of American Association of Physicists in Medicine.

1 | INTRODUCTION

Minibeam and microbeam radiotherapy are spatially fractionated dose delivery approaches of high-dose areas (peaks) alternating with low-dose areas (valleys). To facilitate the following discussion, minibeam radiotherapy (MBRT) is used to represent both spatially fractionated methods. It has been demonstrated that MBRT can widen the therapeutic window in animal experiments. In glioma-bearing rats, even a superior survival rate to standard radiotherapy has also been observed.^{1–3} Minibeam effects include two aspects: (1) sparing the normal tissue and (2) maintaining tumor control. Because of the presence of low-dose regions, it is not hard to understand why MBRT can reduce the lesion of normal tissue. Animal experiments have found that even when there is an inter-fraction shift of beamlets, MBRT can still provide more protection to normal tissue than broad-beam radiotherapy (BBRT).^{4,5} However, the reason MBRT can achieve tumor control when there are underdosed valley regions within tumors is still unknown. Unlike standard radiotherapy in which a treatment can be defined by one parameter, such as the prescribed dose, in MBRT several parameters are used to describe the treatments: peak dose, valley dose, mean dose, peak width, and valley width. Additionally, some other parameters are defined: (1) the peak-valley dose ratio (PVDR), the ratio of peak dose to valley dose; and (2) the center-to-center distance (CTC), the sum of peak width and valley width. Each can only partially represent the minibeam pattern. Even if two treatments have the same CTC, the pattern could be very different due to different peak widths and valley widths. So far, there is not a single variable encompassing all aspects of MBRT. Therefore, it is hard to perform comparisons between different MBRT studies.

Ionizing radiation can cause DNA damage directly or cause water radiolysis first and then damage the DNA by consequent reactive oxygen species (ROS). The human body is roughly 60% water by weight, so water radiolysis plays a vital role in radiation injury. Typically, these radiolytic events occur in three main stages⁶: the physical stage, the physicochemical stage, and the chemical stage, which can last for 10^{-6} s. Because dose is a physical parameter and it is hard to describe MBRT with simple dosimetric quantity, we go further to select a product from the chemical stage as the surrogate of dose.

A previous study⁷ has provided detailed reasons for choosing hydrogen peroxide (H_2O_2) as a potential surrogate of dose, and introduced a H_2O_2 diffusion model based on the convolution method. A Gaussian function representing the H_2O_2 diffusion process over time was obtained through Monte Carlo simulation and data fitting. Then, this Gaussian function was used as a kernel to convolve with the dose distribution. Eventually,

this model could give the irradiation time needed to achieve a certain uniformity of H_2O_2 distribution with different MBRT on pure water. However, there are several problems with this model. First, the arguments of the Gaussian function obtained through Monte Carlo simulation and data fitting could be more accurate. There is always an equation of diffusion model used as the base of Monte Carlo codes that can simulate water radiolysis. If this problem can be solved analytically, it is unnecessary for Monte Carlo simulation and data fitting. Second, this model can only compute the time to achieve a certain uniformity of H_2O_2 distribution. However, the uniformity is not the chemical counterpart of the physical dose if we want to replace the dose with a radiolysis product as an indicator for MBRT. The concentration distribution should be the corresponding quantity to the physical dose. Finally, this model can only simulate radicals' free diffusion in water. As organic tissues consist of cells rather than pure water, and cells can eliminate ROS, a free diffusion model is not enough to simulate MBRT.

To tackle the problems described above, we developed a new diffusion model considering H_2O_2 removal. We proposed that H_2O_2 can be used as a surrogate of dose and therefore modeling the diffusion of H_2O_2 could give some insight into the ability of MBRT to maintain tumor control with a non-uniform dose distribution.

2 | METHODS

2.1 | New H_2O_2 free diffusion model and comparison with the previous convolution-based model

2.1.1 | New H_2O_2 -free diffusion model

Fick's second law describing how diffusion causes the concentration to change with respect to time was used to build the free diffusion model (FDM):

$$\frac{\partial \phi}{\partial t} = D \frac{\partial^2 \phi}{\partial x^2} + \phi_{source} \quad (1)$$

D in Equation 1 is the diffusion coefficient of H_2O_2 in water at room temperature equal to 2.3×10^{-9} m²/s based on a previous report.⁸ ϕ represents the concentration and t is time. Since the dose distribution of each beamlet is uniform, so we can use a one-dimensional model to represent the minibeam pattern. x in the equation is the spatial coordinate. ϕ_{source} in the right hand of the equation is the source term which represents the H_2O_2 distribution generated by each pulse of irradiation.

The time between physical interaction of radiation with medium to the end of the non-homogeneous chemical stage is only 10^{-6} s.^{6,9} Although the H_2O_2 molecules

are generated and diffuse simultaneously in water during this period, it is reasonable to assume there is no diffusion before the end of the stage because of this short time. The FDM assumes dose will be delivered pulse by pulse, with a constant dose per pulse, which means ϕ_{source} is a constant. The Crank-Nicolson method was used to solve the above partial differential equation. We used the inter-pulse time of the beam as the time step of our simulation. The smaller the inter-step used, the smaller the difference between a continuous and discrete approach (smaller errors). To define the best inter-pulse time, we compared three different time steps: 0.01, 0.1, and 1 s. The 1 s time step simulation had a difference of around 5% compared to the 0.1 s time step simulation, and between the 0.1 s time step and the 0.01 s time step simulation, the difference was less than 1%. So, 0.01 s was chosen as the time step in our simulation, and 10 μm was chosen as the spatial step.

The initial H_2O_2 distribution generated by each pulse should be the numerical conversion from the dose distribution, described as follows:

$$\text{H}_2\text{O}_2 \text{ concentration} = \frac{\text{Dose} \times \text{Volume} \times \text{Density} \times G - \text{value}}{N_a \times \text{Volume}} \quad (2)$$

Where N_a stands for the Avogadro constant ($6.02 \times 10^{23}/\text{mol}$), density refers to the density of water (a constant of 10^3 kg/m^3), and the g -value represents how many species are produced per 100 eV by radiation, depending on beam type, LET, temperature, oxygen level, etc. Based on previous Monte Carlo simulations and experimental results,^{9–11} the generally accepted g -value of H_2O_2 is around 0.7/100 eV. Therefore, the conversion factor was 0.0726 $\mu\text{M}/\text{Gy}$ for pure water. The boundary condition was set as ($x \rightarrow \infty$) = 0, which means species could not reach the boundary. In the FDM we also need to set a termination condition, otherwise, it would eventually lead to a homogeneous distribution. Here we chose the same termination condition of the simulation as the previous model⁷: stopping the simulation when the beam is off. Therefore, we need the dose rates to calculate the irradiation time, and divide it by the time step, 0.01 s, to get the number of pulses. The procedure of simulation is described in Figure 1.

The final output of this model is the H_2O_2 distribution when the beam is off.

2.1.2 | Modification of the previous convolution-based model

In order to compare the FDM with the previous model using H_2O_2 to describe treatment outcomes in MBRT,⁷ hereinafter referred to as “old model,” some modifica-

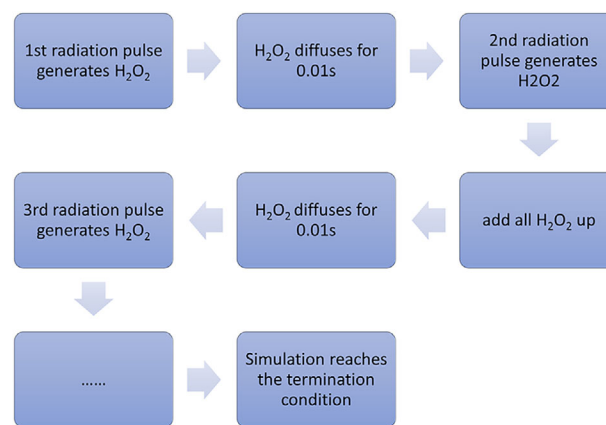


FIGURE 1 The simulation process of FDM.

tions had to be applied. The old model assumed that all radiation would be delivered at once, reaching the medium simultaneously, while FDM was designed to simulate pulsed and continuous irradiation. Hence, we modified the old model accordingly.

The old model is a convolution model of a Gaussian kernel referring to H_2O_2 diffusion with dose distribution. The Gaussian function's standard deviation (σ) was equal to the distance from the beam axis to the position where 68% H_2O_2 molecules were included. In accordance with the data from a Monte Carlo simulation of water radiolysis, the temporal evolution of $\sigma(t)$ was parameterized with the following functional form:

$$\sigma(t) = a \cdot (t/t_0)^b \quad (3)$$

The original parameters used in the model were $a = (4.8 \pm 0.2) \times 10^{-5}$, and $b = (4.3 \pm 0.2) \times 10^{-1}$. These two parameters are not reliable as they were derived from curve fitting and extrapolation from the Monte Carlo simulation of one proton. In addition, the Gaussian kernel for the convolution obtained from the Monte Carlo method is actually the diffusion model already implemented inside the Monte Carlo code that can simulate water radiolysis. Therefore, it is unnecessary to get the approximate value for parameters a and b through data fitting since there is an analytical solution. The diffusion model chosen by most Monte Carlo codes^{12–14} is a Gaussian function whose one-dimensional form is

$$\phi(x, t) = \frac{1}{\sqrt{4\pi Dt}} e^{-\frac{x^2}{4Dt}} \quad (4)$$

D here is the diffusion coefficient of H_2O_2 in water. So, $\sigma(t) = \sqrt{2Dt}$, with $a = \sqrt{2D} = 6.78 \times 10^{-5}$ and $b = 0.5$ in Equation 3.

The old model was further adapted by replacing the dose by the H_2O_2 concentration (calculated through Equation 2) in the convolution. In this way, the output of

the model is the H_2O_2 concentration distribution instead of the time to achieve 95% H_2O_2 uniformity.

2.2 | Diffusion model considering H_2O_2 removal and comparison with the FDM

While H_2O_2 diffusion process in pure water can be described mainly by Fick's second law of diffusion, in cells the antioxidant system can neutralize and eliminate these molecules. Since H_2O_2 is relatively stable, this is the dominating process of elimination. To account for this removal phenomenon, an attenuation term was introduced in a new model, the diffusion model considering removal (DMCR):

$$\frac{\partial \phi}{\partial t} = D \frac{\partial^2 \phi}{\partial x^2} + \phi_{source} - R\phi \quad (5)$$

where R is the removal factor. This factor indicates in general how many molecules have been absorbed by cells per second, not the rate of the biological process of eliminating radicals in cells. The cell density or porosity of tissues decides the removal rate, which varies with each individual, so it is not possible to determine a single value. In an in vitro study about H_2O_2 elimination rate in the rat C6 astrogloma cell line,¹⁵ the highest cell density was 4×10^5 cells/mL and the elimination rate was 1.5×10^{-3} /s. However, the cell densities in human tissues are on the order of 1 billion to 3 billion cells/mL.¹⁶ It is expected that the removal factor in tissues should be higher than that. We studied three different removal factors of increasing orders of magnitudes: 2.3×10^{-1} /s, 2.3×10^{-2} /s, and 2.3×10^{-3} /s to assess the most appropriate removal factor. This means that the concentration of H_2O_2 would decrease by 0.23%, 2.3%, or 23% every second. To show the difference between the FDM and the DMCR, we use the median value, 2.3% per second, as the removal factor in DMCR. In the simulations of the microbeam or minibeam animal studies, we use all three removal factors. Note that the source term ϕ_{source} is a constant when the beam is on as same as FDM. Since DMCR can still run after the beam is off, ϕ_{source} is zero after the dose is delivered.

Figure 2 represents the output of the simulation results of the DMCR: the H_2O_2 that removed by cells in blue and the remaining H_2O_2 in the tissues in green, compared to the dose distribution, which is represented by the red line. Figure 2b shows the result after 60 s post-irradiation. Without further irradiation, the H_2O_2 left in the medium continues to diffuse and is gradually absorbed by the cells. Since there are always some H_2O_2 molecules left in the medium, unlike the termination condition of the simulation we set for FDM, the simulation was stopped once the remaining H_2O_2 reached at least 95% uniformity (as represented by

the green line in Figure 2b) to guarantee that the sum of the remaining and the absorbed H_2O_2 are time-independent. Homogeneous H_2O_2 will be removed homogeneously, so the result will not change afterwards. Figure 3 represents the sum of the remaining and removed H_2O_2 (blue line) compared to the dose (red line), which is the final output of the DMCR and used in the following simulation.

Two tests were performed with FMD and DMCR to determine which model represents H_2O_2 more accurately in MBRT. First, we simulated the H_2O_2 distribution for MBRT with variable dose rates. The same dosimetry parameters were used: peak dose = 100 Gy; PVDR = 12.5; peak width = 400 μm ; valley width = 600 μm ; dose rate = 10 Gy/min and 50 Gy/min. Second, we simulated H_2O_2 distribution after broad beam irradiation. If the H_2O_2 distribution could be a surrogate of dose distribution for MBRT, it should not contradict classical radiotherapy.

2.3 | Comparisons with previous microbeam and minibeam animal experiments

As explained above, MBRT treatments deliver non-uniform dose and still maintain tumor control, which cannot be explained by current radiotherapy theory. Therefore, the dose is not a good indicator of treatment outcomes for MBRT as it is for conventional radiotherapy. We use the DMCR to correlate H_2O_2 concentration with dose. The H_2O_2 concentration distribution could be a surrogate of dose distribution for MBRT since all parameters (peak dose, valley dose, peak width, and valley widths) will have an impact on H_2O_2 distribution. Without a doubt, tens or hundreds Gray of peak dose can directly kill the tumor cells inside the peak region, so we focus on the underdosed region, the valley. The postulate is that MBRT with higher H_2O_2 concentration in the valley region has a better chance of achieving tumor control. Therefore, we analyzed previous animal experiments with different minibeam or microbeam patterns, to try to identify a correlation between H_2O_2 concentration in the valley region and tumor control.

After searching in the literature, we found six previous animal studies using different irradiation patterns where all the required parameters for the simulation were available.^{17–22} We used DMCR to calculate the summed H_2O_2 distribution (removed plus remaining H_2O_2) of the subgroups defined in each study. The minimum value of H_2O_2 in the valley region obtained through the model was used to represent the H_2O_2 concentration in the valley. We then compared the concentration in the valley with the treatment outcomes. The ideal parameters we were looking for from animal experiments were those that could represent the tumor control effect, such as

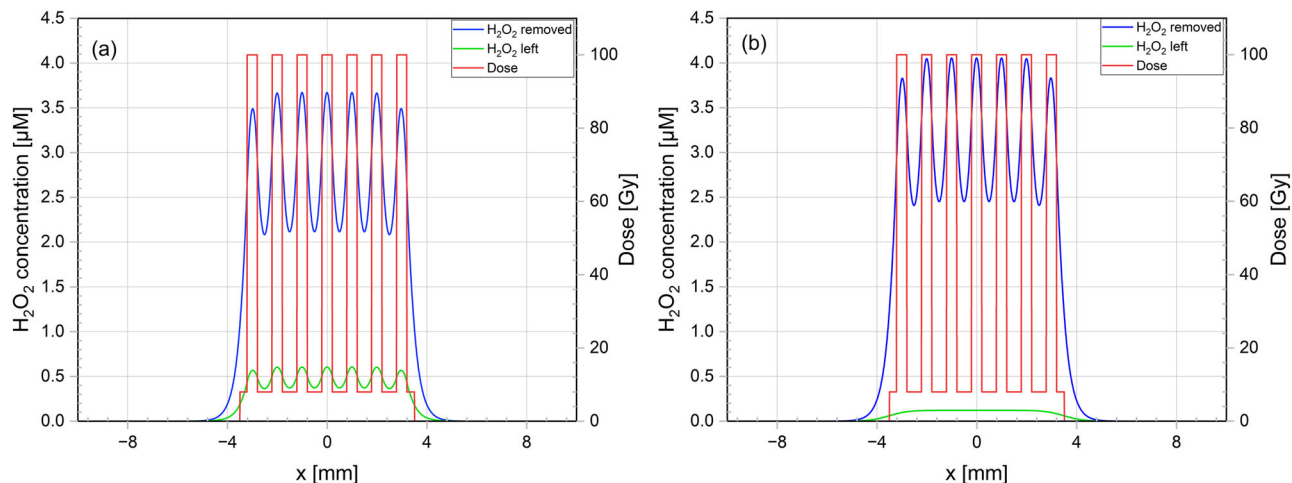


FIGURE 2 Simulation results of the model considering removal. The dosimetry parameters were peak dose = 100 Gy, PVDR = 12.5, dose rate = 20 Gy/min, peak width = 400 μm , and valley width = 600 μm . (a) The simulation result when the radiation stopped; (b) the H₂O₂ distribution 60 s postirradiation.

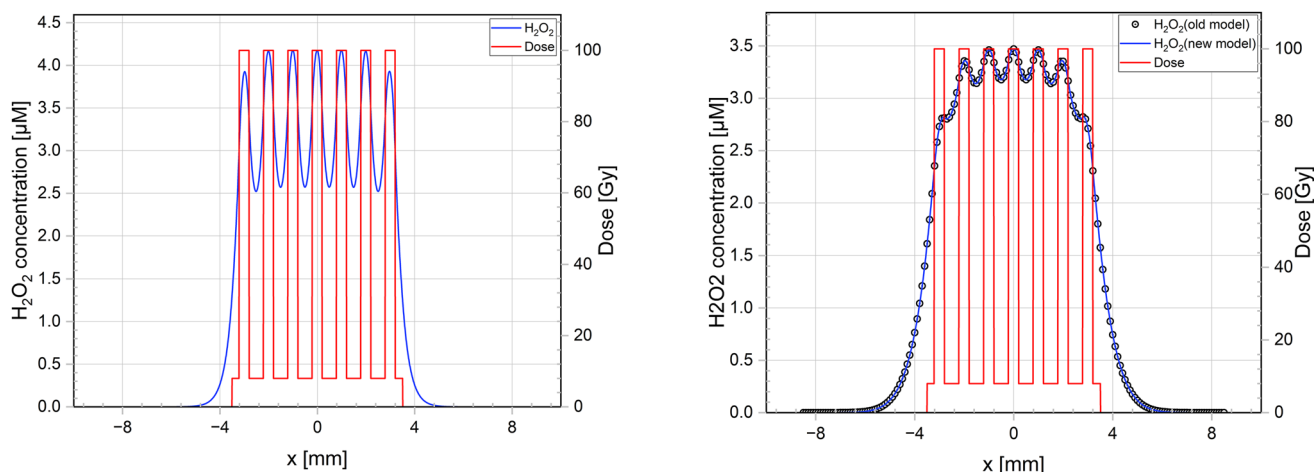


FIGURE 3 The final H₂O₂ distribution from the DMCR. The dosimetry parameters were peak dose = 100 Gy, PVDR = 12.5, dose rate = 20 Gy/min, peak width = 400 μm , and valley width = 600 μm .

FIGURE 4 Under the same MBRT condition (peak dose = 100 Gy, PVDR = 12.5, dose rate = 20 Gy/min, peak width = 400 μm , and valley width = 600 μm), the H₂O₂ distribution from the modified old published model and the FDM.

tumor volume after treatment, but only some studies provided this kind of result, so an alternative index, animal survival, was used in some studies.

3 | RESULTS

Figure 4 shows the comparison between the modified old model and the FDM. The simulation results from the old model (represented by empty dots) matched with the FDM (represented by the blue line). As mentioned in Section 2.A.2., parameters *a* and *b* used in the old model come from fitting the data of the Monte Carlo simulation. In this paper, we modified *a* and *b* with the analytical solution of the diffusion model behind the Monte Carlo codes. The old model also assumed the

total dose of MBRT to be delivered at once. We modified it for simulating pulse irradiation.

The effects of various H₂O₂ removal factors in the DMCR are shown in Figure 5. The minimum removal factor (0.23%, the green line) will result in extra lateral diffusion outside the radiation field; and the maximum removal factor (23%, the blue line) leads to almost no diffusion in the valley.

The comparison between FDM and DMCR is presented in Figures 6 and 7. In the comparison, *R* = 2.3% was chosen for DMCR. Figure 6 shows H₂O₂ distribution for the same radiation dose but under different dose rates (DMCR in Figure 6a and FDM in Figure 6b). FDM resulted in a different distribution with different dose rates, while DMCR led to the same H₂O₂ concentration distribution. In Figure 7, the H₂O₂ distribution

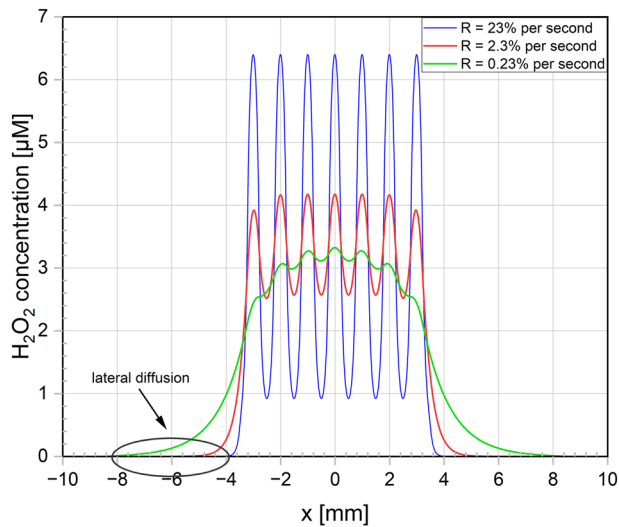


FIGURE 5 Simulated the sum of H_2O_2 distribution (remaining H_2O_2 + removed H_2O_2) from DMCR with various removal factors R (H_2O_2 decreased by 23%, 2.3%, and 0.23% per second) under the same dosimetry parameters (peak dose = 100 Gy, PVDR = 12.5, dose rate = 20 Gy/min, peak width = 400 μm , and valley width = 600 μm).

under uniform irradiation from DMCR was close to the dose profile, while FMD resulted in a Gaussian-shaped distribution for uniform irradiation.

Table 1 shows the parameters of spatially fractionated radiotherapy (SFRT) animal studies and the results of the comparison with DMCR. Note that for the second study, we included two indexes of experimental results: median survival time after irradiation and the longest survival time. That was because 50% of the subgroup's (peak width = 25 μm) animals died within four days after irradiation, but the surviving animals had the longest survival time. Our model was only supposed to predict the tumor control probability of MBRT without considering the normal tissue toxicity, so when toxicity compromised the treatment outcomes, only survival time could not indicate the tumor control.

4 | DISCUSSION

From long-term clinical practice, oncologists have established a connection between physical doses and biological responses. However, the specific mechanism still needs to be clarified. The chemical process is the bridge connecting the physical dose and the biological response. When the physical dose is not a good indicator of biological responses, it is reasonable to study the chemical process further. Therefore, we assume a chemical mechanism should be more suitable to evaluate MBRT efficacy since none of the peak, valley or mean dose can predict the treatment outcome alone. During water radiolysis after irradiation, several radicals are generated. H_2O_2 is the only candidate with relative

stability to allow it to diffuse and reach the valley region and with oxidizability so that it can trigger the following biological response. Therefore, we chose H_2O_2 as the surrogate of dose and developed a diffusion model for it.

As shown in Figure 4, after modifications to the old model, the simulated distribution of H_2O_2 matches the distribution from the FDM, which is not a coincidence. This is because the Gaussian function in Equation 4 is actually the analytical solution for the partial differential Equation 1 when choosing the Dirac delta distribution as the initial condition and zero as the boundary condition. Dirac delta function's value is zero everywhere but at the origin and the function's integral over the entire region is equal to one. This perfectly illustrates what happens at the beginning of radical diffusion: all the radicals concentrate at one point and then start diffusing. This result shows that an analytical method is enough and accurate to simulate the radical distribution of MBRT.

An attenuation term representing the H_2O_2 removal is introduced in DMCR. In reality, the H_2O_2 molecules cannot diffuse freely in tissue because cells can gradually remove them. As mentioned in Section 2.B, the removal factor R is not a coefficient reflecting biological responses. It is the percentage of H_2O_2 that was eliminated by the cell per second. If the cell density of the tumor is relatively high, then R will be larger, meaning the H_2O_2 generated from the peak regions can barely diffuse and reach the valley regions (blue line in Figure 5). In the opposite scenario, if the cell density of the tissue is relatively low, then a smaller R can lead to an H_2O_2 distribution close to free diffusion with extra lateral diffusion at the edge (green line in Figure 5).

As shown in Figure 6, the FDM results are subject to the dose rate. That is because we need to choose a time point to stop the simulation, otherwise the H_2O_2 distribution will eventually become homogeneous, as it is free diffusion. That leads to higher dose rate irradiation having less time for radicals to diffuse. We can see this discrepancy in different dose rate irradiations. Through the comparison between FDM and DMCR in Figure 7, we can find that DMCR results in H_2O_2 distribution that better matches homogeneous broad beam irradiation.

The hypothesis is that higher H_2O_2 concentration in the valley leads to a higher tumor control probability. If it is the case that different dose rate irradiation can generate different H_2O_2 distributions, then based on our hypothesis, it should result in different clinical outcomes. However, this conclusion contradicts previous clinical experience with photon radiotherapy. Flattening-filter-free (FFF) mode with a higher dose rate does not have a different clinical outcome from the low dose rate flattening-filter (FF) mode in broad-beam radiotherapy. Neither should MBRT. Besides, the research object is H_2O_2 , not radiation, so stopping the simulation right after the beam is off is not ideal. By contrast, the dose rate independency of DMCR makes more sense. The nature

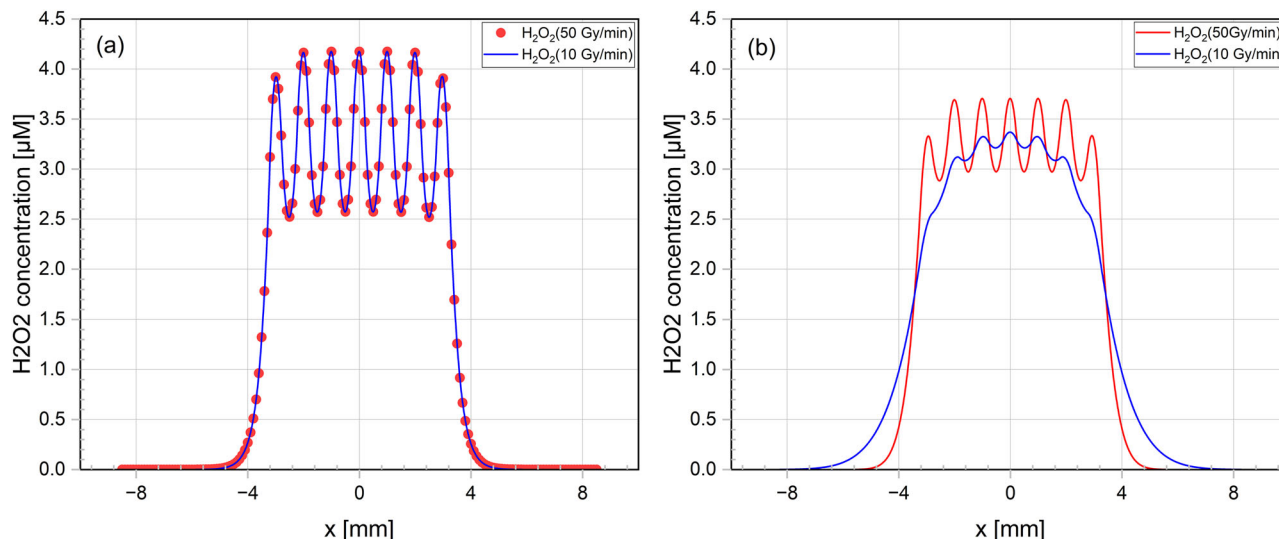


FIGURE 6 Simulated H_2O_2 distribution under different dose rates: 50 Gy/min and 10 Gy/min for (a) the DMCR model (the summed H_2O_2) and (b) the FDM model. Peak dose = 100 Gy, PVDR = 12.5, dose rate = 20 Gy/min, peak width = 400 μm , and valley width = 600 μm .

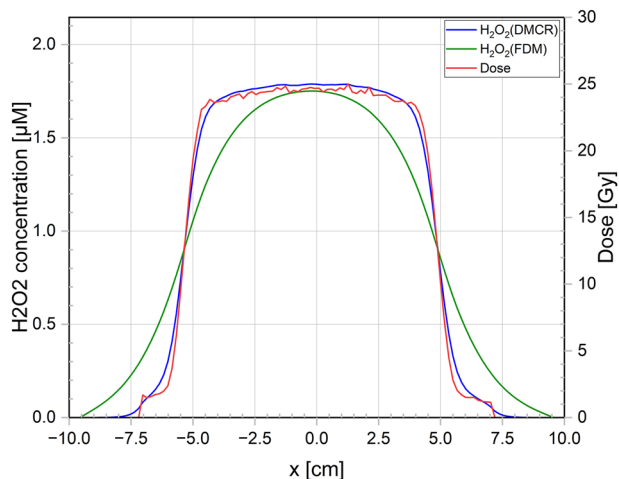


FIGURE 7 Hydrogen peroxide distribution of uniform irradiation from FDM (green line) and DMCR (blue line, summed H_2O_2) compared to dose (red line).

of diffusion is Brownian motion of every single particle. The dose rate only changes the time of the generation of H_2O_2 molecules, not the diffusion. Each H_2O_2 molecule is generated independently, diffused independently, and absorbed by cells independently. The second test shown in Figure 7 is to simulate broad-beam irradiation. Uniform irradiation should not lead to a Gaussian-shape H_2O_2 distribution. Note that in Figure 7 the removal factor of DMCR is 2.3% per second. However, if the lower rate, 0.23% per second, was chosen, then the simulation result from DMCR is close to the Gaussian-shape H_2O_2 distribution from FDM. Because the removal factor 0.0023/s is close to zero, the result tends to be like free diffusion, which suggests 0.0023/s is not a proper

factor for DMCR, otherwise H_2O_2 cannot serve as the surrogate of dose for MBRT.

The above two comparisons have demonstrated the rationality of DMCR. Therefore, it is used to compare with animal experiments (Table 1). The first study in Table 1 indicates irradiation of the same spatial fractionation but different doses. Higher dose leads to longer survival time and our simulated valley concentration of H_2O_2 complies with experimental results. In the second study, half of the rats in the “peak width = 25 μm ” subgroup die within four days after irradiation, probably due to toxicity. We assume that H_2O_2 concentration in the valley can reflect the tumor control probability without considering normal tissue toxicity. So, we can still say that our simulations are consistent with the treatment outcome since the surviving rats have the longest life span. In the third study, our simulations are basically compatible with animal experiments as well. The only exception happened between the rats in the fourth subgroup (peak width = 500 μm , CTC = 1000 μm , peak dose = 180 Gy, valley dose = 7.2 Gy) and the rats in the first subgroup (peak width = 50 μm , CTC = 200 μm , peak dose = 200 Gy, valley dose = 7.7 Gy) when choosing 23% as the removal factor. 23% as the removal factor means that the concentration of H_2O_2 decreases by 23% per second. Previously in the Method section, we mentioned that the removal factor in an in-vitro study is 0.15% per second. Although it should be higher in vivo, 100 times higher may not be appropriate. The rats in the first subgroup have a median survival time of 24 days, while 28 days for the rat in the fourth subgroup. Except for 23% as the removal factor, the simulation results with the other two removal factors match the animal experiments. However, this research does not mention the statistical methods or the threshold for statistical

TABLE 1 Parameters of SFRT animal studies and the simulated H₂O₂ concentration in the valley regions.

Cancer type	Peak width (μm)	CTC (μm) ^a	Peak dose (Gy)	Valley dose (Gy)	Survival/Tumor control	H ₂ O ₂ in the valley region (μM) ^c			
						R = 0.23%	R = 2.3%	R = 23%	
9L gliosarcoma ¹⁷	50	200	400	17.4	Mean survival time	32 days	9.36	9.45	8.45
			200	8.7		23.5 days	4.67	4.73	4.22
9L gliosarcoma ²¹	25	211	860 × 2 ^b	18.0 × 2	Median survival time after irradiation/longest survival time	4/120 days	25.23	25.46	22.18
	50		480 × 2		39/83 days	21.22	21.44	18.85	
	75		320 × 2		26/62 days	18.83	19.04	16.93	
9L gliosarcoma ²⁰	50	200	200	7.7	Median survival time	24 days	4.61	4.68	4.17
			400	15.3		52 days	9.21	9.36	8.34
			600	23.0		110 days	13.82	14.04	12.51
			500	1000	180	7.2		28 days	6.72
9L gliosarcoma ¹⁸	24.6	200	625	8.8	Ablated tumors	2 out of 32	7.13	7.23	6.35
	24.6	100	625	31.3		5 out of 11	14.12	15.01	14.69
U251 glioma ²²	20	100	111 × 2	8.2 × 2	Tumor growth ratios	9.9 ± 7.9 %	5.37	5.62	5.49
	100	500	124 × 2	9.6 × 2		22.0 ± 16.2 %	5.01	4.70	2.97
Rat fibrosarcoma ¹⁹	2200	4200	34.5	6.2	Tumor volume (normalized) on Day 17	4.44	1.14	0.53	0.45
	310	1210	91	6.8		7.45	2.02	1.47	0.56
				225	16.8		1.32	5.00	3.62

^aCTC: center-to-center distance.^bTwo fractions.^cThe minimum value in the valley region was chosen to indicate the H₂O₂ concentration of the valley.

significance. Therefore, we cannot say whether the median survival time of 28 days is significantly longer than 24 days. The fourth study directly presents how many animals have ablated tumors after irradiation for two different configurations. Still, our simulation matches the results. As for the fifth study, the results cannot be explained through any dose theory. There are two configurations in this study with the same ratio of peak region to valley region, which means the same volume of tumors in two subgroups is irradiated by peak dose. Let us assume two subgroups' peak doses are the same. That means that the peak dose, the valley dose, and the mean dose in the two subgroups are all equal. But the tumors in the second subgroup grow faster even with around 10% higher dose. This demonstrates that a narrower beam is more effective for tumor growth suppression. Although the standard deviation of the tumor growth ratios is large, the statistic has shown that the difference is significant ($p < 0.05$). While dose theory cannot explain this effect, H₂O₂ theory can.

Typically, it is assumed that irradiating the whole tumor volume would achieve the highest tumor control probability. SFRT is not supposed to have a uniform dose coverage, but it is theoretically possible that the whole tumor is uniformly treated by H₂O₂. As shown in Figure 8, we keep constant the peak dose, the valley dose, the mean dose, and the ratio of peak region to valley region but gradually narrow the beamlets. The H₂O₂ concentration in the valley increases. With further and further narrowing of the beamlets, the beam widths will eventu-

ally tend to be infinitely small, and the H₂O₂ distribution will tend to be uniform. So, we can say the whole tumor is treated by H₂O₂ and then achieve the theoretically highest tumor control, although the same portion of tumors receives the same dose. Note that narrower beamlets can also cause more damage to the normal tissue, therefore increasing the toxicity of the treatment.²²

The sixth study in Table 1 is the only exception where the DMCR prediction does not match the animal experiments. However, it seems that there is no minibeam effect in that study. MBRT is supposed to expand the therapeutic window with a similar even superior survival rate to BBRT. In that study, BBRT always leads to a much better survival rate than any MBRT, regardless of dose or spatial fractionation. This goes against what previous studies have seen about MBRT.¹ Furthermore, the experimental results can be explained with classical radiotherapy theory: reducing the cold spots (valley regions and valley dose) in the target leads to better treatment outcomes. One example in that paper is the irradiation of only one-half of the tumor, compared to the MBRT irradiation of the whole area (with the MBRT characteristic peaks and valleys). Both treatments lead to similar survival rates and tumor growth suppression. Irradiating only half of the tumor should not lead to comparable results with MBRT. Therefore there is no minibeam effect in this study.

A possible reason is that the minibeam effect may not be observed in all types of tumors. In study 6, fibrosarcoma is studied, while other studies use glioma. Glioma

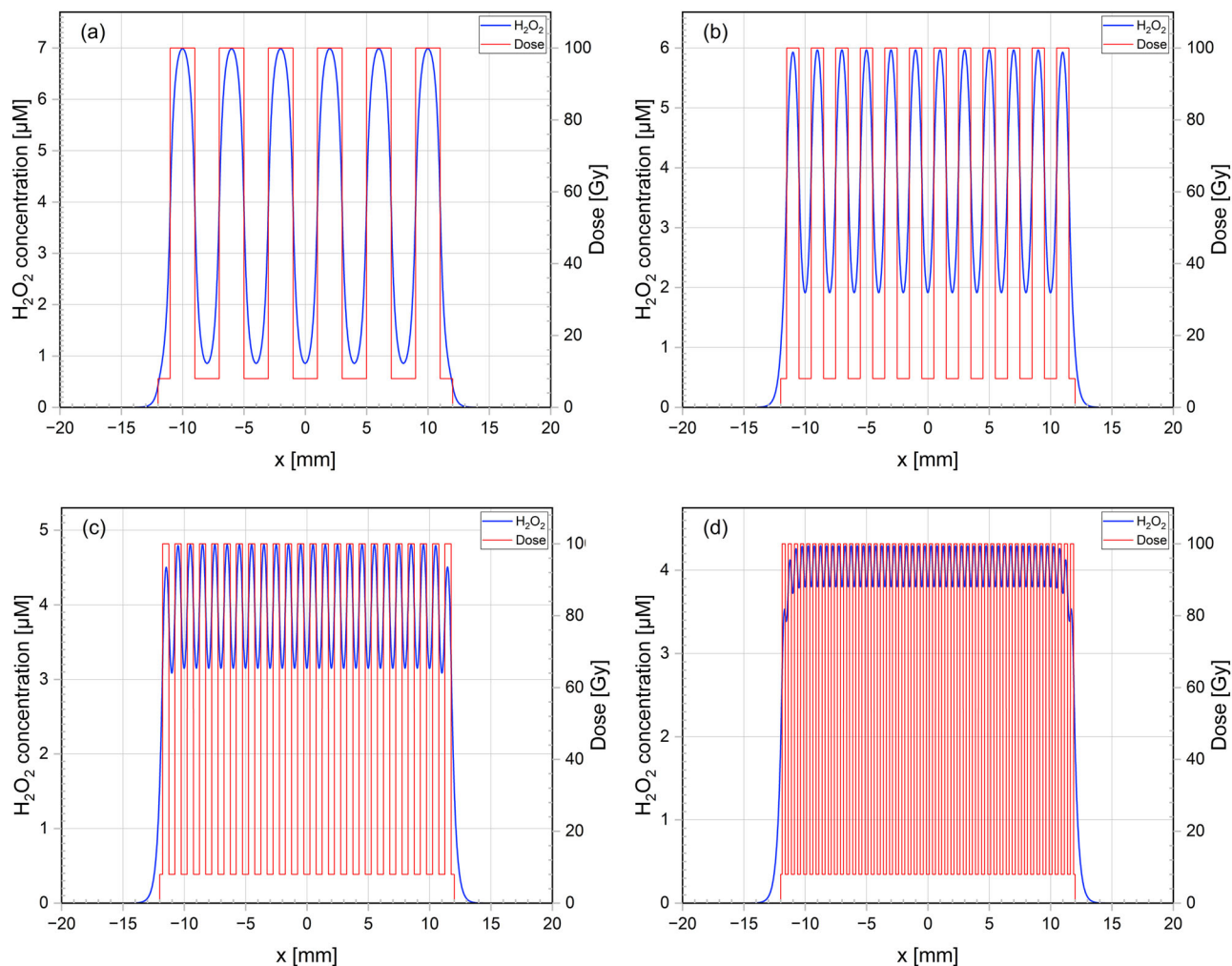


FIGURE 8 Simulation results of the sum of H_2O_2 distribution (remaining H_2O_2 + the removed H_2O_2) of four different patterns under the same peak dose (40 Gy) and valley dose (1.36 Gy) from DMCR. (a) 7 beamlets, peak width = valley width = 2 mm; (b) 14 beamlets, peak width = valley width = 1 mm; (c) 28 beamlets, peak width = valley width = 0.5 mm; (d) 56 beamlets, peak width = valley width = 0.25 mm.

looks like water from imaging, but rat fibrosarcoma is a more solid and firm tumor. As discussed above, firm tumors with higher cell density will have a large removal factor. Therefore, the H_2O_2 generated from the peak region cannot cover the valley region (similar to the blue line in Figure 5). This may be why MBRT does not work for fibrosarcoma but is effective for glioma. The ratio of the removal factor to the diffusion factor could be the key to deciding the efficacy of MBRT. If MBRT only works well for tumors with liquid, then this could be proof that our diffusion model makes sense.

However, there are still several limitations in our model. The first one is that the simulated H_2O_2 concentration may be not accurate because of the inaccuracy of g -value. The latest measurement²³ has shown that g -value of H_2O_2 is $(2.33 \pm 0.05)/100$ eV for 235 MeV proton, $(3.32 \pm 0.07)/100$ eV for 225 keV X-ray, which is much higher than the $0.7/100$ eV we chose in our study. So, the accurate concentration may be several times

higher than our simulation, but the distribution will not change. Also, due to the presence of other biological molecules and different diffusion coefficient in tissues, the g -value in tissue should be different from pure water. However, it is challenging to measure the g -value of H_2O_2 in tissues accurately. The second is that we cannot get the real removal factor for Equation 5. This removal factor is also not a constant due to the heterogeneity of the tumor. Without accurate parameters, we cannot find the specific threshold of H_2O_2 concentration to achieve tumor control. Finally, although we propose to use H_2O_2 as a surrogate of dose and it seems to make sense, we cannot say H_2O_2 is the true mechanism of MBRT achieving tumor control.

Nevertheless, there are several theories about H_2O_2 . The first one is that H_2O_2 as a reactive oxygen species can directly damage the DNA of cells in the valley region. If we choose a higher g -value as mentioned above, the concentration in the valley could be tens of micromolar

or even more than 100 μM . With this high concentration, H_2O_2 can definitely kill the tumor cells.^{24–26} Another theory is that H_2O_2 can change the ratio of glutathione (GSH) to glutathione disulfide (GSSG) and thus change the redox potential of tumor cells, and eventually change the states of cells from proliferation to apoptosis.^{27,28} A recent study suggests that immune response plays a role in MBRT.²⁹ There are also several studies suggesting that H_2O_2 can activate immune response.^{30,31}

5 | CONCLUSION

This study has developed an H_2O_2 diffusion model considering the removal process (DMCR). DMCR has been proven superior to FDM and the old model based on Monte Carlo-convolution method for the simulation of H_2O_2 distribution of MBRT. Meanwhile, the evaluation of previous animal experiments with this model has suggested that H_2O_2 concentration in the valley region could be the surrogate of dose when dealing with MBRT. However, further investigation is needed to find the true mechanism behind MBRT.

ACKNOWLEDGMENTS

The authors acknowledge Riccardo Dal Bello's help from Universitätsspital Zürich (USZ). Daniel García-Calderón was funded by the Deutscher Akademischer Austauschdienst (DAAD) (Graduate School Scholarship Program, 2019, 57450037).

Open access funding enabled and organized by Projekt DEAL.

CONFLICT OF INTEREST STATEMENT

The authors have no relevant conflicts of interest to disclose.

REFERENCES

- Bertho A, Ortiz R, Juchaux M, et al. First evaluation of temporal and spatial fractionation in proton Minibeam radiation therapy of glioma-bearing rats. *Cancers (Basel)*. 2021;13(19):4865.
- Prezado Y, Jouvion G, Guardiola C, et al. Tumor control in RG2 glioma-bearing rats: a comparison between proton Minibeam therapy and standard proton therapy. *Int J Radiat Oncol Biol Phys*. 2019;104(2):266–271.
- Prezado Y, Jouvion G, Patriarca A, et al. Proton minibeam radiation therapy widens the therapeutic index for high-grade gliomas. *Sci Rep*. 2018;8(1):16479.
- Sammer M, Dombrowsky AC, Schauer J, et al. Normal tissue response of combined temporal and spatial fractionation in proton Minibeam radiation therapy. *Int J Radiat Oncol Biol Phys*. 2021;109(1):76–83.
- Dombrowsky AC, Schauer J, Sammer M, et al. Acute skin damage and late radiation-induced fibrosis and inflammation in murine ears after high-dose irradiation. *Cancers (Basel)*. 2019;11(5):727.
- Le Caër S. Water radiolysis: influence of oxide surfaces on H_2 production under ionizing radiation. *Water*. 2011;3(1):235–253.

- Dal Bello R, Becher T, Fuss MC, Krämer M, Seco J. Proposal of a chemical mechanism for mini-beam and micro-beam efficacy. *Front Phys*. 2020;8:564836.
- Ballarini F, Biaggi M, Merzagora M, et al. Stochastic aspects and uncertainties in the prechemical and chemical stages of electron tracks in liquid water: a quantitative analysis based on Monte Carlo simulations. *Radiat Environ Biophys*. 2000;39(3):179–188.
- Boscolo D, Kramer M, Durante M, Fuss MC, Scifoni E. TRAX-CHEM: a pre-chemical and chemical stage extension of the particle track structure code TRAX in water targets. *Chem Phys Lett*. 2018;698:11–18.
- Meesungnoen J, Jay-Gerin J. Radiation chemistry of liquid water with heavy ions: Monte Carlo simulation studies. *Charged Particle and Photon Interactions with Matter: Recent Advances, Applications, and Interfaces*. Taylor & Francis; 2011:355–400.
- Ramos-Mendez J, Perl J, Schuemann J, McNamara A, Paganetti H, Faddegon B. Monte Carlo simulation of chemistry following radiolysis with TOPAS-nBio. *Phys Med Biol*. 2018;63(10):105014.
- Karamitros M, Luan S, Bernal MA, et al. Diffusion-controlled reactions modeling in Geant4-DNA. *J Comput Phys*. 2014;274:841–882.
- Plante I. A review of simulation codes and approaches for radiation chemistry. *Phys Med Biol*. 2021;66(3):03TR02.
- Tian Z, Jiang SB, Jia X. Accelerated Monte Carlo simulation on the chemical stage in water radiolysis using GPU. *Phys Med Biol*. 2017;62(8):3081–3096.
- Gülden M, Jess A, Kammann J, Maser E, Seibert H. Cytotoxic potency of H_2O_2 in cell cultures: impact of cell concentration and exposure time. *Free Radical Biol Med*. 2010;49(8):1298–1305.
- McClelland RE, Dennis R, Reid LM, Stegemann JP, Palsson B, Macdonald JM. Chapter 6 - Tissue Engineering. In: Enderle JD, Bronzino JD, eds. *Introduction to Biomedical Engineering (Third Edition)*. Academic Press; 2012:273–357.
- Bouchet A, Brauer-Krisch E, Prezado Y, et al. Better efficacy of synchrotron spatially microfractionated radiation therapy than uniform radiation therapy on glioma. *Int J Radiat Oncol Biol Phys*. 2016;95(5):1485–1494.
- Regnard P, Le Duc G, Brauer-Krisch E, et al. Irradiation of intracerebral 9L gliosarcoma by a single array of microplanar x-ray beams from a synchrotron: balance between curing and sparing. *Phys Med Biol*. 2008;53(4):861–878.
- Rivera JN, Kierski TM, Kasoji SK, Abrantes AS, Dayton PA, Chang SX. Conventional dose rate spatially-fractionated radiation therapy (SFRT) treatment response and its association with dosimetric parameters: a preclinical study in a Fischer 344 rat model. *PLoS One*. 2020;15(6):e0229053.
- Romano M, Bravin A, Mittone A, et al. A multi-scale and multi-technique approach for the characterization of the effects of spatially fractionated X-ray radiation therapies in a preclinical model. *Cancers (Basel)*. 2021;13(19):4953.
- Serduc R, Bouchet A, Brauer-Krisch E, et al. Synchrotron microbeam radiation therapy for rat brain tumor palliation—influence of the microbeam width at constant valley dose. *Phys Med Biol*. 2009;54(21):6711–6724.
- Uyama A, Kondoh T, Nariyama N, et al. A narrow microbeam is more effective for tumor growth suppression than a wide microbeam: an in vivo study using implanted human glioma cells. *J Synchrotron Radiat*. 2011;18(4):671–678.
- Kacem H, Psoroulas S, Boivin G, et al. Comparing radiolytic production of H_2O_2 and development of Zebrafish embryos after ultra high dose rate exposure with electron and transmission proton beams. *Radiother Oncol*. 2022;175:197–202.
- Dahm-Daphi J, Sass C, Alberti W. Comparison of biological effects of DNA damage induced by ionizing radiation and hydrogen peroxide in CHO cells. *Int J Radiat Biol*. 2000;76(1):67–75.
- Ogawa Y. Paradigm shift in radiation biology/radiation oncology—exploitation of the “ H_2O_2 effect” for radiotherapy

- using low-LET (linear energy transfer) radiation such as X-rays and high-energy electrons. *Cancers*. 2016;8(3):28.
26. Park WH. Hydrogen peroxide inhibits the growth of lung cancer cells via the induction of cell death and G1-phase arrest. *Oncol Rep*. 2018;40(3):1787-1794.
27. Aw TY. Cellular redox: a modulator of intestinal epithelial cell proliferation. *News Physiol Sci*. 2003;18(5):201-204.
28. Jones DP. Redox potential of GSH/GSSG couple: assay and biological significance. In: Sies H, Packer L, eds. *Methods in Enzymology*. Academic Press; 2002:93-112.
29. Bertho A, Iturri L, Brisebard E, et al. Evaluation of the role of the immune system response after Minibeam radiation therapy. *Int J Radiat Oncol Biol Phys*. 2023;115(2):426-439.
30. Herrera-Ortiz A, Martínez-Barnetche J, Smit N, Rodríguez MH, Lanz-Mendoza H. The effect of nitric oxide and hydrogen peroxide in the activation of the systemic immune response of *Anopheles albimanus* infected with *Plasmodium berghei*. *Dev Comp Immunol*. 2011;35(1):44-50.
31. Reth M. Hydrogen peroxide as second messenger in lymphocyte activation. *Nat Immunol*. 2002;3(12):1129-1134.

How to cite this article: Zhang T, García-Calderón D, Molina-Hernández M, Leitão J, Hesser J, Seco J. A theoretical study of H₂O₂ as the surrogate of dose in minibeam radiotherapy, with a diffusion model considering radical removal process. *Med Phys*. 2023;50:5262–5272.
<https://doi.org/10.1002/mp.16570>

3. DISCUSSION

The two studies presented in this dissertation address a central challenge in modern radiotherapy research: explaining and predicting biological outcomes in novel high-dose-rate and spatially fractionated delivery techniques through chemical rather than purely physical dose concepts. Specifically, both works focused on the role of hydrogen peroxide (H_2O_2)—a relatively stable reactive oxygen species (ROS)—as a potential surrogate for the dose and an indicator of radiation-induced oxidative stress.

In conventional radiotherapy, a single dose parameter (e.g., the prescribed dose) usually suffices to predict outcomes. However, with ultra-high dose-rate irradiation (often referred to as FLASH) and minibeam radiation therapy (MBRT), the time structure of the dose (FLASH) or its spatial pattern (MBRT) can decouple the physical dose distribution from the ensuing biological effect. Consequently, a purely physical dose metric may fail to explain why healthy tissue is better spared or why tumor control remains robust in these novel approaches.

In the first publication, the experiments focused on how hydrogen peroxide production in pure water depends on dose rate (UHDR vs. CONV) and the underlying mechanistic explanations for any differences. The work clearly showed that H_2O_2 yield in pure water is reduced at UHDR compared to conventional dose rates, contrasting with certain Monte Carlo studies that predicted an opposite effect. By attributing this discrepancy to the scavenging of $\bullet\text{OH}$ by e_{aq}^- , we established a mechanistic link: in UHDR, the instantaneous concentration of free radicals is so large that competing reactions—especially the third-order $e_{\text{aq}}^- + \bullet\text{OH}$ reaction—can decrease net H_2O_2 formation. Furthermore, the study demonstrated that adding scavengers for e_{aq}^- (e.g., N_2O , NaNO_3) eliminates the observed dose-rate dependence, offering strong experimental support for this radical-competition hypothesis.

In the second publication, the spotlight shifts from time structure to spatial structure. Minibeams, with their array of high-dose peaks and low-dose valleys, can achieve remarkable normal tissue sparing while maintaining tumor control. This study proposed H_2O_2 as a chemical surrogate of physical dose in MBRT by developing two theoretical models of radical transport: one describing free diffusion of H_2O_2 (FDM) and another (DMCR) that incorporates a removal term reflecting biologically realistic antioxidant processes. The DMCR model better reconciled theoretical predictions with *in vivo* animal data. Its key insight was that H_2O_2 , being both diffusible and subject to cellular clearance, might effectively “bridge” the dose gap between peaks and valleys. Hence, even though a tumor subvolume is underdosed in terms of immediate physical dose, H_2O_2 generated in the peaks can diffuse into these valleys, potentially contributing to tumor cell killing. Meanwhile, healthy tissue with higher metabolic activity and antioxidant capacity may remove H_2O_2 more readily, thus experiencing reduced toxicity.

To examine this bridging effect in detail, we next employed the Crank–Nicolson (CN) method to solve the corresponding diffusion–reaction equations. As an unconditionally stable, second-order accurate finite-difference scheme, the CN approach captured how H_2O_2 is generated, diffuses laterally, and is subsequently removed by cells—even under the large dose gradients characteristic of MBRT. The term representing the radiation source in the equation varies over time (e.g., the simulation continues even when the beam is off), which precludes straightforward

analytical formulas and makes a numerical approach, such as CN method, more robust and flexible.

Although FLASH and MBRT operate on different principles (dose-rate vs. spatial fractionation), these two studies share a unifying theme: that ROS-driven chemistry is central to understanding the normal tissue sparing and tumor control observed in emerging radiotherapy modalities. By focusing on H_2O_2 , both works provide a chemical explanation for these phenomena that extends beyond conventional physical dose descriptors.

Despite the advances outlined, important questions remain:

1. Both works either employed or modeled relatively simple conditions (pure water in experiments, idealized diffusion in theoretical models). In living tissue, robust antioxidant systems (e.g., glutathione, catalase), cellular architectures, and varying oxygen tensions create a dynamic environment where H_2O_2 can be rapidly neutralized or further converted. Validating these models in increasingly realistic settings (e.g., multicellular spheroids, in vivo tumor models) remains a high priority.
2. H_2O_2 is only one of many ROS produced during water radiolysis; superoxide, peroxy radicals, and short-lived hydroxyl radicals may also play substantial roles in DNA damage and stress signaling. Although H_2O_2 is more stable and therefore easier to measure, the overall radiochemical “network” is complex. Future studies might involve time-resolved spectroscopy or advanced molecular imaging techniques to track multiple reactive species in real-time.
3. In FLASH, the magnitude and duration of radical bursts can exceed the recombination capacity of normal cells, but the exact relationship between short pulse spacing, radical lifetimes, and subsequent biological responses is not fully understood. Similarly, in MBRT, the temporal sequencing of beamlets or fractionated delivery could affect the eventual pattern of H_2O_2 accumulation. Further mechanistic studies—potentially combining radiation chemistry with cell-level data—are required to clarify these phenomena.
4. Due to technical limitations, we were unable to precisely control the concentration of N_2O gas dissolved in water, despite its saturation solubility of ~ 25 mM at 25°C and standard atmospheric pressure. Additionally, CO_2 plays a strong role in radical reactions, and although our study is the first to report this phenomenon, the underlying mechanisms require further investigation in future research.

The overall research question posed in the dissertation concerns how spatiotemporal modulation of radiation dose might be leveraged to optimize therapeutic index beyond what conventional approaches can achieve. Looking ahead, continuing this line of inquiry entails moving from controlled in vitro or theoretical contexts to progressively more complex biological systems. In conclusion, the two research projects have jointly highlighted the central role of radiochemical processes in explaining dose-rate and spatial-fractionation effects. By bridging physical dose descriptions and the complex kinetics of radical formation, diffusion, and removal, they offer fresh insights into how advanced radiotherapy paradigms might work—and how they might be optimized. Through continued experimental validation and model refinement, radiochemical concept could become a valuable indicator for designing and evaluating FLASH and MBRT strategies that deliver maximal tumor control with minimal normal tissue damage.

4. SUMMARY

FLASH-RT, delivered at UHDR, has demonstrated a remarkable capacity to spare normal tissues while maintaining effective tumor control. Among the various modalities, proton conformal FLASH-RT stands out due to its superior dose conformity and its feasibility for UHDR delivery using modern beam delivery systems. This dissertation presents a comprehensive exploration of its development, implementation, and optimization, integrating both technical advancements and mechanistic insights.

A key unresolved question has been why UHDR produces less H_2O_2 , with conflicting results in previous studies. This dissertation addresses this issue, demonstrating through experimental data that solvated electrons are responsible for the lower H_2O_2 yield in UHDR. By employing solvated electron scavengers, we show that the dose rate dependency of H_2O_2 production disappears, providing the first clear resolution to this longstanding debate.

Furthermore, we establish an analytical model to simulate H_2O_2 distribution under MBRT conditions and validate our model through comparisons with animal experiments. The results indicate that our simulation accurately predicts animal experimental data, offering new insights into the underlying mechanisms of the minibeam effect, which spares normal tissues while maintaining tumor control, similar to FLASH-RT. This dissertation thus presents a comprehensive exploration of these advancements, integrating both technical innovations and mechanistic understanding to further optimize next-generation radiotherapy approaches.

4.1 Technical Advances in Proton Conformal FLASH-RT

Various techniques have been developed to achieve conformal proton FLASH-RT:

- TB: The most clinically tested method, capable of achieving the highest dose rate but with unavoidable exit dose.
- SEBP: Provides improved conformity by eliminating exit dose but requires patient-specific RCs.
- SESOBP: Uses RFs to broaden the BP, enabling single-field FLASH delivery while increasing neutron contamination.
- Hybrid FLASH-RT: Combines TB with SEBP or SESOBP to enhance FLASH dose rate coverage while reducing normal tissue toxicity.
- MESOBP: Enabled by superconducting gantries, allowing ultra-fast energy switching for optimized dose rate delivery.

Despite these advancements, several challenges persist, including the insufficient beam current of existing cyclotron/synchrotron systems, the complexities of dose rate optimization, and the need for robust TPS. Various dose rate models, such as DADR, PBSDR, and DTDR, have been proposed to quantify dose rate in PBS approaches. However, these models often yield differing results, complicating efforts to standardize FLASH dose rate definitions. Additionally, the biological mechanisms underlying the FLASH effect require further clarification to optimize treatment strategies across different tumor types and anatomical sites. Expanding the accessibility of FLASH-optimized TPS and integrating real-time dose rate monitoring into clinical workflows will be critical for achieving widespread adoption. Future

research should also explore novel accelerator technologies capable of delivering consistent UHDR across larger treatment volumes. While numerous preclinical and computational studies support the feasibility of proton FLASH-RT, clinical validation remains a crucial next step, necessitating well-designed trials that assess both efficacy and long-term safety in human patients.

4.2 Biological and Mechanistic Insights into FLASH-RT

Despite its promising therapeutic index, the mechanism behind FLASH remains unclear. Several hypotheses have been proposed:

- **Oxygen Depletion Hypothesis:** Suggests that UHDR rapidly consumes oxygen, inducing transient hypoxia and reducing radiation-induced damage. However, recent studies indicate that oxygen depletion alone is insufficient, particularly for high-LET radiation.
- **RRR Hypothesis:** Proposes that FLASH promotes radical recombination, reducing oxidative damage. However, conflicting experimental results challenge this as the primary mechanism.

A major focus of this dissertation is H_2O_2 under UHDR, as it is a key oxidative species implicated in radiation-induced damage. Previous studies have debated whether UHDR increases or decreases H_2O_2 production, with Monte Carlo simulations often predicting a higher yield and attributing this to long-lived radical interactions. However, our research provides the first definitive resolution to this debate by demonstrating that solvated electrons are responsible for the lower H_2O_2 yield in UHDR. We show through experimental data that when solvated electron scavengers are introduced, the dose rate dependency of H_2O_2 production disappears, confirming that e_{aq}^- plays a dominant role in suppressing H_2O_2 formation under UHDR conditions. Furthermore, our study uniquely investigates the effect of different LETs on H_2O_2 production. By comparing low-LET sources such as electrons with high-LET radiation like carbon ions, we observe distinct differences in radical production and recombination kinetics, further reinforcing the role of solvated electrons in UHDR conditions.

Additionally, our 1-spilled vs. 3-spilled UHDR experiments provide critical evidence refuting the assumption in Monte Carlo studies that UHDR produces more H_2O_2 . While theoretical models suggested that long-lived radicals might contribute to decreased yields under CONV, our experimental findings demonstrate otherwise, proving that Monte Carlo simulations overestimate radical concentration and their impact on H_2O_2 production. This correction to existing models is crucial for improving future simulations and guiding accurate predictions of FLASH radiochemistry.

Moreover, this dissertation is the first to incorporate CO_2 into the analysis of FLASH-RT radiochemistry, revealing its significant influence on ROS dynamics. Our data show that CO_2 modulates the chemical environment of irradiated media, affecting radical recombination and stabilizing oxidative products. The inclusion of CO_2 offers a new dimension to understanding FLASH effects, particularly in the context of biological tissues where CO_2 levels vary dynamically.

4.3 H₂O₂ as a Surrogate in MBRT

SFRT, particularly MBRT, has been explored as an alternative approach to enhance the therapeutic window. Unlike BBRT, MBRT employs sub-millimeter beamlets, creating alternating high-dose peaks and low-dose valleys. Preclinical studies have demonstrated that MBRT can reduce normal tissue toxicity while maintaining tumor control. However, defining an appropriate surrogate metric for MBRT remains a challenge. This dissertation investigates the feasibility of using H₂O₂ distribution as a radiochemical surrogate for MBRT. We have significantly improved upon previous diffusion models, addressing critical limitations in prior approaches. Traditional free diffusion models assumed radiation was delivered simultaneously across the entire target, an assumption that does not reflect the sequential nature of real radiation delivery. Our model corrects this by incorporating a time-dependent approach, improving its predictive accuracy. Another major enhancement in our model is the consideration of H₂O₂ removal mechanisms. Unlike prior models, which only simulated free diffusion, we implemented a more realistic framework where H₂O₂ is actively eliminated in biological environments. This refinement allows for a more accurate representation of ROS dynamics under MBRT conditions.

To validate our model, we compared simulated H₂O₂ distributions with experimental data from previous MBRT animal studies. The results show that our model accurately predicts treatment outcomes based on H₂O₂ concentration in valley regions, reinforcing the idea that H₂O₂ could serve as a reliable surrogate for MBRT dose distribution. Furthermore, our findings suggest that the balance between H₂O₂ diffusion and removal plays a crucial role in determining the effectiveness of MBRT. Overall, our research provides a more comprehensive framework for understanding MBRT by refining diffusion modeling, incorporating scavenging processes, and integrating experimental validation. These advancements offer new perspectives for optimizing MBRT to enhance therapeutic efficacy while minimizing normal tissue damage.

4.4 Future Directions in FLASH-RT and MBRT

The translation of FLASH-RT and MBRT into clinical practice requires addressing several key scientific and technological challenges. These include improving machine capabilities, optimizing dose rate models, further elucidating underlying biological mechanisms, and integrating these advancements into clinical workflows.

Existing particle accelerators lack the beam current necessary to sustain UHDR treatments over large tumor volumes. Future developments should focus on high-current cyclotrons and synchrotrons, as well as emerging laser-driven proton acceleration techniques, to enable broader clinical adoption of FLASH-RT. Novel beam delivery methods, such as real-time adaptive scanning, could further enhance treatment precision. Furthermore, the inconsistent definitions of dose rate in FLASH-RT research pose a significant hurdle. Standardization of metrics such as DADR, PBSDR, and DTDR is crucial for ensuring comparability across studies and guiding clinical implementation. More sophisticated dose rate models that incorporate biological responses in real-time could further refine treatment planning.

Although significant progress has been made in elucidating the FLASH effect, gaps remain in our understanding of ROS dynamics, redox balance, and immune

modulation. Future studies should investigate the interaction between oxidative stress and cellular response pathways, with a focus on validating these mechanisms in human tissue models. Additionally, the impact of different LETs on ROS formation and their implications for treatment efficacy should be further explored.

In the end, MBRT shares similarities with FLASH-RT in its ability to spare normal tissues while maintaining tumor control. This dissertation has established H_2O_2 as a potential surrogate for MBRT dose distribution, addressing limitations in previous diffusion models. Further research should explore the combination of MBRT with FLASH-RT principles to enhance therapeutic benefits. The integration of refined H_2O_2 -based models into treatment planning systems could provide a novel approach to optimizing MBRT protocols.

4.5 Conclusion

This dissertation contributes to the field of FLASH-RT by advancing technical methodologies, exploring fundamental radiochemical mechanisms, and evaluating MBRT as a complementary approach. While substantial preclinical evidence supports the potential of FLASH-RT, further experimental validation and clinical trials are essential to establish its role as a standard-of-care modality in oncology.

5. ZUSAMMENFASSUNG

Die FLASH-Strahlentherapie (FLASH-RT), die mit ultrahoher Dosisleistung (UHDR) verabreicht wird, hat eine bemerkenswerte Fähigkeit zur Schonung von gesundem Gewebe bei gleichzeitig effektiver Tumorkontrolle gezeigt. Unter den verschiedenen Modalitäten zeichnet sich die protonen-konforme FLASH-RT durch ihre überlegene Dosis-Konjungierung und die Machbarkeit der UHDR-Applikation mittels moderner Strahlführungssysteme aus. Diese Dissertation bietet eine umfassende Untersuchung ihrer Entwicklung, Implementierung und Optimierung und integriert sowohl technische Fortschritte als auch mechanistische Erkenntnisse.

Eine zentrale ungeklärte Frage war bisher, warum UHDR eine geringere Wasserstoffperoxid-(H_2O_2)-Produktion aufweist, da frühere Studien widersprüchliche Ergebnisse lieferten. Diese Dissertation adressiert dieses Problem und zeigt anhand experimenteller Daten, dass solvatisierte Elektronen für die reduzierte H_2O_2 -Bildung unter UHDR-Bedingungen verantwortlich sind. Durch den Einsatz von Scavengern für solvatisierte Elektronen demonstrieren wir, dass die Dosisratenabhängigkeit der H_2O_2 -Produktion verschwindet, womit wir erstmals eine eindeutige Klärung dieser langjährigen Debatte liefern.

Darüber hinaus entwickeln wir ein analytisches Modell zur Simulation der H_2O_2 -Verteilung unter Mikrostrahlentherapie-(MBRT)-Bedingungen und validieren dieses Modell durch den Vergleich mit Tierexperimenten. Die Ergebnisse zeigen, dass unsere Simulation die experimentellen Daten präzise vorhersagt und neue Einblicke in die zugrundeliegenden Mechanismen des Minibeam-Effekts liefert. Dieser trägt, ähnlich wie die FLASH-RT, zur Schonung von gesundem Gewebe bei, während die Tumorkontrolle erhalten bleibt. Diese Dissertation integriert somit technische Innovationen und mechanistische Erkenntnisse zur weiteren Optimierung der nächsten Generation der Strahlentherapie.

5.1 Technische Fortschritte in der protonen-konformen FLASH-RT

Verschiedene Techniken wurden entwickelt, um eine konforme protonen-basierte FLASH-RT zu ermöglichen:

- Transmission Beam (TB): Die klinisch am besten untersuchte Methode, die die höchste Dosisleistung erreicht, jedoch eine unvermeidbare Austrittsdosis aufweist.
- Single-Energy Bragg Peak (SEBP): Verbessert die Konformität durch Eliminierung der Austrittsdosis, erfordert jedoch patientenspezifische Reichweitenkompensatoren.
- Single-Energy Spread-Out Bragg Peak (SESOBP): Verwendet Reichweitenmodulationsfolien, um den Bragg-Peak zu erweitern, ermöglicht die Einzelfeld-FLASH-Applikation, erhöht jedoch die Neutronenkontamination.
- Hybrid FLASH-RT: Kombiniert TB mit SEBP oder SESOBP, um eine breitere FLASH-Dosisrate-Abdeckung zu erreichen und gleichzeitig die normale Gewebetoxizität zu reduzieren.
- Multi-Energy Spread-Out Bragg Peak (MESOBP): Wird durch supraleitende Gantries ermöglicht und erlaubt eine ultraschnelle Energieschaltung zur Optimierung der Dosisratenverteilung.

Trotz dieser Fortschritte bestehen weiterhin Herausforderungen, darunter die unzureichende Strahlstromkapazität bestehender Zyklotron-/Synchrotron-Systeme, die Komplexität der Dosisratenoptimierung und der Bedarf an robusten Behandlungsplanungssystemen (TPS). Verschiedene Modelle zur Quantifizierung der Dosisrate in der Punkt-Scanning-Technik (PBS) wurden vorgeschlagen, darunter DADR (Dose-Averaged Dose Rate), PBSDR (Pencil Beam Scanning Dose Rate) und DTDR (Differential Temporal Dose Rate). Diese Modelle liefern jedoch oft unterschiedliche Ergebnisse, was die Standardisierung von FLASH-Dosisraten erschwert. Zudem sind die biologischen Mechanismen des FLASH-Effekts noch nicht vollständig verstanden, was die Optimierung von Behandlungsstrategien für verschiedene Tumorarten und anatomische Regionen behindert.

Ein zentraler Aspekt zukünftiger Forschung ist die Entwicklung von TPS, die FLASH-spezifische Dosisraten berücksichtigen und eine Echtzeitüberwachung der Dosisrate in klinische Abläufe integrieren. Darüber hinaus sollten neue Beschleunigertechnologien erforscht werden, die eine konsistente UHDR-Applikation über größere Behandlungsvolumina ermöglichen. Obwohl zahlreiche präklinische und rechnergestützte Studien die Machbarkeit der Protonen-FLASH-RT belegen, ist die klinische Validierung durch gut konzipierte Studien unerlässlich, um sowohl die Wirksamkeit als auch die Langzeitsicherheit in Patienten zu bewerten.

5.2 Biologische und mechanistische Erkenntnisse zur FLASH-RT

Trotz des vielversprechenden therapeutischen Potenzials ist der Mechanismus hinter der FLASH-RT noch nicht vollständig geklärt. Mehrere Hypothesen wurden vorgeschlagen:

- Oxygen Depletion Hypothesis: Besagt, dass UHDR den Sauerstoff schnell verbraucht, was zu einer vorübergehenden Hypoxie führt und die strahleninduzierte Schädigung reduziert. Neuere Studien zeigen jedoch, dass Sauerstoffverbrauch allein insbesondere bei Hoch-LET-Strahlung nicht ausreicht.
- RRR Hypothesis: FLASH-RT fördert die Rekombination von Radikalen und reduziert so oxidative Schäden. Widersprüchliche experimentelle Ergebnisse stellen jedoch diese Hypothese infrage.

Ein Hauptfokus dieser Dissertation liegt auf der H_2O_2 -Dynamik unter UHDR, da dieses Molekül eine Schlüsselrolle in der strahleninduzierten Zellschädigung spielt. Während Monte-Carlo-Simulationen oft eine erhöhte H_2O_2 -Bildung unter UHDR vorhersagen, zeigen unsere experimentellen Daten eindeutig, dass solvatisierte Elektronen für die reduzierte H_2O_2 -Produktion verantwortlich sind. Wir zeigen, dass die Dosisratenabhängigkeit der H_2O_2 -Bildung verschwindet, wenn Scavenger für solvatisierte Elektronen hinzugefügt werden, was die zentrale Rolle von e_{aq}^- bei der Unterdrückung der H_2O_2 -Bildung unter UHDR bestätigt.

Zusätzlich liefern unsere 1-Spill- versus 3-Spill-UHDR-Experimente entscheidende Beweise, die die Annahme in Monte-Carlo-Studien widerlegen, dass UHDR eine erhöhte H_2O_2 -Produktion verursacht. Während theoretische Modelle nahelegten, dass langlebige Radikale zu einer reduzierten Ausbeute unter konventionellen (CONV) Bedingungen beitragen könnten, zeigen unsere experimentellen Ergebnisse das Gegenteil. Sie belegen, dass Monte-Carlo-Simulationen die Radikalkonzentration

und deren Einfluss auf die H₂O₂-Produktion überschätzen. Diese Korrektur bestehender Modelle ist entscheidend für die Verbesserung zukünftiger Simulationen und die präzise Vorhersage der FLASH-Radiochemie.

Darüber hinaus ist diese Dissertation die erste, die CO₂ in die Analyse der FLASH-RT-Radiochemie einbezieht und dessen erheblichen Einfluss auf die Dynamik reaktiver Sauerstoffspezies (ROS) aufzeigt. Unsere Daten zeigen, dass CO₂ die chemische Umgebung des bestrahlten Mediums moduliert, die Radikalrekombination beeinflusst und oxidative Produkte stabilisiert. Die Einbeziehung von CO₂ eröffnet eine neue Perspektive für das Verständnis der FLASH-Effekte, insbesondere im Kontext biologischer Gewebe, in denen die CO₂-Konzentrationen dynamisch variieren.

5.3 H₂O₂ als Surrogat in der MBRT

SFRT, insbesondere MBRT, wurde als alternative Methode zur Erweiterung des therapeutischen Fensters untersucht. Im Gegensatz zu BBRT verwendet MBRT submillimeterfeine Strahlenbündel, die abwechselnd Hochdosis-Peaks und Niedrigdosis-Täler erzeugen. Präklinische Studien haben gezeigt, dass MBRT die normale Gewebetoxizität reduzieren kann, während die Tumorkontrolle erhalten bleibt. Dennoch bleibt die Definition eines geeigneten Surrogatparameters für MBRT eine Herausforderung.

Diese Dissertation untersucht die Machbarkeit der Verwendung der H₂O₂-Verteilung als radiochemisches Surrogat für MBRT. Wir haben bestehende Diffusionsmodelle erheblich verbessert und dabei kritische Einschränkungen früherer Ansätze adressiert. Traditionelle Modelle freier Diffusion gingen davon aus, dass die Strahlung simultan über das gesamte Zielvolumen appliziert wird – eine Annahme, die nicht die sequentielle Natur der realen Strahlenapplikation widerspiegelt. Unser Modell korrigiert dies durch die Integration eines zeitabhängigen Ansatzes, was die Vorhersagegenauigkeit verbessert. Eine weitere bedeutende Verbesserung unseres Modells ist die Berücksichtigung der H₂O₂-Eliminationsmechanismen. Im Gegensatz zu früheren Modellen, die nur die freie Diffusion simulierten, haben wir ein realistischeres Framework implementiert, in dem H₂O₂ aktiv in biologischen Umgebungen eliminiert wird. Diese Verfeinerung ermöglicht eine genauere Darstellung der ROS-Dynamik unter MBRT-Bedingungen.

Zur Validierung unseres Modells haben wir simulierte H₂O₂-Verteilungen mit experimentellen Daten aus früheren MBRT-Tierstudien verglichen. Die Ergebnisse zeigen, dass unser Modell die Behandlungsergebnisse basierend auf der H₂O₂-Konzentration in den Talregionen präzise vorhersagt und damit die Idee stärkt, dass H₂O₂ als verlässliches Surrogat für die MBRT-Dosisverteilung dienen könnte. Darüber hinaus legen unsere Ergebnisse nahe, dass das Gleichgewicht zwischen H₂O₂-Diffusion und -Elimination eine entscheidende Rolle für die Wirksamkeit der MBRT spielt. Insgesamt liefert unsere Forschung ein umfassenderes Framework zum Verständnis der MBRT, indem sie Diffusionsmodellierung verfeinert, Scavenger-Prozesse integriert und experimentelle Validierung einbezieht. Diese Fortschritte eröffnen neue Perspektiven für die Optimierung der MBRT, um die therapeutische Wirksamkeit zu verbessern und gleichzeitig normale Gewebeschäden zu minimieren.

5.4 Zukünftige Entwicklungen in FLASH-RT und MBRT

Die klinische Umsetzung von FLASH-RT und MBRT erfordert die Bewältigung mehrerer zentraler wissenschaftlicher und technologischer Herausforderungen. Dazu gehören die Verbesserung der Maschinenkapazitäten, die Optimierung von Dosisratenmodellen, die weitere Aufklärung zugrunde liegender biologischer Mechanismen und die Integration dieser Fortschritte in klinische Arbeitsabläufe.

Bestehende Teilchenbeschleuniger verfügen nicht über den erforderlichen Strahlstrom, um UHDR-Behandlungen für große Tumervolumina aufrechtzuerhalten. Zukünftige Entwicklungen sollten sich auf Hochstrom-Zyklotrone und -Synchrotrone sowie auf neue lasergetriebene Protonenbeschleunigungstechniken konzentrieren, um eine breitere klinische Anwendung von FLASH-RT zu ermöglichen. Neue Strahlführungsmethoden, wie beispielsweise das adaptive Scanning in Echtzeit, könnten die Behandlungspräzision weiter verbessern. Darüber hinaus stellen die uneinheitlichen Definitionen der Dosisrate in der FLASH-RT-Forschung ein erhebliches Hindernis dar. Die Standardisierung von Metriken wie DADR, PBSDR und DTDR ist entscheidend, um die Vergleichbarkeit zwischen Studien sicherzustellen und die klinische Umsetzung zu erleichtern. Fortschrittlichere Dosisratenmodelle, die biologische Reaktionen in Echtzeit berücksichtigen, könnten die Behandlungsplanung weiter verfeinern.

Obwohl bedeutende Fortschritte bei der Aufklärung des FLASH-Effekts erzielt wurden, bestehen weiterhin Wissenslücken in Bezug auf die Dynamik reaktiver Sauerstoffspezies (ROS), das Redox-Gleichgewicht und die Immunmodulation. Zukünftige Studien sollten die Wechselwirkung zwischen oxidativem Stress und zellulären Signalwegen untersuchen, mit einem besonderen Fokus auf die Validierung dieser Mechanismen in humanen Gewebemodellen. Darüber hinaus sollte der Einfluss unterschiedlicher LETs auf die ROS-Bildung und deren Auswirkungen auf die Behandlungseffizienz weiter erforscht werden.

Letztendlich weist MBRT Ähnlichkeiten mit FLASH-RT auf, da beide Methoden normales Gewebe schonen und gleichzeitig die Tumorkontrolle aufrechterhalten. Diese Dissertation hat H_2O_2 als potenzielles Surrogat für die MBRT-Dosisverteilung etabliert und dabei Einschränkungen früherer Diffusionsmodelle adressiert. Weitere Forschung sollte die Kombination von MBRT mit FLASH-RT-Prinzipien untersuchen, um die therapeutischen Vorteile zu maximieren. Die Integration verfeinerter H_2O_2 -basierter Modelle in Behandlungsplanungssysteme könnte einen neuartigen Ansatz zur Optimierung von MBRT-Protokollen bieten.

5.5 Abschluss

Diese Dissertation leistet einen Beitrag zum Bereich der FLASH-RT, indem sie technische Methoden weiterentwickelt, grundlegende radiochemische Mechanismen untersucht und MBRT als komplementären Ansatz bewertet. Während umfangreiche präklinische Evidenz das Potenzial der FLASH-RT unterstützt, sind weitere experimentelle Validierungen und klinische Studien erforderlich, um ihre Rolle als Standardtherapie in der Onkologie zu etablieren.

6. LITERATURE

1. Daugherty EC, Zhang Y, Xiao Z, et al. FLASH radiotherapy for the treatment of symptomatic bone metastases in the thorax (FAST-02): protocol for a prospective study of a novel radiotherapy approach. *Radiation Oncology*. 2024/03/12 2024;19(1):34. doi:10.1186/s13014-024-02419-4
2. Mascia AE, Daugherty EC, Zhang Y, et al. Proton FLASH Radiotherapy for the Treatment of Symptomatic Bone Metastases: The FAST-01 Nonrandomized Trial. *JAMA Oncology*. 2023;9(1):62-69. doi:10.1001/jamaoncol.2022.5843
3. Vozenin M-C, De Fornel P, Petersson K, et al. The Advantage of FLASH Radiotherapy Confirmed in Mini-pig and Cat-cancer Patients. *Clin Cancer Res*. 2019;25(1):35-42. doi:10.1158/1078-0432.Ccr-17-3375
4. Vozenin MC, Hendry JH, Limoli CL. Biological Benefits of Ultra-high Dose Rate FLASH Radiotherapy: Sleeping Beauty Awoken. *Clin Oncol*. 2019;31(7):407-415. doi:10.1016/j.clon.2019.04.001
5. Bourhis J, Montay-Gruel P, Gonçalves Jorge P, et al. Clinical translation of FLASH radiotherapy: Why and how? *Radiother Oncol*. 2019;139:11-17. doi:10.1016/j.radonc.2019.04.008
6. Sørensen BS, Sitarz MK, Ankjærgaard C, et al. Pencil beam scanning proton FLASH maintains tumor control while normal tissue damage is reduced in a mouse model. *Radiother Oncol*. 2022;175:178-184. doi:10.1016/j.radonc.2022.05.014
7. Friedl AA, Prise KM, Butterworth KT, Montay-Gruel P, Favaudon V. Radiobiology of the FLASH effect. *Med Phys*. 2022;49(3):1993-2013. doi:10.1002/mp.15184
8. Jolly S, Owen H, Schippers M, Welsch C. Technical challenges for FLASH proton therapy. *Phys Med*. 2020;78:71-82. doi:10.1016/j.ejmp.2020.08.005
9. Jin J-Y, Gu A, Wang W, Oleinick NL, Machtay M, Kong F-M. Ultra-high dose rate effect on circulating immune cells: A potential mechanism for FLASH effect? *Radiother Oncol*. 2020;149:55-62. doi:10.1016/j.radonc.2020.04.054
10. Favaudon V, Caplier L, Monceau V, et al. Ultrahigh dose-rate FLASH irradiation increases the differential response between normal and tumor tissue in mice. *Sci Transl Med*. 2014;6(245):245ra93-245ra93. doi:10.1126/scitranslmed.3008973
11. Newhauser WD, Zhang R. The physics of proton therapy. *Phys Med Biol*. 2015;60(8):R155. doi:10.1088/0031-9155/60/8/R155
12. Wei S, Lin H, Choi JI, et al. FLASH Radiotherapy Using Single-Energy Proton PBS Transmission Beams for Hypofractionation Liver Cancer: Dose and Dose Rate Quantification. Original Research. *Front Oncol*. 2022-January-13 2022;11doi:10.3389/fonc.2021.813063
13. Kang M, Wei S, Choi JI, Simone CB, Lin H. Quantitative Assessment of 3D Dose Rate for Proton Pencil Beam Scanning FLASH Radiotherapy and Its Application for Lung Hypofractionation Treatment Planning. *Cancers (Basel)*. 2021;13(14):3549. doi:10.3390/cancers13143549
14. Shen J, Tryggestad E, Younkin JE, et al. Technical Note: Using experimentally determined proton spot scanning timing parameters to accurately model beam delivery time. *Med Phys*. 2017;44(10):5081-5088. doi:<https://doi.org/10.1002/mp.12504>
15. Koschik A, Bula C, Duppich J, et al. Gantry 3: further development of the PSI PROSCAN proton therapy facility. Joint Accelerator Conferences Website-JACoW; 2015:2275-2277.

-
16. Esplen N, Mendonca MS, Bazalova-Carter M. Physics and biology of ultrahigh dose-rate (FLASH) radiotherapy: a topical review. *Phys Med Biol*. 2020/12/01 2020;65(23):23TR03. doi:10.1088/1361-6560/abaa28
 17. Van De Water S, Safai S, Schippers JM, Weber DC, Lomax AJ. Towards FLASH proton therapy: the impact of treatment planning and machine characteristics on achievable dose rates. *Acta Oncol*. 2019;58(10):1463-1469. doi:10.1080/0284186X.2019.1627416
 18. Schwarz M, Traneus E, Safai S, Kolano A, van de Water S. Treatment planning for Flash radiotherapy: General aspects and applications to proton beams. *Med Phys*. 2022;49(4):2861-2874. doi:10.1002/mp.15579
 19. Wei S, Lin H, Shi C, et al. Use of single-energy proton pencil beam scanning Bragg peak for intensity-modulated proton therapy FLASH treatment planning in liver-hypofractionated radiation therapy. *Med Phys*. 2022;49(10):6560-6574. doi:10.1002/mp.15894
 20. Folkerts MM, Abel E, Busold S, Perez JR, Krishnamurthi V, Ling CC. A framework for defining FLASH dose rate for pencil beam scanning. *Med Phys*. 2020;47(12):6396-6404. doi:doi.org/10.1002/mp.14456
 21. Zeng Y, Li H, Wang W, et al. Feasibility study of multiple-energy Bragg peak proton FLASH on a superconducting gantry with large momentum acceptance. *Med Phys*. 2024;51(3):2164-2174. doi:10.1002/mp.16932
 22. Liu G, Zhao L, Li X, et al. A Novel Ultrahigh-Dose-Rate Proton Therapy Technology: Spot-Scanning Proton Arc Therapy + FLASH (SPLASH). *Int J Radiat Oncol Biol Phys*. 2023/11/01/ 2023;117(3):730-737. doi:<https://doi.org/10.1016/j.ijrobp.2023.05.012>
 23. Rothwell B, Bertolet A, Schuemann J. Proton FLASH-arc therapy (PFAT): A feasibility study for meeting FLASH dose-rate requirements in the clinic. *Radiother Oncol*. 2025/01/01/ 2025;202:110623. doi:<https://doi.org/10.1016/j.radonc.2024.110623>
 24. van Marlen P, Dahele M, Folkerts M, Abel E, Slotman BJ, Verbakel W. Ultra-High Dose Rate Transmission Beam Proton Therapy for Conventionally Fractionated Head and Neck Cancer: Treatment Planning and Dose Rate Distributions. *Cancers (Basel)*. 2021;13(8):1859. doi:10.3390/cancers13081859
 25. Diffenderfer ES, Verginadis II, Kim MM, et al. Design, Implementation, and in Vivo Validation of a Novel Proton FLASH Radiation Therapy System. *Int J Radiat Oncol Biol Phys*. 2020/02/01/ 2020;106(2):440-448. doi:10.1016/j.ijrobp.2019.10.049
 26. Verhaegen F, Wanders R-G, Wolfs C, Eekers D. Considerations for shoot-through FLASH proton therapy. *Phys Med Biol*. 2021/03/02 2021;66(6):06NT01. doi:10.1088/1361-6560/abe55a
 27. Wei S, Lin H, Huang S, et al. Dose rate and dose robustness for proton transmission FLASH-RT treatment in lung cancer. Original Research. *Front Oncol*. 2022-August-15 2022;12doi:10.3389/fonc.2022.970602
 28. van Marlen P, Dahele M, Folkerts M, Abel E, Slotman BJ, Verbakel WFAR. Bringing FLASH to the Clinic: Treatment Planning Considerations for Ultrahigh Dose-Rate Proton Beams. *Int J Radiat Oncol Biol Phys*. 2020/03/01/ 2020;106(3):621-629. doi:10.1016/j.ijrobp.2019.11.011
 29. Gao H, Lin B, Lin Y, et al. Simultaneous dose and dose rate optimization (SDDRO) for FLASH proton therapy. *Med Phys*. 2020;47(12):6388-6395. doi:10.1002/mp.14531

-
30. Kneepkens E, Wolfs C, Wanders R-G, Traneus E, Eekers D, Verhaegen F. Shoot-through proton FLASH irradiation lowers linear energy transfer in organs at risk for neurological tumors and is robust against density variations. *Phys Med Biol.* 2023/11/02 2023;68(21):215020. doi:10.1088/1361-6560/ad0280
 31. Gao H, Liu J, Lin Y, et al. Simultaneous dose and dose rate optimization (SDDRO) of the FLASH effect for pencil-beam-scanning proton therapy. *Med Phys.* 2022;49(3):2014-2025. doi:10.1002/mp.15356
 32. Kang M, Wei S, Choi JI, Lin H, Simone CB. A Universal Range Shifter and Range Compensator Can Enable Proton Pencil Beam Scanning Single-Energy Bragg Peak FLASH-RT Treatment Using Current Commercially Available Proton Systems. *Int J Radiat Oncol Biol Phys.* 2022/05/01/ 2022;113(1):203-213. doi:10.1016/j.ijrobp.2022.01.009
 33. Vyfhuis MAL, Onyeuku N, Diwanji T, et al. Advances in proton therapy in lung cancer. *Ther Adv Respir Dis.* 2018;12:1753466618783878. doi:10.1177/1753466618783878
 34. Siddon RL. Prism representation: a 3D ray-tracing algorithm for radiotherapy applications. *Phys Med Biol.* 1985/08/01 1985;30(8):817. doi:10.1088/0031-9155/30/8/005
 35. Girdhani S, Labarbe R, Traneus E. IBA ConformalFLASH. <https://www.iba-protontherapy.com/conformalflash-0>
 36. Gata-Danil G, Parajpan M, Timoshenko G. Ridge filter design for carbon radiotherapy. 2008:14. [http://www1.jinr.ru/Preprints/2008/136\(E16-2008-136\).pdf](http://www1.jinr.ru/Preprints/2008/136(E16-2008-136).pdf)
 37. Fujimoto R, Takayanagi T, Fujitaka S. Design of a ridge filter structure based on the analysis of dose distributions. *Phys Med Biol.* 2009/06/17 2009;54(13):N273. doi:10.1088/0031-9155/54/13/N03
 38. Courneyea L, Beltran C, Tseung HSWC, Yu J, Herman MG. Optimizing mini-ridge filter thickness to reduce proton treatment times in a spot-scanning synchrotron system. *Med Phys.* 2014;41(6Part1):061713. doi:10.1118/1.4876276
 39. O'Grady F, Janson M, Rao AD, et al. The use of a mini-ridge filter with cyclotron-based pencil beam scanning proton therapy. *Med Phys.* 2023;50(4):1999-2008. doi:10.1002/mp.16254
 40. Kim MM, Verginadis II, Goia D, et al. Comparison of FLASH Proton Entrance and the Spread-Out Bragg Peak Dose Regions in the Spruing of Mouse Intestinal Crypts and in a Pancreatic Tumor Model. *Cancers (Basel).* 2021;13(16):4244. doi:10.3390/cancers13164244
 41. Patriarca A, Fouillade C, Auger M, et al. Experimental Set-up for FLASH Proton Irradiation of Small Animals Using a Clinical System. *Int J Radiat Oncol Biol Phys.* 2018/11/01/ 2018;102(3):619-626. doi:10.1016/j.ijrobp.2018.06.403
 42. Evans T, Cooley J, Wagner M, Yu T, Zwart T. Demonstration of the FLASH Effect Within the Spread-out Bragg Peak After Abdominal Irradiation of Mice. *Int J Part Ther.* 2022/03/01/ 2022;8(4):68-75. doi:10.14338/IJPT-20-00095
 43. Kristensen L, Poulsen PR, Kanouta E, et al. Spread-out Bragg peak FLASH: quantifying normal tissue toxicity in a murine model. Original Research. *Front Oncol.* 2024-July-03 2024;14doi:10.3389/fonc.2024.1427667
 44. Chen D, Motlagh SAO, Stappen FV, et al. Secondary neutron dosimetry for conformal FLASH proton therapy. *Med Phys.* 2024;51(7):5081-5093. doi:10.1002/mp.17050

-
45. Uli W, Gerhard K. Design and construction of a ripple filter for a smoothed depth dose distribution in conformal particle therapy. *Phys Med Biol.* 1999/11/01 1999;44(11):2765. doi:10.1088/0031-9155/44/11/306
 46. Sakae T, Nohtomi A, Maruhashi A, et al. Multi-layer energy filter for realizing conformal irradiation in charged particle therapy. *Med Phys.* 2000;27(2):368-373. doi:10.1118/1.598840
 47. Nakagawa T, Yoda K. A method for achieving variable widths of the spread-out Bragg peak using a ridge filter. *Med Phys.* 2000;27(4):712-715. doi:10.1118/1.598933
 48. Kostjuchenko V, Nichiporov D, Luckjashin V. A compact ridge filter for spread out Bragg peak production in pulsed proton clinical beams. *Med Phys.* 2001;28(7):1427-1430. doi:10.1118/1.1380433
 49. Tansho R, Furukawa T, Hara Y, et al. Development of a new ridge filter with honeycomb geometry for a pencil beam scanning system in particle radiotherapy. *Nucl Instrum Methods Phys Res, Sect B.* 2017/09/01/ 2017;406:352-355. doi:10.1016/j.nimb.2016.10.009
 50. Takashi A, Akio H, Hironobu T, Hidenobu S, Yasutaka M, Yoshio H. Ridge filter design for proton therapy at Hyogo Ion Beam Medical Center. *Phys Med Biol.* 2003/10/24 2003;48(22):N301. doi:10.1088/0031-9155/48/22/N01
 51. Liu R, Charyyev S, Wahl N, et al. An Integrated Physical Optimization Framework for Proton Stereotactic Body Radiation Therapy FLASH Treatment Planning Allows Dose, Dose Rate, and Linear Energy Transfer Optimization Using Patient-Specific Ridge Filters. *Int J Radiat Oncol Biol Phys.* 2023;116(4):949-959. doi:10.1016/j.ijrobp.2023.01.048
 52. Simeonov Y, Weber U, Penchev P, et al. 3D range-modulator for scanned particle therapy: development, Monte Carlo simulations and experimental evaluation. *Phys Med Biol.* 2017/08/11 2017;62(17):7075. doi:10.1088/1361-6560/aa81f4
 53. Zhang Z, Zhao W, Butkus M, Wu X. Conformal dose modulator for proton beam therapy: A simulation study. *Research Square.* 2023;doi:10.21203/rs.3.rs-2488761/v1
 54. Jeon C, Ahn S, Amano D, et al. FLASH dose rate calculation based on log files in proton pencil beam scanning therapy. *Med Phys.* 2023;50(11):7154-7166. doi:10.1002/mp.16575
 55. Zhang G, Gao W, Peng H. Design of static and dynamic ridge filters for FLASH-IMPT: A simulation study. *Med Phys.* 2022;49(8):5387-5399. doi:10.1002/mp.15717
 56. Maradia V, Colizzi I, Meer D, et al. Universal and dynamic ridge filter for pencil beam scanning particle therapy: a novel concept for ultra-fast treatment delivery. *Phys Med Biol.* 2022/11/07 2022;67(22):225005. doi:10.1088/1361-6560/ac9d1f
 57. Ma C, Zhou J, Chang C-W, et al. Streamlined pin-ridge-filter design for single-energy proton FLASH planning. *Med Phys.* 2024;51(4):2955-2966. doi:10.1002/mp.16939
 58. Simeonov Y, Weber U, Schuy C, et al. Development, Monte Carlo simulations and experimental evaluation of a 3D range-modulator for a complex target in scanned proton therapy. *Biomed Phys Eng Express.* 2022/03/11 2022;8(3):035006. doi:10.1088/2057-1976/ac5937
 59. Hachadorian R, Cascio E, Schuemann J. Increased flexibility and efficiency of a double-scattering FLASH proton beamline configuration for in vivo SOBP

-
- radiotherapy treatments. *Phys Med Biol.* 2023/07/24 2023;68(15):15NT01. doi:10.1088/1361-6560/ace23c
60. Ma J, Lin Y, Tang M, et al. Simultaneous dose and dose rate optimization via dose modifying factor modeling for FLASH effective dose. *Med Phys.* 2024;51(8):5190-5203. doi:10.1002/mp.17251
61. Luo Y, Zhu Y, Setianegara J, al. e. Single-field-uniform-dose-per-fraction simultaneous dose and dose rate optimization (SFUDPF-SDDRO) method for proton FLASH therapy. *Submitted.* 2024;
62. Bowman E, Luevano R, Mohr S, Hellstern C, Djurovic B. Dynamic three-dimensional beam modification for radiation therapy. Varian Medical Systems, Inc (Palo Alto, CA); 2018.
63. Lin Y, Lin B, Fu S, et al. SDDRO-joint: simultaneous dose and dose rate optimization with the joint use of transmission beams and Bragg peaks for FLASH proton therapy. *Phys Med Biol.* 2021/06/14 2021;66(12):125011. doi:10.1088/1361-6560/ac02d8
64. Ma C, Yang X, Chang C-W, et al. Feasibility study of hybrid inverse planning with transmission beams and single-energy spread-out Bragg peaks for proton FLASH radiotherapy. *Med Phys.* 2023;50(6):3687-3700. doi:10.1002/mp.16370
65. MacKay R, Burnet N, Lowe M, et al. FLASH radiotherapy: Considerations for multibeam and hypofractionation dose delivery. *Radiother Oncol.* 2021;164:122-127. doi:10.1016/j.radonc.2021.09.011
66. Wilson P, Jones B, Yokoi T, Hill M, Vojnovic B. Revisiting the ultra-high dose rate effect: implications for charged particle radiotherapy using protons and light ions. *Br J Radiol.* 2014;85(1018):e933-e939. doi:10.1259/bjr/17827549
67. Sørensen BS, Kanouta E, Ankjærgaard C, et al. Proton FLASH: Impact of Dose Rate and Split Dose on Acute Skin Toxicity in a Murine Model. *Int J Radiat Oncol Biol Phys.* doi:10.1016/j.ijrobp.2024.04.071
68. Montay-Gruel P, Petersson K, Jaccard M, et al. Irradiation in a flash: Unique sparing of memory in mice after whole brain irradiation with dose rates above 100Gy/s. *Radiother Oncol.* 2017;124(3):365-369. doi:10.1016/j.radonc.2017.05.003
69. Hornsey S, Bewley DK. Hypoxia in Mouse Intestine Induced by Electron Irradiation at High Dose-rates. *International Journal of Radiation Biology and Related Studies in Physics, Chemistry and Medicine.* 1971/01/01 1971;19(5):479-483. doi:10.1080/09553007114550611
70. Chabi S, To THV, Leavitt R, et al. Ultra-high-dose-rate FLASH and Conventional-Dose-Rate Irradiation Differentially Affect Human Acute Lymphoblastic Leukemia and Normal Hematopoiesis. *Int J Radiat Oncol Biol Phys.* 2021;109(3):819-829. doi:10.1016/j.ijrobp.2020.10.012
71. Prax G, Kapp DS. A computational model of radiolytic oxygen depletion during FLASH irradiation and its effect on the oxygen enhancement ratio. *Phys Med Biol.* 2019;64(18):185005.
72. Mascia A, McCauley S, Speth J, et al. Impact of Multiple Beams on the FLASH Effect in Soft Tissue and Skin in Mice. *Int J Radiat Oncol Biol Phys.* 2024;118(1):253-261. doi:10.1016/j.ijrobp.2023.07.024
73. Galts A, Hammi A. FLASH radiotherapy sparing effect on the circulating lymphocytes in pencil beam scanning proton therapy: impact of hypofractionation and dose rate. *Phys Med Biol.* 2024/01/05 2024;69(2):025006. doi:10.1088/1361-6560/ad144e

-
74. Montay-Gruel P, Acharya MM, Petersson K, et al. Long-term neurocognitive benefits of FLASH radiotherapy driven by reduced reactive oxygen species. *Proc Natl Acad Sci U S A*. May 28 2019;116(22):10943-10951. doi:10.1073/pnas.1901777116
 75. Levy K, Natarajan S, Wang J, et al. Abdominal FLASH irradiation reduces radiation-induced gastrointestinal toxicity for the treatment of ovarian cancer in mice. *Scientific Reports*. 2020/12/10 2020;10(1):21600. doi:10.1038/s41598-020-78017-7
 76. Valdés Zayas A, Kumari N, Liu K, et al. Independent Reproduction of the FLASH Effect on the Gastrointestinal Tract: A Multi-Institutional Comparative Study. *Cancers (Basel)*. 2023;15(7):2121.
 77. Børresen B, Arendt ML, Konradsson E, et al. Evaluation of single-fraction high dose FLASH radiotherapy in a cohort of canine oral cancer patients. *Original Research. Front Oncol*. 2023-September-11 2023;13doi:10.3389/fonc.2023.1256760
 78. Rohrer Bley C, Wolf F, Gonçalves Jorge P, et al. Dose- and Volume-Limiting Late Toxicity of FLASH Radiotherapy in Cats with Squamous Cell Carcinoma of the Nasal Planum and in Mini Pigs. *Clin Cancer Res*. 2022;28(17):3814-3823. doi:10.1158/1078-0432.Ccr-22-0262
 79. Pennock M, Wei S, Cheng C, et al. Proton Bragg Peak FLASH Enables Organ Sparing and Ultra-High Dose-Rate Delivery: Proof of Principle in Recurrent Head and Neck Cancer. *Cancers (Basel)*. 2023;15(15):3828. doi:10.3390/cancers15153828
 80. Wei S, Lin H, Isabelle Choi J, Shi C, Simone CB, Kang M. Advanced pencil beam scanning Bragg peak FLASH-RT delivery technique can enhance lung cancer planning treatment outcomes compared to conventional multiple-energy proton PBS techniques. *Radiother Oncol*. 2022/10/01/ 2022;175:238-247. doi:10.1016/j.radonc.2022.08.005
 81. van Marlen P, van de Water S, Dahele M, Slotman BJ, Verbakel WFA. Single Ultra-High Dose Rate Proton Transmission Beam for Whole Breast FLASH-Irradiation: Quantification of FLASH-Dose and Relation with Beam Parameters. *Cancers (Basel)*. 2023;15(9):2579. doi:10.3390/cancers15092579
 82. Lattery G, Kaulfers T, Cheng C, et al. Pencil Beam Scanning Bragg Peak FLASH Technique for Ultra-High Dose Rate Intensity-Modulated Proton Therapy in Early-Stage Breast Cancer Treatment. *Cancers (Basel)*. 2023;15(18):4560. doi:10.3390/cancers15184560
 83. Kaulfers T, Lattery G, Cheng C, et al. Pencil Beam Scanning Proton Bragg Peak Conformal FLASH in Prostate Cancer Stereotactic Body Radiotherapy. *Cancers (Basel)*. 2024;16(4):798. doi:10.3390/cancers16040798
 84. Krieger M, van de Water S, Folkerts MM, et al. A quantitative FLASH effectiveness model to reveal potentials and pitfalls of high dose rate proton therapy. *Med Phys*. 2022;49(3):2026-2038. doi:10.1002/mp.15459
 85. José Santo R, Habraken SJM, Breedveld S, Hoogeman MS. Pencil-beam Delivery Pattern Optimization Increases Dose Rate for Stereotactic FLASH Proton Therapy. *Int J Radiat Oncol Biol Phys*. 2023;115(3):759-767. doi:10.1016/j.ijrobp.2022.08.053
 86. Zhao X, Huang S, Lin H, et al. A Novel Dose Rate Optimization Method to Maximize Ultrahigh-Dose-Rate Coverage of Critical Organs at Risk Without Compromising Dosimetry Metrics in Proton Pencil Beam Scanning FLASH Radiation Therapy. *Int J Radiat Oncol Biol Phys*. 2024;Epub ahead of printdoi:10.1016/j.ijrobp.2024.06.002

-
87. Wieser H-P, Cisternas E, Wahl N, et al. Development of the open-source dose calculation and optimization toolkit matRad. *Med Phys*. 2017;44(6):2556-2568. doi:10.1002/mp.12251
 88. Alex B, M K, L L. Implementation of a novel pencil beam scanning Bragg peak FLASH technique to a commercial treatment planning system. 2024;
 89. Adrian G, Konradsson E, Lempart M, Bäck S, Ceberg C, Petersson K. The FLASH effect depends on oxygen concentration. *The British journal of radiology*. 2020;93(1106):20190702.
 90. Tessonnier T, Mein S, Walsh DW, et al. FLASH dose rate helium ion beams: first in vitro investigations. *Int J Radiat Oncol Biol Phys*. 2021;111(4):1011-1022.
 91. Cooper CR, Jones D, Jones GD, Petersson K. FLASH irradiation induces lower levels of DNA damage ex vivo, an effect modulated by oxygen tension, dose, and dose rate. *The British Journal of Radiology*. 2022;95(1133):20211150.
 92. Grimes DR, Partridge M. A mechanistic investigation of the oxygen fixation hypothesis and oxygen enhancement ratio. *Biomed Phys Eng Express*. 2015;1(4):045209.
 93. Ewing D. The oxygen fixation hypothesis: a reevaluation. *Am J Clin Oncol*. 1998;21(4):355-361.
 94. Gray LH, Conger AD, Ebert M, Hornsey S, Scott O. The concentration of oxygen dissolved in tissues at the time of irradiation as a factor in radiotherapy. *The British journal of radiology*. 1953;26(312):638-648.
 95. Wenzl T, Wilkens JJ. Modelling of the oxygen enhancement ratio for ion beam radiation therapy. *Phys Med Biol*. 2011;56(11):3251.
 96. Tinganelli W, Durante M. Carbon Ion Radiobiology. *Cancers (Basel)*. 2020;12(10):3022.
 97. Scifoni E, Tinganelli W, Weyrather W, Durante M, Maier A, Krämer M. Including oxygen enhancement ratio in ion beam treatment planning: model implementation and experimental verification. *Phys Med Biol*. 2013;58(11):3871.
 98. Tinganelli W, Sokol O, Quartieri M, et al. Ultra-high dose rate (FLASH) carbon ion irradiation: dosimetry and first cell experiments. *Int J Radiat Oncol Biol Phys*. 2022;112(4):1012-1022.
 99. Tinganelli W, Puspitasari-Kokko A, Sokol O, et al. FLASH Bragg-peak irradiation with a therapeutic carbon ion beam: first in vivo results. *Int J Radiat Oncol Biol Phys*. 2024;
 100. El Khatib M, Motlagh AO, Beyer JN, et al. Direct Measurements of FLASH-Induced Changes in Intracellular Oxygenation. *Int J Radiat Oncol Biol Phys*. Sep 18 2023;doi:10.1016/j.ijrobp.2023.09.019
 101. Cao X, Zhang R, Esipova TV, et al. Quantification of Oxygen Depletion During FLASH Irradiation In Vitro and In Vivo. *Int J Radiat Oncol Biol Phys*. Sep 1 2021;111(1):240-248. doi:10.1016/j.ijrobp.2021.03.056
 102. Jansen J, Knoll J, Beyreuther E, et al. Does FLASH deplete oxygen? Experimental evaluation for photons, protons, and carbon ions. *Med Phys*. 2021;48(7):3982-3990.
 103. Bogaerts E, Macaeva E, Isebaert S, Haustermans K. Potential Molecular Mechanisms behind the Ultra-High Dose Rate "FLASH" Effect. *International Journal of Molecular Sciences*. 2022;23(20):12109.

-
104. Boyd A, Carver M, Dixon R. Computed and experimental product concentrations in the radiolysis of water. *Radiation Physics and Chemistry*. 1980;15(2-3):177-185. doi:10.1016/0146-5724(80)90129-6
 105. Buxton GV, Greenstock CL, Helman WP, Ross AB. Critical Review of rate constants for reactions of hydrated electrons, hydrogen atoms and hydroxyl radicals ($\cdot\text{OH}/\cdot\text{O}^-$ in Aqueous Solution. *Journal of physical and chemical reference data*. 1988;17(2):513-886. doi:10.1063/1.555805
 106. Frongillo Y, Goulet T, Fraser MJ, Cobut V, Patau JP, Jay-Gerin J-P. Monte Carlo simulation of fast electron and proton tracks in liquid water -- II. nonhomogeneous chemistry. *Radiation Physics and Chemistry*. 1998;51:245-254.
 107. Gervais B, Beuve M, Olivera G, Galassi ME. Numerical simulation of multiple ionization and high LET effects in liquid water radiolysis. *Radiation Physics and Chemistry*. 2006;75(4):493-513.
 108. LaVerne JA. OH radicals and oxidizing products in the gamma radiolysis of water. *Radiation research*. 2000;153(2):196-200.
 109. Plante I. A review of simulation codes and approaches for radiation chemistry. *Phys Med Biol*. Jan 30 2021;66(3):03TR02. doi:10.1088/1361-6560/abbd19
 110. Sunnerberg JP, Zhang R, Gladstone DJ, Swartz HM, Gui J, Pogue BW. Mean dose rate in ultra-high dose rate electron irradiation is a significant predictor for O₂ consumption and H₂O₂ yield. *Phys Med Biol*. 2023;68(16):165014. doi:10.1088/1361-6560/ace877
 111. Thomas W, Sunnerberg J, Reed M, et al. Proton and Electron Ultrahigh-Dose-Rate Isodose Irradiations Produce Differences in Reactive Oxygen Species Yields. *Int J Radiat Oncol Biol Phys*. Jan 1 2024;118(1):262-267. doi:10.1016/j.ijrobp.2023.07.042
 112. Kacem H, Psoroulas S, Boivin G, et al. Comparing radiolytic production of H₂O₂ and development of Zebrafish embryos after ultra high dose rate exposure with electron and transmission proton beams. *Radiother Oncol*. Oct 2022;175:197-202. doi:10.1016/j.radonc.2022.07.011
 113. Cooper CR, Jones DJ, Jones GD, Petersson K. Comet assay profiling of FLASH-induced damage: mechanistic insights into the effects of FLASH irradiation. *International Journal of Molecular Sciences*. 2023;24(8):7195.
 114. Limoli CL, Vozenin M-C. Reinventing radiobiology in the light of FLASH radiotherapy. *Annual Review of Cancer Biology*. 2023;7:1-21.
 115. Ward JF. DNA damage produced by ionizing radiation in mammalian cells: identities, mechanisms of formation, and reparability. *Progress in nucleic acid research and molecular biology*. 1988;35:95-125.
 116. Eric J. Hall, Giaccia AJ. *Radiobiology for the radiologist, 8th*. Springer; 2018.
 117. Valentin J. *The 2007 recommendations of the international commission on radiological protection*. vol 37. Elsevier Oxford; 2007.
 118. Le Caër S. Water radiolysis: influence of oxide surfaces on H₂ production under ionizing radiation. *Water*. 2011;3(1):235-253.
 119. Guo Z, Kozlov S, Lavin MF, Person MD, Paull TT. ATM activation by oxidative stress. *Science*. 2010;330(6003):517-521.
 120. Barzilai A, Yamamoto K-I. DNA damage responses to oxidative stress. *DNA Repair*. 2004;3(8-9):1109-1115.
 121. Ditch S, Paull TT. The ATM protein kinase and cellular redox signaling: beyond the DNA damage response. *Trends in biochemical sciences*. 2012;37(1):15-22.

-
122. Burrows CJ. Oxidative nucleobase modifications leading to strand scission. *Chem Rev.* 1998;98:1109-1151.
 123. Pogożelski WK, Tullius TD. Oxidative strand scission of nucleic acids: routes initiated by hydrogen abstraction from the sugar moiety. *Chem Rev.* 1998;98(3):1089-1108.
 124. Tullius TD, Greenbaum JA. Mapping nucleic acid structure by hydroxyl radical cleavage. *Curr Opin Chem Biol.* 2005;9(2):127-134.
 125. JN DK, Garcia-Garcia OR, LaVerne JA, et al. An integrated Monte Carlo track-structure simulation framework for modeling inter and intra-track effects on homogenous chemistry. *Phys Med Biol.* Jun 9 2023;68(12)doi:10.1088/1361-6560/acd6d0
 126. Wardman P. Radiotherapy Using High-Intensity Pulsed Radiation Beams (FLASH): A Radiation-Chemical Perspective. *Radiat Res.* Dec 1 2020;194(6):607-617. doi:10.1667/RADE-19-00016
 127. Derksen L, Flatten V, Engenhardt-Cabillic R, Zink K, Baumann K-S. A method to implement inter-track interactions in Monte Carlo simulations with TOPAS-nBio and their influence on simulated radical yields following water radiolysis. *Physics in Medicine and Biology.* 2023;doi:10.1088/1361-6560/acdc7d
 128. Abolfath R, Grosshans D, Mohan R. Oxygen depletion in FLASH ultra-high-dose-rate radiotherapy: A molecular dynamics simulation. *Med Phys.* Dec 2020;47(12):6551-6561. doi:10.1002/mp.14548
 129. Wardman P. Mechanisms of the 'FLASH' effect: radiation chemistry should not be ignored in developing models. *Radiother Oncol.* 2023;184
 130. Lai Y, Jia X, Chi Y. Modeling the effect of oxygen on the chemical stage of water radiolysis using GPU-based microscopic Monte Carlo simulations, with an application in FLASH radiotherapy. *Phys Med Biol.* Jan 26 2021;66(2):025004. doi:10.1088/1361-6560/abc93b
 131. Boscolo D, Kramer M, Durante M, Fuss MC, Scifoni E. TRAX-CHEM: A pre-chemical and chemical stage extension of the particle track structure code TRAX in water targets. *Chemical Physics Letters.* Apr 16 2018;698:11-18. doi:10.1016/j.cplett.2018.02.051
 132. Spinks JW, Woods RJ. An introduction to radiation chemistry. 1990;
 133. Von Sonntag C. The Chemical Basis of Radiation Biology. Taylor & Francis; 1987.
 134. Halliwell B, Gutteridge JM. *Free radicals in biology and medicine.* Oxford university press, USA; 2015.
 135. Baikalov A, Abolfath R, Schüler E, Mohan R, Wilkens JJ, Bartzsch S. Intertrack interaction at ultra-high dose rates and its role in the FLASH effect. *Frontiers in Physics.* 2023;11
 136. Renault JP, Pommeret S. Seeing the solvated electron in action: First-principles molecular dynamics of NO₃⁻ and N₂O reduction. *Radiation Physics and Chemistry.* 2022;190:109810.
 137. Köhler A. Theorie einer Methode, bisher unmöglich anwendbar hohe Dosen Röntgenstrahlen in der Tiefe des Gewebes zur therapeutischen Wirksamkeit zu bringen ohne schwere Schädigung des Patienten, zugleich eine Methode des Schutzes gegen Röntgenverbrennungen überhaupt. *Forsch Geb Röntg.* 1910;14:27.
 138. Marks H. Clinical experience with irradiation through a grid. *Radiology.* 1952;58(3):338-342.

-
139. LE J. Grid depth dose investigation for 200 and 400 kilovolts at the center and edge of the field. *The American Journal of Roentgenology, Radium Therapy, and Nuclear Medicine*. 1953;69(6):991-1000.
 140. Marks H, Rudinger G. Inoperable carcinoma of the lungs; report of a five year survival after roentgen-grid therapy. Some considerations of the physical factors in grip therapy. *Mississippi Valley Medical Journal (Quincy, Ill)*. 1954;76(6):222-225.
 141. Bouchet A, Serduc R, Laissue JA, Djonov V. Effects of microbeam radiation therapy on normal and tumoral blood vessels. *Phys Med*. 2015;31(6):634-641.
 142. Crosbie JC, Anderson RL, Rothkamm K, et al. Tumor cell response to synchrotron microbeam radiation therapy differs markedly from cells in normal tissues. *Int J Radiat Oncol Biol Phys*. 2010;77(3):886-894.
 143. Bertho A, Ortiz R, Juchaux M, et al. First Evaluation of Temporal and Spatial Fractionation in Proton Minibeam Radiation Therapy of Glioma-Bearing Rats. *Cancers (Basel)*. Sep 28 2021;13(19)doi:10.3390/cancers13194865
 144. Bertho A, Ortiz R, Juchaux M, et al. First Evaluation of Temporal and Spatial Fractionation in Proton Minibeam Radiation Therapy of Glioma-Bearing Rats. *Cancers (Basel)*. Sep 28 2021;13(19):4865. doi:10.3390/cancers13194865
 145. Prezado Y, Jouvion G, Guardiola C, et al. Tumor Control in RG2 Glioma-Bearing Rats: A Comparison Between Proton Minibeam Therapy and Standard Proton Therapy. *International Journal of Radiation Oncology Biology Physics*. Jun 1 2019;104(2):266-271. doi:10.1016/j.ijrobp.2019.01.080
 146. Prezado Y, Jouvion G, Patriarca A, et al. Proton minibeam radiation therapy widens the therapeutic index for high-grade gliomas. *Sci Rep*. Nov 7 2018;8(1):16479. doi:10.1038/s41598-018-34796-8
 147. Lamirault C, Brisebard E, Patriarca A, et al. Spatially modulated proton minibeam results in the same increase of lifespan as a uniform target dose coverage in F98-glioma-bearing rats. *Radiation Research*. 2020;194(6):715-723.
 148. Rivera JN, Kierski TM, Kasoji SK, Abrantes AS, Dayton PA, Chang SX. Conventional dose rate spatially-fractionated radiation therapy (SFRT) treatment response and its association with dosimetric parameters-A preclinical study in a Fischer 344 rat model. *PLoS One*. 2020;15(6):e0229053. doi:10.1371/journal.pone.0229053
 149. Sammer M, Dombrowsky AC, Schauer J, et al. Normal Tissue Response of Combined Temporal and Spatial Fractionation in Proton Minibeam Radiation Therapy. *Int J Radiat Oncol Biol Phys*. Jan 1 2021;109(1):76-83. doi:10.1016/j.ijrobp.2020.08.027
 150. Dombrowsky AC, Schauer J, Sammer M, et al. Acute Skin Damage and Late Radiation-Induced Fibrosis and Inflammation in Murine Ears after High-Dose Irradiation. *Cancers (Basel)*. May 25 2019;11(5):727. doi:10.3390/cancers11050727
 151. Dal Bello R, Becher T, Fuss MC, Krämer M, Seco J. Proposal of a chemical mechanism for mini-beam and micro-beam efficacy. *Frontiers in Physics*. 2020;8:564836.

7. APPENDIX

Journal Publications:

- 1, [Zhang T](#), Stengl C, Derksen L, Palskis K, Koritsidis K, Zink K, Adeberg S, Major G, Weishaar D, Theiß U, Jin J, Spadea M, Hesser J, Baumann KS, Seco J, Analysis of Hydrogen Peroxide Production in Pure Water: Ultrahigh vs. Conventional Dose-Rate Irradiation and Mechanistic Insights, *Medical Physics*, 2024 August 02, doi: 10.1002/mp.17335. **Editor's Choice**
- 2, [Zhang T](#), García-Calderón D, Molina-Hernández M, Leitão J, Hesser J, Seco J, A theoretical study of H₂O₂ as the surrogate of dose in minibeam radiotherapy, with a diffusion model considering radical removal process, *Medical Physics*, 2023 June 22, doi: 10.1002/mp.16570. **Editor's Choice**
- 3, Ma Y, [Zhang T \(co-first\)](#), Selvaraj B, Shen J, Wei S, Cheng C, Gao H, Poulsen P, Li H, Diffenderfer E, Schuemann J, Lin L, Folkerts M, Morris Z, Durkee B, Hesser J, Lin H, Simone II C, Kang M, Wu H, Advancing Proton Conformal FLASH Radiation Therapy: Innovations, Techniques, and Clinical Potentials, under review.

Conference Abstract:

1. [Zhang T](#), García-Calderón D, Molina-Hernández M, Leitão J, Hesser J, Seco J, Studying H₂O₂ as the surrogate of physical dose in Minibeam radiotherapy. **Oral presentation** (FRPT 2023).
2. [Zhang T](#), Stengl C, Derksen L, Zink K, Adeberg S, Major G, Hesser J, Baumann KS, Seco J, Unveiling the enigma: does Flash generate more or less H₂O₂ than the conventional dose rate irradiation, and what is its underlying mechanism? **Oral presentation, top score** (FRPT 2023).
3. [Zhang T](#), Stengl C, Derksen L, Zink K, Adeberg S, Major G, Hesser J, Baumann KS, Seco J, Hydrogen Peroxide Production in Flash Vs. Conventional Dose-Rate Irradiation: Investigating the Mechanisms. **Oral presentation** (AAPM 2024).

8. CURRICULUM VITAE

PERSONAL INFORMATION

Last and first name: Zhang, Tengda
Date of birth: 21.07.1990
Place of birth: Liaoning, China

HIGH SCHOOL

(2006) – (2009) Shenyang No.20 Middle School
(10.06.2009) High school diploma

UNIVERSITY CAREER

(2009) – (2013) Southern Medical University, China
Bachelor, Biomedical Engineering;
(2013) – (2016) Peking Union Medical College & Tsinghua University, China
Master, Biomedical Engineering;
(2021) – present Heidelberg University, Germany
PhD, Dr. sc. hum.

9. ACKNOWLEDGMENT

I would like to express my deepest gratitude to Prof. Jürgen Hesser from the Mannheim Medical Faculty, Heidelberg University, for his invaluable supervision and continuous support throughout my PhD journey. His guidance has been instrumental in shaping my research and academic growth.

I am particularly indebted to Dr. Kilian-Simon Baumann from the Marburg Ion Beam Therapy Center (MIT), whose unwavering support made it possible for me to carry out my experiments. Kilian provided everything I needed for my experiments and consistently supported me throughout the process.

My sincere thanks also go to PD Dr. Stefan Bartzsch from TUM, with whom I collaborated closely on experiments and discussions. Working with Kilian and Stefan has been a truly enriching experience, not only in terms of scientific knowledge but also in forging meaningful friendships.

Furthermore, I am grateful to Christina Stengl and Prof. Oliver Jäkel from DKFZ E040, whose tremendous support enabled me to successfully conduct our experiments at MIT.

I also extend my heartfelt thanks to my friends in Heidelberg—Hugo, Mariana, Daniel, Joana, Francesca, Alex, Joao, and Miguel—for their unwavering support. As a foreign researcher, their friendship and companionship have made my time here much less lonely.

Finally, I wish to express my deepest appreciation to my family, especially my wife, whose unconditional support has been the foundation of my PhD journey. Without her encouragement and sacrifices, completing this PhD would not have been possible.